

2014

Sediment Deposition and Reworking: A Modeling Study using Isotopically Tagged Sediment Classes

Justin J. Birchler

College of William and Mary - Virginia Institute of Marine Science

Follow this and additional works at: <https://scholarworks.wm.edu/etd>



Part of the [Geology Commons](#), [Oceanography Commons](#), and the [Sedimentology Commons](#)

Recommended Citation

Birchler, Justin J., "Sediment Deposition and Reworking: A Modeling Study using Isotopically Tagged Sediment Classes" (2014). *Dissertations, Theses, and Masters Projects*. Paper 1539617950.

<https://dx.doi.org/doi:10.25773/v5-0r4h-r256>

This Thesis is brought to you for free and open access by the Theses, Dissertations, & Master Projects at W&M ScholarWorks. It has been accepted for inclusion in Dissertations, Theses, and Masters Projects by an authorized administrator of W&M ScholarWorks. For more information, please contact scholarworks@wm.edu.

Sediment Deposition and Reworking:
A Modeling Study Using Isotopically Tagged Sediment Classes

A Thesis

Presented to

The Faculty of the School of Marine Science
The College of William and Mary in Virginia

In Partial Fulfillment
of the Requirements for the Degree of
Master of Science

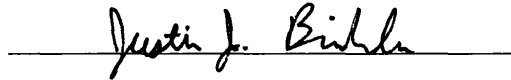
by

Justin J. Birchler

2014

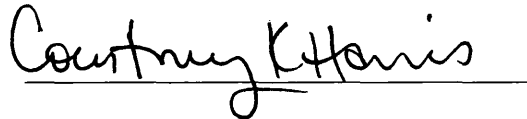
APPROVAL SHEET

This thesis is submitted in partial fulfillment of
the requirements for the degree of
Master of Science



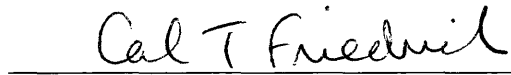
Justin J. Birchler

Approved, by the Committee, February, 2014

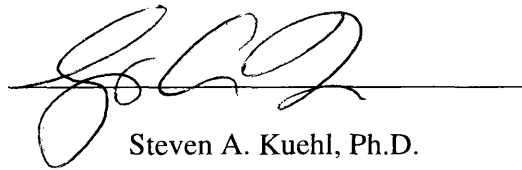


Courtney K. Harris, Ph.D.

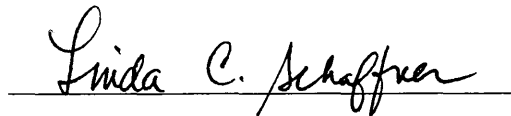
Committee Chairman/ Advisor



Carl T. Friedrichs, Ph.D.



Steven A. Kuehl, Ph.D.



Linda C. Schaffner, Ph.D.

TABLE OF CONTENTS

ACKNOWLEDGEMENTS.....	v
LIST OF TABLES.....	vi
LIST OF FIGURES.....	vii
ABSTRACT.....	viii
CHAPTER 1: Introduction.....	1-2
1.1 Motivation.....	1-2
1.2 Short-lived Radioisotopes.....	1-3
1.3 Event Bed Generation and Preservation.....	1-3
1.4 Coupled Hydrodynamic – Sediment Transport Model; ROMS.....	1-10
1.5 Research Questions.....	1-11
1.6 Approach.....	1-12
Figures.....	1-14
CHAPTER 2: Methods and Proof of Concept for a Numerical Model of Radioisotopic Activity within a Coastal Sediment Bed.....	2-1
2.1 Abstract.....	2-1
2.2 Introduction and Motivation.....	2-2
2.3 Model Approach.....	2-4
2.4 Model Implementation.....	2-10
2.5 Example Application: Results.....	2-12
2.5.1 Behavior of the Standard Model.....	2-13
2.5.2 Sensitivity to Biodiffusion Coefficient.....	2-15
2.5.3 Sensitivity to Resuspension Intensity.....	2-16
2.5.4 Sensitivity to Flood Deposit Thickness.....	2-17
2.6 Discussion of Example Application.....	2-18
2.6.1 Relative Effect of Biodiffusion, Resuspension and Deposit Thickness.....	2-19

2.6.2	Vertical Profile Comparisons.....	2-21
2.6.3	Synthesis of Event Bed Tracer Metrics	2-23
2.7	Summary and Future Work.....	2-24
	Tables.....	2-27
	Figures.....	2-29
CHAPTER 3: Comparative Study of Modeled and Observed Radioisotope Profiles		3-1
3.1	Abstract	3-1
3.2	Introduction and Motivation	3-2
3.3	Example from the Gulf of Mexico.....	3-10
3.4	Methods.....	3-12
3.5	Results.....	3-19
3.5.1	Standard Calm Model Run.....	3-20
3.5.2	Standard Storm Model Run	3-23
3.5.3	Deposition Rates	3-25
3.6	Discussion	3-28
3.6.1	Sensitivity to Bioturbation	3-28
3.6.2	Sensitivity to Flood Thickness.....	3-29
3.6.3	Application to Mississippi Delta Field Site	3-30
3.7	Conclusions and Future Work	3-32
	Tables.....	3-34
	Figures.....	3-35
CHAPTER 4: Summary and Future Directions.....		4-1
REFERENCES		R-1
APPENDIX: Model Input Files		A-1
	sedbiotoy.h.....	A-5
	ocean_sedbiotoy.in.....	A-8
	sediment_sedbio.in.....	A-30
VITA		A-37

ACKNOWLEDGEMENTS

Many people have influenced me while at VIMS. Most importantly, I would like to thank my advisor, Dr. Courtney Harris, who provided an immense amount of guidance and support throughout my time at VIMS. I would also like to thank my Masters Thesis Committee; Drs. Carl Friedrichs, Steve Kuehl, and Linda Schaffner, for their support, advice, and insight. I am also grateful to the faculty, staff, and students who took part in my experience of study and research at VIMS.

This thesis benefitted from the support provided by a number of individuals. Julia Moriarty provided computational assistance and support on a daily basis. Tara Kniskern helped with the radioisotope calculations. Adam Miller, Mary Ann Bynum, and Dave Weiss dispensed technical assistance for using the computational facilities at VIMS.

Funding for this thesis was provided by a BOEM grant.

Finally, I would like to thank my family and friends for all their love, as well as helping to make the last few years a wonderful chapter of my life.

LIST OF TABLES

Table 2-1: Model Sensitivity Test Parameters.....	2-27
Table 2-2: Standard Model and Sensitivity Test Results.....	2-28
Table 3-1: Sediment Deposition Rates	3-34

LIST OF FIGURES

Figure 1-1: One-dimensional Model Illustration	1-14
Figure 2-1: Comparison of Observed ⁷ Be Activity and Modeled Sediment Deposition.....	2-29
Figure 2-2: One-dimensional Model Illustration	2-30
Figure 2-3: Standard Model Timeseries	2-31
Figure 2-4: Profiles for the Standard Model	2-32
Figure 2-5: Profiles Varying by the Biodiffusion Coefficient (D_b)	2-33
Figure 2-6: Profiles Varying by Resuspension Intensity	2-34
Figure 2-7: Profiles Varying by Flood Deposit Thickness	2-35
Figure 2-8: Profiles Varying by the Active Layer Thickness	2-36
Figure 3-1: Study Site Map.....	3-35
Figure 3-2: Radioisotope Profiles from Corbett <i>et al.</i> , (2004).....	3-36
Figure 3-3: Calm Model Timeseries	3-37
Figure 3-4: Storm Model Timeseries.....	3-38
Figure 3-5: Calm Model Grain Size and Radioisotope Profiles	3-39
Figure 3-6: Calm Model Comparison with Observations.....	3-40
Figure 3-7: Calm Model Timeseries of Bed Inventory and Surface Activity.....	3-41
Figure 3-8: ⁷ Be: ²³⁴ Th Ratio for Bed Inventory and Surface Activity.....	3-42
Figure 3-9: Calm Model Penetration Depth.....	3-43
Figure 3-10: Storm Model Grain Size and Radioisotope Profiles	3-44
Figure 3-11: Storm Model Comparison with Observations.....	3-45
Figure 3-12: Storm Model Timeseries of Bed Inventory and Surface Activity	3-46
Figure 3-13: Storm Model Penetration Depth	3-47
Figure 3-14: Model Deposition Rates.....	3-48
Figure 3-15: Calm Model Sensitivity to D_b	3-49
Figure 3-16: Storm Model Sensitivity to D_b	3-50
Figure 3-17: Calm Model Sensitivity to Deposition.....	3-51
Figure 3-18: Storm Model Sensitivity to Deposition.....	3-52

ABSTRACT

A sediment transport model within the Regional Ocean Modeling System (ROMS) was used to examine how repeated cycles of deposition, erosion, and bioturbation influence flood and storm event bed character offshore of a significant fluvial source. Short-lived radioisotopes Beryllium-7 (^7Be) and Thorium-234 (^{234}Th) can be used as tracers of deposition and reworking on the continental shelf, and modeled profiles of these radioisotopes, along with simulated profiles of sediment bed grain size distributions, were analyzed for various model runs. The presence of an atmospherically derived radionuclide, ^7Be , in seafloor sediment indicates terrestrial (riverine derived) sediment deposition offshore of a fluvial source. In contrast, ^{234}Th naturally occurs in seawater through the decay of its generally conservative parent, ^{238}U , and its presence in the seabed indicates the recent suspension of sediment in oceanographic water. Simulated profiles of ^7Be and ^{234}Th were directly related to the flood and storm sequences used as model input. The model results showed that the radioisotopic profiles are sensitive to the timing of ^7Be input, phasing of wave and current energy, and intensity of bioturbation; complicating the relationship between simulated profiles and model input of flood and hydrodynamic forcing. Sediment grain size and geochronological tracers were used as markers of event beds for flood and storm deposition scenarios.

Sediment Deposition and Reworking:

A Modeling Study Using Isotopically Tagged Sediment Classes

CHAPTER 1: Introduction

1.1 Motivation

Numerical sediment transport models have been developed that estimate deposition as well as physical reworking of sediment via resuspension (e.g. Harris and Wiberg, 2001; Warner *et al.*, 2008). Because sediment availability impacts erosion depths (Sanford and Maa, 2001), many sediment transport models represent multiple grain classes that have different hydrodynamic properties (critical shear stress, settling velocity), and represent the sediment grain size distribution with depth in the bed using a layered bed model (Harris and Wiberg, 1997; Warner *et al.*, 2008). Biological processes, however, also impact the seabed via bioturbation which can act to vertically mix sediment and is especially intense near the sediment-water interface (Wheatcroft *et al.*, 1990). Only a few sediment transport studies (e.g. Harris and Wiberg, 1997), have included biodiffusion, though recently, Sherwood *et al.*, (in prep) added it to the Community Sediment Transport Modeling System (CSTMS), along with other modifications.

Radioisotopic tracers have long been used to infer the depositional history of marine sediment, based on conceptual models that rely on assumed rates of mixing and burial (e.g. Nittrouer *et al.*, 1979; Sommerfield and Nittrouer, 1999; Waples *et al.*, 2006). The geochronological data, however, have not been suitable for direct comparison to

numerical models that deal solely with sediment grain size. This disconnect has perpetuated a difficulty in evaluating the relative importances of bioturbation, resuspension, erosion, and deposition in marine sedimentation.

1.2 Short-lived Radioisotopes

The radioisotope tracers Beryllium-7 (^7Be) and Thorium-234 (^{234}Th) have been widely used by marine geologists to characterize sediment transport pathways over short time scales (days-months). These two radionuclides are highly particle-reactive and therefore quite useful as tracers of sediment transport (Baskaran and Santschi, 1993). The half-life for decay determines the temporal period over which a tracer remains useful; the half-lives ($t_{1/2}$) of ^7Be and ^{234}Th are 53.3 and 24.1 days, respectively. Radioisotopes can generally be detected for about 4 – 5 half-lives; therefore ^7Be and ^{234}Th are useful as indicators of a depositional or resuspension episode for as long as 250 days and 100 days following an event, respectively (Corbett *et al.*, 2007).

1.3 Event Bed Generation and Preservation

All sediment deposited on the seabed is subject to post-depositional alteration by physical, biological, and chemical processes before it becomes preserved in the stratigraphic record. Consolidation occurs in all sedimentary environments; the burden of overlying sediment causes pore water to escape the sediment bed, decreasing porosity within the seabed over time. Muddy sediments are particularly prone to consolidation; in cohesive sediments, consolidation has a greater effect on critical shear stress than grain

size. Consolidation decreases the erodibility of the sediment bed and increases the likelihood of event bed preservation (Wheatcroft *et al.*, 2007).

Physical alteration in the form of sediment erosion, transport, and redeposition impacts sediment bed layers, and is driven by energetic waves and currents. Shelf geometry, wave climate, and tidal energy greatly influence sediment accumulation on continental margins (Nittrouer *et al.*, 1985; Nittrouer and Wright, 1994). Waves are often the dominant control on sediment resuspension in open-shelf environments (Komar *et al.*, 1972; Drake and Cacchione, 1985; Wright and Nittrouer, 1995; Allison *et al.*, 2000). While oceanographic currents may often be too weak to mobilize sediment independently of waves, they dictate the direction and rate of transport (Sherwood *et al.*, 1994).

Sanford and Maa, (2001) expressed the sediment entrainment rate (E , kg/m²/s) as:

$$E = M(\tau_b - \tau_{cr})^n \quad (1)$$

where M is the erosion rate parameter, n is an empirical coefficient, and τ_b and τ_{cr} (Pa) are the bed shear stress and critical shear stress of sediment, respectively. In cohesive sediments, τ_{cr} can vary both with depth in the bed and time, and does not depend strongly on disaggregated grain size (Sanford and Maa, 2001). For well sorted beds of non-cohesive sands, however, τ_{cr} varies with grain size (Miller *et al.*, 1977). In beds with a range of non-cohesive grain sizes, the entrainment rate (E) for each size class depends on its abundance at the bed surface (Harris and Wiberg, 2001; Wheatcroft *et al.*, 2007). Fine sediment is more readily suspended than coarse sediment and therefore becomes depleted at the surface, i.e., winnowed, creating a coarsened, armored layer that prevents

underlying fine sediment from being suspended (Kachel and Smith, 1986; Wiberg *et al.*, 1994; Reed *et al.*, 1999).

Sediment is mobilized when waves and currents produce a bed shear stress exceeding its critical shear stress (Miller *et al.*, 1977). An event bed formed by an immense amount of sediment mobilization on the continental shelf is referred to as a storm bed (Wiberg, 2000). A storm bed is diagnostic of energetic flow conditions with little or no apparent input of new sediment. Characteristics of storm beds include a graded layer of reworked sediment that fines upward that may be armored by a coarse lag layer at its base (Reineck and Singh, 1972; Nittrouer and Sternberg, 1981; Myrow and Southard, 1996). Storm beds also often have signs of an erosive base indicated by a sharp discontinuity in grain size and truncation of features relative to the underlying layer. Under non-uniform flow and bed conditions, spatial variations in flux cause net erosion and deposition over the course of a storm, modifying the grain size distribution of the bed and possibly creating thick deposits at some locations (see Harris and Wiberg, 2002). Corbett *et al.*, (2007) suggest that ^{234}Th could be used as evidence of storm layers produced within its detection window of ~ 100 days, because resuspension can “recharge” marine sediments with ^{234}Th and create elevated ^{234}Th inventories.

Hurricanes Katrina and Rita, two large hurricanes that impacted the Gulf of Mexico in August and September 2005, respectively, did not induce especially large discharge pulses of the Mississippi River, but created storm bed deposits on the continental shelf. Walsh *et al.*, (2006) showed that cores in the Mississippi delta region, with the exception of one site, contained one or two layers of physically stratified

sediment and elevated excess ^{234}Th activities; indicating sediment reworking and/or deposition within the timeframe of the hurricanes. The total event layer thickness for both hurricanes exceeded 20 cm at several sites in water shallower than 40 m. These data suggest the event layer(s) were related to wave and current – driven suspended transport during the two hurricanes. Keen *et al.*, (2006) also found thick event beds ranging from 5-30cm at roughly 25 m on the western Louisiana shelf following these two hurricanes.

An event bed formed by input of flood sediment, often during peak river discharges, with or without substantial sediment mobilization on the continental shelf is referred to as a flood bed (Wheatcroft, 2000). Much attention of late has been paid to coherent systems, common in small mountainous river systems, where river flood conditions often coincide with energetic oceanic wave and/or wind-driven currents (Wheatcroft, 2000; Guillen *et al.*, 2006). Sommerfield *et al.*, (1999) identified flood event beds from the 1995 and 1997 Eel River floods by analyzing ^7Be and grain size on the continental shelf. Clay content and ^7Be inventories of the flood deposits were much greater than those of ambient shelf sediments. Drake (1999) was able to clearly identify the flood bed after the same 1995 Eel River flood by the predominance of particles smaller than 20 μm , which accounted for as much as 96% of the deposit.

Prior to preservation in the geologic record, however, both physical and biological reworking likely modify a flood bed. Drake (1999) found that after creation of a flood bed on the Eel River shelf, physical alteration, new sediment, and bioturbation modified the normally graded layer that had small spatial variability into a layer that was inversely graded with high spatial variability. Benthic organisms play three roles in post-

depositional alteration and preservation of strata. (1) They alter dynamically important properties of bottom sediments, e.g. porosity and grain size, which can influence consolidation and erosion. (2) Bioturbation, the stirring of bulk sediment by organisms (Richter, 1952), can destruct strata and redistribute material within the seabed, reorganizing bulk properties in the seabed. (3) Finally, animals produce sedimentary structures such as burrows and feeding traces that replace the primary physical sedimentary structures and bedding with a bioturbate texture or 'ichnofabric' (Frey and Pemberton, 1990; Wheatcroft *et al.*, 2007). Virtually all animals that come into contact with the sea bed cause some degree of bioturbation. Bioturbating macro benthic organisms are present in most marine environments excluding, e.g., oxygen minimum zones and areas of rapid sediment accumulation. Bioturbation causes particle displacement in the surface mixing layer that destroys physically produced sedimentary structures and mixes transient signals so that they cannot be recognized (Wheatcroft and Drake, 2003).

Measurement and modeling of the short-lived radionuclide ^{234}Th is the primary approach to quantifying bioturbation, parameterized by the biodiffusion coefficient, (Wheatcroft and Drake, 2003; Wheatcroft, 2006), though other radioisotopes have been used including ^7Be , ^{210}Pb , ^{137}Cs , and $^{239,240}\text{Pu}$. The biodiffusion coefficient, D_b , is used to model the vertical mixing within the sediment bed. Many studies, at numerous locations have tried to constrain the biodiffusion coefficient (see Table 1 from Boudreau, 1994). However, D_b varies considerably (10^{-2} to $10^2 \text{ cm}^2 \text{ y}^{-1}$) depending on water depth, geographical location, and the tracer used to infer it (Boudreau, 1994; Wheatcroft *et al.*,

2007), though Wheatcroft and Drake, (2003) identify that continental shelf sediments are mixed vigorously and that in general D_b on shelves ranges from $\sim 10\text{-}100\text{ cm}^2/\text{yr}$. Under dominantly mixing conditions, radioisotopes are used to quantify bioturbation with the biodiffusion coefficient, D_b (e.g. Aller and Cochran, 1976; Nittrouer *et al.*, 1984, Wheatcroft, 2006):

$$D_b = \lambda \left[\frac{z}{\ln(A_0 / A_z)} \right]^2 \quad (2)$$

where A_0 is the activity of the radionuclide near the sediment surface, A_z is the activity of the radionuclide at depth z , and λ is the decay constant of the radionuclide; assuming sediment accumulation is negligible, i.e. $S^2 \ll 4D_b\lambda$, where S is the steady state accumulation rate.

Preservation of sedimentary strata depends on sediment accumulation rate, bioturbation, surface mixing layer thickness, and event deposit thickness (Nittrouer and Sternberg, 1981; Wheatcroft, 1990; Bentley and Nittrouer, 2003; Wheatcroft and Drake, 2003). The relative timescales for transit through the mixed layer, and dissipation of the signal determine whether an event layer will be preserved. Transit time, a function of sediment accumulation rate, surface mixing layer thickness, and the event layer thickness, can be defined as the period of time required to advect an event layer through the surface mixed layer, while dissipation time is the time necessary to destroy the signals that mark an event bed. If the dissipation time exceeds the transit time, a portion of the event bed can be preserved (Wheatcroft, 1990).

Wheatcroft and Drake, (2003) showed that the probability of event layers being preserved on the Eel River shelf was extremely low because, on average, transit time (decades) greatly exceeded dissipation time (months to years). However, studies on the Eel River shelf have identified clearly preserved event beds over the Pleistocene (Leithold, 1989) as well as over the last ~500 years (Bentley and Nittrouer, 2003). Accumulation rates are extremely variable on river dominated margins, however, with long periods of low sedimentation punctuated by short bursts of rapid deposition during floods or storms that mobilize recently delivered sediment. For example, on the Eel River shelf, episodic sedimentation events, such as floods during the northern California storms of 1995 and 1997 deposited enough sediment to rapidly bury layers and signals below the surface mixing layer, thereby enhancing the preservation potential of any flood layers that had been recently formed. In this manner, episodic sedimentation events can decrease the transit time of the events that preceded them by more than one order of magnitude, which is key in determining preservation potential (Wheatcroft *et al.*, 2007).

Previous attempts to model event beds and preservability include a one-dimensional sedimentation-bioturbation model (Bentley and Sheremet, 2003) that simply deals with preservability, the two-dimensional model of Harris and Wiberg, (2002) that analyzed storm-driven across-shelf sediment transport and the two-dimensional model that Bentley *et al.*, (2002) and Keen *et al.*, (2004) used to investigate storm beds, but treated grain size only. To date, models have not represented tracers, such as ^7Be and ^{234}Th , which are used to infer event bed presence.

1.4 Coupled Hydrodynamic – Sediment Transport Model; ROMS

Warner *et al.*, (2008) described the implementation of a sediment-transport module in the Regional Ocean Modeling System (ROMS). To estimate suspended sediment transport, ROMS solves the scalar transport equations for advection and diffusion for an unlimited number of user-defined sediment classes; with each having fixed attributes of grain diameter, density, settling velocity, and erosion rate parameter. ROMS treats these sediment classes as non-reactive, i.e. conservative tracers, in a manner similar to temperature and salinity, but with an added downward vertical velocity to account for sediment settling, and a bottom boundary condition to represent erosion from, and deposition to the sediment bed.

In addition to these conservative tracers, however, ROMS can account for the transport of reactive (i.e. non-conservative) tracers, and the biogeochemical research community, for example, have developed modules within the community model to account for the transport of biological tracers such as plankton, and geochemical constituents such as oxygen and organic matter (e.g. Hetland and DiMarco, 2008; Fennel *et al.*, 2013). Tracer concentrations are estimated using the advection-diffusion-reaction equation that takes into account physical movement within the model domain as well as reaction terms to represent biological processes such as mortality, growth, and birth; and chemical reactions.

Recent enhancements to the sediment transport model have allowed it to include reaction terms, so that it can account for both particulate and dissolved geochemically reactive tracers in the seabed and the water column (Harris *et al.*, 2012). To account for

mixing between sediment bed layers, biodiffusion has also been added (Sherwood *et al.*, in prep.). With these new capabilities, the sediment transport model can be used to account for any number of reactive components within the water column and seabed, including radioisotopes such as ^7Be and ^{234}Th which would enable us to address, within a numerical modeling framework, relevant questions regarding the generation and preservation of geochronological tracers within coastal systems.

1.5 Research Questions

The CSTMS can now be used to directly evaluate the modifications expected from both bioturbation and physical reworking, to both grain size and geochronological tracers. This gives us the ability to address the following questions:

1. The magnitude of flood deposition has been inferred by grain size patterns, and surface activities and depth of penetration of ^7Be . How does bioturbation, resuspension intensity, and the magnitude of the source term impact proxies for flood event sedimentation inferred from profiles of ^7Be and grain size?
2. Post-depositional reworking of flood deposits via resuspension impacts grain size and radioisotopic profiles. Can ^{234}Th be useful in combination with the ^7Be and grain size profiles to evaluate the role that physical reworking may play in event bed character?

1.6 Approach

These questions are addressed using a one-dimensional sediment and biogeochemical implementation of ROMS that includes sediment transport based on the CSTMS. Harris *et al.*, (2012) modified this one-dimensional model to incorporate particulate and dissolved reactive tracers within the sediment bed, with the goal of developing a diagenetic model coupled to the water column Nutrient-Phytoplankton-Zooplankton-Detritus (NPZD) biogeochemical model developed by Fennel *et al.*, (2006). Biodiffusion of particles and dissolved components was calculated by solving for diffusive fluxes at the layer interfaces (Sherwood *et al.*, in prep.).

Using Harris *et al.*, (2012)'s framework to represent geochronological components instead of biological tracers (i.e. organic matter, oxygen, and nutrients), the model can directly estimate the activities of radioisotopes such as ^7Be and ^{234}Th . Reaction terms for these tracers account for constant decay according to their known half-lives, as well as sorption within the water column for ^{234}Th (Figure 1-1). The model was used to simulate erosional and depositional processes for timescales of up to a year, and examined the effect of biodiffusion and resuspension on grain size and geochronological profiles within the sediment bed. In addition to developing the capability of the model to account for geochronological tracers, this thesis also explores the sensitivity of radioisotopic profiles to parameters such as the biodiffusion coefficient and source term activities.

Chapter 2 uses an idealized one-dimensional (vertical) model to explore the processes that impact grain size and radioisotope profiles. Chapter 2 explains in detail

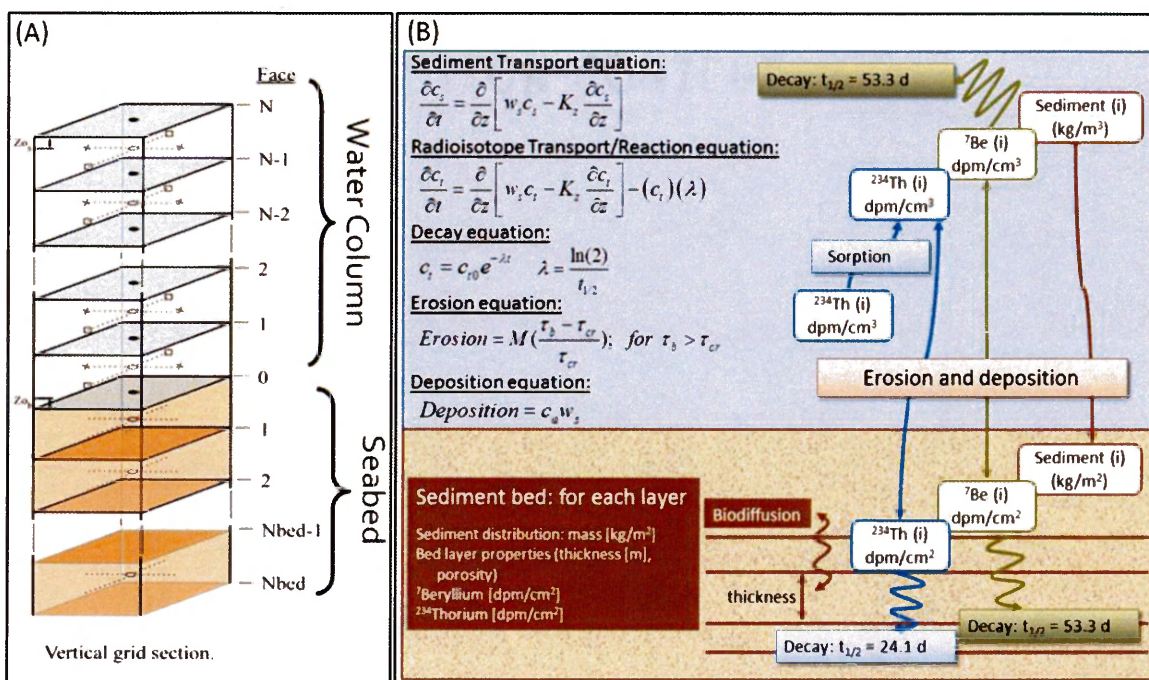
how the model works. A range of biodiffusion coefficients, resuspension intensities, and flood deposit thicknesses were used to examine how these parameters affected sediment bed profiles of grain size and geochronology over a year long time period using idealized wave forcing.

Chapter 3 then applies the model to a more realistic set of waves. The one-dimensional model was compared to field observations from the northern Gulf of Mexico. Corbett *et al.*, (2004) measured radioisotope profiles from sediment cores taken in April and October, 2000 at a 50 meter site just offshore of the Mississippi River. Two versions of the model were run; a standard calm model representing a low energy period of the year, from April, 2000 to October, 2000 and a standard storm model representing the high wave period of the year, from October, 1999 to April, 2000. Using these standard calm and storm models, the profiles measured by Corbett *et al.*, (2004) were reproduced within our model framework. Then, sensitivity of modeled profiles of grain size and radioisotopes were examined for a range of biodiffusion coefficients and deposition thicknesses.

Figures

Figure 1-1: One-dimensional Model Illustration

(A) One-dimensional vertical model illustration (Warner *et al.*, 2008). Water column layers of constant thickness overlie seabed layers of variable thickness. (B) Schematic of the combined CSTMS sediment transport and geochronology model.



CHAPTER 2: Methods and Proof of Concept for a Numerical Model of Radioisotopic Activity within a Coastal Sediment Bed

2.1 Abstract

Sediment transport models that represent flood and storm sedimentation for coastal areas typically estimate grain size patterns and deposit thicknesses and are therefore disconnected from field observations that rely on geochronological tracers to infer event bed character. For example, observations of Beryllium-7 (^7Be) offshore of a fluvial source provide an indicator of riverine derived terrestrial sediment deposition. Conversely, Thorium-234 (^{234}Th) naturally occurs in seawater and its presence indicates recent sediment suspension. Interpreting field data based on radioisotopes presents challenges that stem from the source terms for the tracers, as well as confounding effects of sediment transport processes and physical and biological mixing, but numerical models for these processes are lacking. To address this, a sediment transport model capable of estimating sediment bed profiles of ^7Be and ^{234}Th has been developed by expanding the Community Sediment Transport Modeling System (CSTMS), implemented within the Regional Ocean Modeling System (ROMS) to account for reactive tracers. In addition to the processes of sediment erosion, deposition, and suspension, the model also includes mixing within the sediment bed via biodiffusion.

A one-dimensional (vertical) test case that includes a non-cohesive sediment bed, three classes of sediment, and reactive tracers for ^7Be and ^{234}Th was subjected to flood

deposition and storm resuspension. The model was initialized with fine and medium sediment in suspension which settled to become a flood deposit. These two sediment classes were initially labeled with ^7Be , and became labeled with ^{234}Th upon resuspension. The sediment bed was then subjected to idealized storm events that resuspended sediment. Sensitivity tests were run to compare the effects of flood input, resuspension and bioturbation on grain size and radioisotope profiles. The model results showed that the radioisotopic profiles were sensitive to the flood deposit thickness, wave resuspension, and intensity of bioturbation. Post-depositional reworking of a flood deposit via resuspension modified the ^7Be profile in a manner similar to bioturbation, but created a signature within the ^{234}Th and grain size profiles.

2.2 Introduction and Motivation

Radioisotopic tracers, such as ^7Be and ^{234}Th , have long been used to infer the depositional history of marine sediment, based on conceptual or analytical models that rely on assumed rates of mixing and burial (e.g. Nittrouer *et al.*, 1979; Sommerfield and Nittrouer, 1999; Waples *et al.*, 2006). The geochronological data, however, have not been suitable for direct comparison to numerical sediment transport models that deal solely with sediment grain size, such as Warner *et al.*, 2008, Harris *et al.*, 2008, and Bever *et al.*, 2009 (Figure 2-1). This disconnect has perpetuated a difficulty in using either the numerical models or the radioisotopic profiles to evaluate the relative importance of bioturbation, physical mixing, resuspension, erosion, and deposition in marine sediment. Several processes impact profiles of geochronological tracers, including timing of input,

bioturbation within the seabed and dilution. The biodiffusion coefficient, D_b , in the marine environment varies considerably (10^{-2} to 10^2 $\text{cm}^2 \text{y}^{-1}$) depending on water depth, geographical location, and tracer used to infer it (Boudreau, 1994; Wheatcroft *et al.*, 2007), however, the biodiffusion rates for upper continental margins around the world can be constrained to typically $10\text{-}100$ $\text{cm}^2 \text{y}^{-1}$ (Wheatcroft and Drake, 2003).

Previous attempts to explore these problems by numerical modeling have included a one-dimensional sedimentation-bioturbation model (Bentley and Sheremet, 2003) and a simple two-dimensional gravity flow model (Ma *et al.*, 2010). Bentley and Sheremet, (2003) presented a model for preservation of sedimentary fabric under deposition and bioturbation assuming negligible physical mixing. The authors analyzed the “preservation quotient”, the fraction of the original unit volume that retains its primary depositional fabric, for both depth-constant and depth-dependent bioturbation of sediments. Ma *et al.*, (2010) used a model to represent gravity-driven sediment transport and deposition on the Waiapu shelf, New Zealand. The deposit thickness after 10 discrete time segments was multiplied by a ^7Be activity decay factor to determine a relative ^7Be activity within the continental shelf flood deposit. The authors then compared this relative ^7Be activity to ^7Be observations on the shelf.

The addition of geochronological tracers to a sediment transport model would provide a tool for addressing these problems and facilitate direct comparisons between observations and model estimates. The objective of this study is to therefore include reactive tracers within a sediment transport model so that it can be used to estimate the distribution of various chemical constituents, including radionuclides within coastal

waters and sediment. By developing this within a community model, we hope to provide a tool useful for many applications.

2.3 Model Approach

The Community Sediment Transport Modeling System (CSTMS) provides a sediment-transport module within the Regional Ocean Modeling System (ROMS), as described by Warner *et al.*, (2008). The CSTMS can represent multiple grain types (typically size classes) of sediment, each having a characteristic grain diameter (D_i), particle settling velocity ($w_{s,i}$), critical shear stress for erosion ($\tau_{cr,i}$) and sediment density ($\rho_{quartz}=2650 \text{ kg m}^{-3}$), where i represents an index used to differentiate sediment classes.

Beneath each horizontal water-column grid cell, the model represents the seafloor using a number of sediment bed layers (Figure 2-2A). Model input files specify the number of bed layers, along with the initial thickness, and sediment-class distribution. The sediment bed layer thicknesses and grain size distribution are adjusted every time step to account for erosion and deposition. Additionally, changes to the active layer thickness, which is the layer of sediment at the seabed surface available for erosion (Harris and Wiberg, 1997), can modify the thicknesses of the surficial bed layers. When the calculated active layer exceeds the thickness of the top layer, the model entrains sediment from underlying layers until the top layer is as thick as the active layer. If an entire bed layer is removed via erosion, or by being absorbed into the active layer, the model splits the bottom layer to maintain a constant number of bed layers (Warner *et al.*, 2008; Sherwood *et al.*, in prep). When sediment deposition onto the bed exceeds a user-

defined thickness, a new bed layer is produced, and the bottom-most two layers are merged, again to maintain a constant number of bed layers (Warner *et al.*, 2008).

The model estimates the sediment entrainment rate dependent on the bed shear stress (τ_b) and the sediment erodibility as quantified by the critical shear stress for erosion (τ_{cr}). The sediment entrainment rate (E) was based on the Partheniades (1965) equation:

$$E = M \left[\frac{(\tau_b - \tau_{cr,i})}{\tau_{cr,i}} \right] \quad (1)$$

Sediment can be mobilized when the bed shear stress (τ_b) exceeds the critical shear stress. The erosion rate is assumed to be proportional to the excess shear stress ($S = \tau_b - \tau_{cr,i}$), and to the “erosion rate parameter”, M . The values of $\tau_{cr,i}$ and M are both specified as model input, and can be different for each sediment class. Less erodible sediments, i.e. those having higher critical shear stress and/or lower erosion rate parameters, are less likely to be entrained into the water column than more erodible sediment and can armor the seabed during resuspension episodes.

The model assumes simultaneous erosion and deposition, where sediment constantly settles within the water column at a rate proportional to the sediment class’ settling velocity ($w_{s,i}$) and its suspended concentration near the bed. The deposition rate calculated for each sediment class (D_i) is therefore:

$$D_i = w_{s,i} c_{s,i} \quad (2)$$

where $c_{s,i}$ is the near-bed suspended sediment concentration. Whether net deposition or net erosion occurs for a sediment class depends on whether the deposition rate exceeds the entrainment rate for that sediment class, or vice versa.

The model calculates transport in the water column by solving the advection-diffusion equation. For suspended-sediment, an additional source and sink term is added to incorporate exchange with the seabed via net erosion and deposition. Representation of the bottom boundary layer is critical for sediment-transport formulations because bottom stress influences sediment concentrations and resuspension rates. ROMS offers multiple choices for representing BBL processes, including simpler drag-coefficient expressions and more complex formulations that represent the interactions of waves and currents over a moveable bed. For many applications, the bottom boundary layer formulation must resolve subgrid-scale processes such as the production and dissipation of turbulent kinetic energy, presence of a wave boundary layer, and gradients in velocity and suspended-sediment concentration.

ROMS accounts for the transport of tracers that undergo diffusion and travel with the ambient ocean currents. For example, it treats salinity and temperature as conservative dissolved tracers, and sediment classes as conservative tracers that have an added vertical velocity component to account for settling. Biogeochemical models have used ROMS tracers to account for the transport of reactive (i.e. non-conservative) constituents such as biological tracers like plankton; and biogeochemical constituents such as oxygen and organic matter (e.g. Hetland and DiMarco, 2008; Fennel *et al.*, 2013). Tracer concentrations for biogeochemical constituents are estimated using the advection-diffusion-reaction equation that accounts for physical movement within the model domain and reaction terms such as mortality, birth, and chemical reactions.

Recently, the sediment transport model has been modified to account for reactive terms and to include geochemically reactive particulate and dissolved tracers within the sediment bed (Harris *et al.*, 2012). To account for mixing between sediment bed layers, biodiffusion was also added (Sherwood *et al.*, in prep.). These modifications, both to the model's representation of porewater chemistry and particulate matter, have enhanced the CSTMS's ability to address critical issues for coastal and marine waters.

The CSTMS already accounts for a user – specified number of sediment classes, which are treated as particulate tracers and exchange particulate mass between the water column and the sediment bed via erosion and deposition (Warner *et al.*, 2008). To this, we added reactive tracers to store the concentration of some geochemical constituent that is associated with a sediment tracer. Within the model, indices were used to link various reactive particulate tracers, like ^7Be and ^{234}Th , to sediment classes. For example, both the sediment tracer and reactive tracer for a particular grain size are stored in terms of a concentration. The model tracks sediment concentration (kg/m^3) in the water column, and sediment mass in each bed layer (kg/m^2); while the reactive tracer (e.g. ^7Be) associated with that grain size is stored as dpm/m^3 in the water column, and dpm/m^2 in a bed layer. To obtain the activity of the sediment, the reactive tracer concentration can be divided by the sediment concentration to yield dpm/kg . Particulate matter tracers were assigned hydrodynamic properties (e.g. settling velocity, critical shear stress, and erodibility) equivalent to those of their associated sediment class, but only the sediment tracers add mass to the bed upon deposition.

A transport-reaction equation was added for particulate reactive tracers in the water column:

$$\frac{\partial c_{t,i}}{\partial t} = \frac{\partial}{\partial z} \left[w_{s,i} c_{s,i} - K_z \frac{\partial c_{t,i}}{\partial z} \right] - (c_{t,i})(\lambda) \quad (3)$$

where $c_{t,i}$ was the suspended tracer concentration (dpm/m³), $c_{s,i}$ was the suspended sediment concentration (kg/m³), $w_{s,i}$ was the sediment settling velocity of the tracer and its associated sediment (m/s), K_z was the eddy viscosity (m²/s), λ was the tracer decay constant (1/day), and the index, i , was used to denote each size class.

Erosion and deposition can impact the concentration of geochemical tracers within the water column and the sediment bed. When eroded, reactive tracers linked to the sediment classes were added to the water column and removed from the top sediment bed layer. Upon deposition, reactive tracers linked to sediment were removed from the water column; and added back to the sediment bed. If a geochemical tracer is assumed to be present as dissolved in the water column, such as ²³⁴Th, suspended sediment can sorb ‘fresh’ tracer therefore increasing the concentration of a particulate – bound tracer, and increasing the sediment bed inventory upon deposition of the sediment to which it is linked. For this study, geochemical tracers decayed based on their half-lives within both the water column and sediment bed.

Biodiffusion mixed tracer concentrations and sediment type distributions across sediment layers. As described in Sherwood *et al.*, (in prep.), the model included seabed mixing using a diffusion equation where the diffusive flux across bed layers was proportional to the concentration gradient with the constant of proportionality being the biodiffusion coefficient, D_b . The depth to which mixing occurred was determined by the

model input parameter $Z_{b,max}$. The model assumed that the intensity of biodiffusion was largest near the sediment – water interface, and $D_b = D_{b,max}$ for $z_{b,k} < Z_{b,max}$. The biodiffusion coefficient then decayed linearly until it reached a small value specified as $D_{b,min}$, at depths below twice $Z_{b,max}$. The equation used for the linear decay of the biodiffusion coefficient was

$$D_{b,k} = D_{b,min} + (2Z_{b,max} - z_{b,k}) \frac{(D_{b,max} - D_{b,min})}{Z_{b,max}} \quad (4)$$

where $D_{b,k}$ represented a biodiffusion coefficient for bed layer k at depth $z_{b,k}$. Note that the coordinate system for the sediment bed model assumed that z_b represented the depth in the sediment bed, so that $z_b = 0$ at the sediment – water interface, and z_b increased with depth.

Two particulate geochronological tracers to represent short-lived radioisotopes ^7Be and ^{234}Th were added to the sediment transport model (Figure 2-2B). The radioisotopes ^7Be and ^{234}Th were linked to the model's two finest sediment classes, and their activities decayed based on half-lives of 53.3 and 24.1 days, respectively. The model treated these two tracers similarly, except for differences in source terms. Precipitation and subsequent river runoff provide the primary source of ^7Be from the atmosphere to the Earth's surface and the coastal ocean, so ^7Be was assumed to be a tracer of river sedimentation. Within our model it can be added as either a specified initial condition or at a riverine point source. For the one-dimensional (vertical) case shown here, sediment suspended at model initiation was assumed to have a ^7Be activity of 5 dpm/g. For the case of a three-dimensional model, sediment delivered by a riverine point source could be specified to have ^7Be associated with the fluvial sediment. In

contrast, ^{234}Th is continuously produced in the coastal ocean due to decay of its parent ^{238}U , which is conservative in seawater (McKee *et al.*, 1984). Our model therefore assumed ^{234}Th to be a tracer of marine water and resuspension, and the ^{234}Th activity of any sediment suspended in the water column was instantaneously set to be 5 dpm/g. Then, when that sediment settled, the resuspended sediment provided a source of ^{234}Th to the seabed. In the model, ^7Be decayed both in the water column and sediment bed, but ^{234}Th decayed only within the sediment bed.

2.4 Model Implementation

As a proof-of-concept, the one-dimensional model was configured to represent deposition and reworking of a flood deposit using the radioisotopes ^7Be and ^{234}Th at a 20 meter deep site from the Louisiana continental shelf in the northern Gulf of Mexico. The water column had 30 layers with constant thickness, and an approximately ten centimeter thick sediment bed was represented using 20 layers whose thickness varied depending on erosion and deposition. The model run used three sediment classes; fine (micro-floc), medium (macro-floc) and coarse (sand), which had settling velocities (w_s) of 0.1, 1.0, and 10.0 mm/s; nominal grain sizes (D_i) of 0.015 mm, 0.063 mm, and 0.125mm; and critical shear stresses (t_{cr}) of 0.03, 0.08, and 0.1 Pa, respectively. The erosion rate parameter (M) was $1 \times 10^{-5} \text{ kg m}^{-2} \text{ s}^{-1}$. At the beginning of the model run, the sediment bed grain size distribution was assumed uniform with depth, and sediment from the two finest grain sizes was suspended. During the first few days of the model run, the suspended sediment settled to the bed, which created a fining-upward layer. This was then disturbed during an

idealized 130 day stormy period that contained nine consecutive two-week long episodes of increasing and subsequently decreasing bed stress that simulated storm reworking of the flood deposit. Each of these two-week periods included a wave-driven storm that persisted for 6 days, followed by 8 days of calm conditions. Finally, the end of the model run included a 230 day quiescent period (Figure 2-3A-C).

The radioisotopic profiles responded to the changing physical forcing. Initially the model assumed that there was no ^7Be or ^{234}Th on the sediment bed. Sediment suspended at the start of the model run was tagged with ^7Be , and as it settled to the bed it also was assigned ^{234}Th activities of 5 dpm/g. The ^7Be continuously decayed with respect to its half-life in both the water column and sediment bed; ^{234}Th assumed instantaneous sorption in the water column, and then decayed within the sediment bed (Figure 2-3D-E).

This study examined the sensitivity of penetration depth, surface activity, and bed inventory of each tracer to the biodiffusion coefficient (indicated by $D_{b,max}$), resuspension intensity, and initial flood sediment input. The penetration depth (cm) was defined as the depth at which tracer activity equaled our specified detection limit, 0.1 dpm/g. It was calculated by finding the sediment bed layers whose activities bracketed the detection limit, and then linearly interpolating the modeled activities to find the depth at which the activity would fall below 0.1 dpm/g. The surface activity (dpm/g) was estimated as the average activity of the top centimeter of the sediment bed. The bed inventory (dpm/cm²) was obtained by integrating the tracer activity with depth in the seabed and accounting for mineral density (assumed 2650 kg/m³) and porosity (assumed 0.8). Three sets of

sensitivity tests compared: (1) biodiffusion coefficients of 0, 1 and 25 cm² yr⁻¹, (2) resuspension intensity, including no, moderate and high resuspension; and (3) flood input including low (0.38 cm), moderate (0.75 cm), and high (1.5 cm) flood deposition.

It was expected that increased $D_{b,max}$ would enhance mixing of the short-lived radioisotopes, creating a more uniform profile with depth and reduced surface activity. A reduced $D_{b,max}$ would limit mixing within our model; if a chosen $D_{b,max}$ was low enough (though still greater than zero) the effective biodiffusion will be zero due to the short-lived nature of the radioisotopes of interest. We expected resuspension intensity to increase the ²³⁴Th inventory of the bed, while flood input would increase both the ⁷Be and ²³⁴Th inventories.

2.5 Example Application: Results

In this section, we demonstrate that the model behaved reasonably for the case where a flood deposit was modified by bioturbation and storm reworking. The sensitivity of the vertical profiles of grain size distributions, and geochronological tracers to flood deposition, storm disturbance and bioturbation were investigated. Several different implementations of the model were run, so that estimates could be made using a range of biodiffusion coefficients, flood deposit thicknesses, and storm intensities. This section first describes the version which serves as a “standard model” for comparisons to the other model runs, and then describes model sensitivity to various parameters. Eight sensitivity tests were examined for the sediment transport – geochronological model. The standard case (Model run 1 in Table 2-1) used intermediate values, other models

varied the biodiffusion coefficient (Model runs 2 and 3), resuspension intensity (Model runs 4 and 5), the initial flood deposit thickness (Model runs 6 and 7), and the active layer thickness (Model run 8).

2.5.1 Behavior of the Standard Model

The standard model of the sediment-transport geochronological model assumed a low but non-zero $D_{b,max}$, medium storm resuspension intensity, and a medium (0.75 cm) flood thickness (see Table 2-1, model run 1). The sediment bed was subjected to nine storm events (Figure 2-3); during which sediment was eroded under high bed stresses (~ 2.7 Pa) and subsequently deposited when bed stresses returned to background levels. The one-dimensional (vertical) model did not account for horizontal flux convergence or divergence, and therefore any sediment that was eroded during a storm was redeposited when conditions subsided. During resuspension events, depth-averaged sediment concentrations peaked at around 0.12 kg/m^3 , and the eroded depth of the bed was about 0.46 cm, which was about one-half of the initial flood deposit thickness (0.75 cm).

The grain size profile changed with time due to flood deposition, and reworking by resuspension and biodiffusion (Figure 2-4A-E). The initial deposition and resuspension events produced a fining upward signal within the sediment bed due to the lower critical shear stress for erosion of the finer grains and differential settling of grains. Biodiffusion then attenuated this signal by mixing coarser material upward and finer material downward, so that by the end of the model run, the sediment grain size distribution returned to being nearly uniform with depth.

The bed inventories of ^7Be and ^{234}Th behaved differently due to their distinct treatments in the model (Figure 2-3D). The only source of ^7Be was that initially present on suspended sediment that settled in the flood deposit, and the model assumed that ^7Be decayed both in the bed and water column. With every storm event, the bed inventory of ^7Be sorbed to the fine size class decreased with the erosion, and then increased during the depositional phase as the fine size class was redeposited. The surface activity of ^7Be behaved similarly to the total inventory for ^7Be ; activity decreased upon resuspension and decayed with time (Figure 2-3E). In contrast, injection of the fine and medium sediment into suspension enriched the ^{234}Th bed inventory with each storm event. There was a larger change in the inventory of ^{234}Th sorbed to the fine size class as it accounted for most of the suspended load. The surface activity of ^{234}Th also behaved similarly to the total inventory of ^{234}Th ; activity decreased during resuspension, increased upon deposition, and decayed with time after the resuspension events ceased.

The ^7Be and ^{234}Th profiles changed with time due to decay, resuspension and biodiffusion (Figure 2-4F-J). Surficial sediment had the highest activity due to the large initial input of ^7Be -rich flood sediment, and continued enrichment of ^{234}Th due to resuspension events. After the flood pulse, resuspension and biodiffusion mixed both radioisotopes deeper into the bed. Over time, biodiffusion and decay produced a more uniform profile within the top few cm. Decay continuously decreased ^7Be and ^{234}Th activity throughout the bed, so that by day 250 of the model run, 125 days after the last storm episode, both radioisotopes had decayed below detection limit throughout the sediment bed.

2.5.2 Sensitivity to Biodiffusion Coefficient

The sensitivity of model estimates to biodiffusion was investigated by using values for $D_{b,max}$ that ranged from full neglect of mixing between bed layers ($0 \text{ cm}^2 \text{ yr}^{-1}$) to one of the larger values that has been reported for a continental shelf ($25 \text{ cm}^2 \text{ yr}^{-1}$). Results from these models (Model runs 2 and 3) were compared to the standard model that used $1 \text{ cm}^2 \text{ yr}^{-1}$ (Model run 1). Interestingly, the peak erosion depths of successive resuspension events in Model run 3 decreased by about 10% with time as the mixing processes coarsened the surficial sediment distribution, whereas the peak erosion depths stayed fairly constant in the standard model. Vertical profiles of grain size distribution were compared for days 100 and 240 in the model run, which represented the end of the storm period and ~ 3 months into the quiescent period (Figure 2-5A-C). Neglecting biodiffusion, the sediment distribution was unchanged from the fining upward layer produced by the resuspension events (Figure 2-5A). With inclusion of biodiffusion, the fining upward trend was attenuated as the grain size distribution was mixed, and ranged from a slight decrease in the fining upward trend when $D_{b,max}$ was $1 \text{ cm}^2 \text{ yr}^{-1}$ (Figure 2-5B), to a nearly uniform profile with depth when $D_{b,max}$ was $25 \text{ cm}^2 \text{ yr}^{-1}$ (Figure 2-5C).

Independent of resuspension intensity and flood deposit thickness, the biodiffusion coefficient had a clear signal with respect to surface activity, penetration depth and inventory (Figure 2-5D-F). Figure 2-5D-F show the ^7Be and ^{234}Th profiles for two different times in the model: day 20, after the first resuspension event, and day 100, representing resuspension events in the model run while radioisotope activities were high.

With increasing $D_{b,max}$, surface activity decreased and penetration depth increased. For ^7Be , the bed inventory remained unchanged with increasing $D_{b,max}$, while the bed inventory increased with increasing $D_{b,max}$ for ^{234}Th , because the mixing process brought sediment having reduced activities of ^{234}Th upward where it became available for suspension.

2.5.3 Sensitivity to Resuspension Intensity

To investigate how resuspension intensity affected the character of the flood bed, the model was run using significant wave heights that ranged from 0 to 10 m with a bottom wave period of 14 s (Model runs 4 and 5), but with the same timing and frequency of resuspension events as for the standard model (Model run 1). Peak bed stress estimated for each of these model runs was 0, 2.7 and 6.0 Pa for runs 4, 1 and 5, respectively. These represented no resuspension (peak bed stress < critical shear stress for erosion) and medium, and high resuspension intensity; and yielded mean erosion depths of 0, 0.46 and 0.56 cm, respectively (Table 2-1). Note that the thickness of the standard model flood deposit of 0.75 cm exceeded the peak erosion depths calculated for all of these model runs.

Resuspension impacted the persistence of the fining upward flood event layer in the grain size profiles (Figure 2-6A-C). For the case that neglected resuspension, the grain size signature of the initial flood layer was quickly attenuated by biodiffusion, so that by day 100, there was a weakly fining upward layer in the seabed surface (Figure 2-6A). While biodiffusion also occurred under medium and high resuspension intensities,

it was unable to attenuate the fining upward signal while the resuspension events were ongoing (Figure 2-6B, C).

For ^7Be , resuspension intensity did not impact bed inventory (Figure 2-6D-F), which depended only on the initial flood deposit. The physical mixing caused by increased resuspension, however, acted to slightly lower the surface activity and slightly deepen the penetration of ^7Be (Figure 2-6D-F). The case that neglected resuspension had a much lower ^{234}Th surface activity than the cases with medium and high resuspension intensity. The surface activity of ^{234}Th increased along with the amount of resuspension, as did its penetration depth. For the case of no resuspension, the estimated penetration depth of ^{234}Th became shallow early in the model run (Figure 2-6D).

2.5.4 Sensitivity to Flood Deposit Thickness

The final set of sensitivity model runs compared calculations made for a range of initial flood deposit thicknesses, including the standard model (0.75 cm thick, Model run 1) and 0.38 and 1.5 cm (Model runs 6 and 7, respectively). For comparison, the standard model had a resuspension depth of 0.46 cm. The mean resuspension depth for the case having the thick flood deposit increased to 0.60 cm, as it had less coarse sediment present at the surface to armor the bed.

The initial flood deposit added fine and medium sediment to the sediment bed which caused less coarse sediment to be present at the seabed surface for a thicker deposit (Figure 2-7A-C). By day 20 the signature of the grain size profiles was similar for thin and medium deposit thicknesses because resuspension acted deeper than the

initial thickness of the flood deposits (Figure 2-7A, B). The fining upward layer produced by the thick flood layer on day 20 started deeper in the bed than the layer produced by thinner flood layers (Figure 2-7C). While bioturbation and resuspension modified the grain size profile for the thick flood deposit by day 100, the fining upward layer started to be evident at a depth of 3cm and the amount of coarse sediment in the bed surface was still very low.

Because the initial flood deposit provided the primary flux of radioisotopes to the seabed, penetration depth and bed inventory increased with increasing deposit thickness for both radioisotopes and surface activity increased for ^7Be with a thicker deposit (Figure 2-7D-F). Doubling the flood deposit thickness doubled the ^7Be bed inventory, but had a lesser effect on the ^{234}Th inventory which was enriched by resuspension episodes (Table 2-2). Compared to the standard model, doubling the flood deposit thickness increased the ^7Be surface activity by 60% and the ^7Be penetration depth by 30%; the ^7Be penetration depth did not decrease as quickly with time compared to the standard case. Doubling the flood thickness increased the ^{234}Th surface activity by 14% and the ^{234}Th penetration depth by 25%.

2.6 Discussion of Example Application

This section synthesizes the results learned from the sensitivity tests, and suggests future directions for the development of the coupled geochemistry – sediment transport model.

2.6.1 Relative Effect of Biodiffusion, Resuspension and Deposit Thickness

To evaluate the degree to which the range in biodiffusion coefficients, resuspension intensity, and flood deposit thickness influenced likelihood that the flood bed could be detected using geochronology, we evaluated the “detection timescale”. This metric represented the number of half-lives for which the surface activities exceeded the detection limit, assumed to be 0.1 dpm/g. The “detection timescale” was estimated by taking the average activity in the top centimeter of the bed for each radioisotope, finding the number of days this exceeded the detection limit, and calculating the number of half-lives that this represented. For the case that did not include resuspension (Model run 4), the detection length was calculated as time elapsed since the flood event, the first day of the model run for both ^7Be and ^{234}Th . For cases that included resuspension events, the detection timescale for ^{234}Th was calculated relative to Day 125, which marked the end of the last resuspension event.

The detection timescale (represented as the number of half-lives) was similar for both ^7Be and ^{234}Th (Table 2-2). The detection timescale was inversely related to $D_{b,max}$. The higher the $D_{b,max}$, the more widely each radioisotope was mixed through the bed, and therefore surficial sediment activity fell below the detection limit more quickly, even though the total inventory varied little with $D_{b,max}$. Flood thickness also played a role in detection timescale, with thicker flood deposits remaining detectable for longer periods of time. The initial activity of ^7Be and ^{234}Th in the flood layer was identical for the different deposit thicknesses, but the thicker flood layer was more slowly diluted via biodiffusion of the low-activity sediment. For the case studied which had a $D_{b,max}$ of

$1\text{ cm}^2\text{ yr}^{-1}$, however, changing the flood thickness by a factor of two only increased the detection timescale by roughly 15% for ^7Be and 2% for ^{234}Th .

The thickness of the active layer, defined as the surficial sediment available for suspension, increases with increasing bed stress in the model (Harris and Wiberg, 1997). A thick active layer allows for more sediment to be available for suspension, especially the easily suspended fine and medium sediment, and reduces bed armoring by coarse sediment. In the standard model (Model run 1), the active layer thickness was limited to 5 mm or less so that the model produced resuspension depths that seemed reasonable compared to erodibility experiments from the site reported in Xu *et al.*, (in prep.). This limit prevented the resuspension episodes from fully reworking the flood deposit, even though the flood deposit was fairly thin.

To evaluate the degree to which more intense resuspension events would rework a flood deposit, the active layer thickness for Model run 8 was allowed to increase with bed stress, following Harris and Wiberg, (1997). The bed stresses were identical in Model runs 1 and 8, but the amount of suspended sediment and the eroded depth was almost doubled in run 8 when the active layer reached nearly 1.8 cm during the peak bed stress, thereby exceeding the thickness of the initial flood deposit (Table 2-1, Figure 2-8). The grain size signature was greatly influenced by the thicker active layer. While the concentration profile of coarse sediment in Model run 8 was similar to that in the standard model, the fining upward layer in Model run 8 was evident almost to a depth of 4cm (Figure 2-8A, B). The ^7Be bed inventory depended on the initial flood deposit, and was not influenced by the thicker resuspended layer. The increased physical mixing of

the surficial few centimeters of the bed, however, reduced the surface activity for ^7Be (Figure 2-8C, D). The increased active layer thickness and resultant resuspension depths nearly doubled the ^{234}Th inventory for Model run 8 compared to the standard model, however (Figure 2-8C, D). The surface activity of ^{234}Th was not much influenced because it was replenished during resuspension events (Table 2-2, Figure 2-8C, D).

2.6.2 Vertical Profile Comparisons

In this section, we synthesize the results of multiple sensitivity tests by comparing the degree to which the grain size and geochronological tracer profiles were influenced by the range of biodiffusion coefficients, flood thicknesses, and resuspension intensities that were considered. The initial flood deposit was an event layer at the sediment surface with high ^7Be and ^{234}Th activity, and having a fining upward grain size distribution. Each of these indicated the presence of an event bed, but over time the signatures were reworked by resuspension and bioturbation.

Grain Size Profiles: After initial flood deposition, the grain size profiles had a fining upward signature (Figure 2-4A), but different processes modified the grain size signature over time. Biodiffusion attenuated the grain size signature produced by the initial flood deposit and the resuspension events, even for the standard model which used a conservative value for $D_{b,max}$ (Figure 2-5B). Over time, the various flood deposits did not leave a discernible signal within the grain size distribution profile, except that reduced concentrations of coarse sediment persisted near the sediment surface for the cases having a thicker initial flood layer (Figure 2-7A-C). For the case where the

resuspension thickness exceeded the flood deposit thickness (Model run 8), the thick active layer quickly mixed the fining upward layer deeper into the bed, which accentuated the fining upward signal in the sediment surface (Figure 2-8A, B).

Beryllium-7 Profiles: For the standard model, the flood bed began as a 0.75cm thick layer of high ^7Be activity. Biodiffusion and resuspension mixed the sediment enriched in ^7Be down to 2cm, though with time the signal decayed according to the ^7Be half-life (Figure 2-4F). The resuspension events maintained a nearly uniform ^7Be activity in the top centimeter of the bed (Figure 2-6). Because the length scale assumed for biodiffusion ($Z_{b,max} = 3$ cm) exceeded the standard model's resuspension thickness (0.46 cm), biodiffusion more effectively mixed ^7Be into the bed than resuspension (Figure 2-5). For the case where a thicker flood deposit was used (Model run 7), the flood deposit was less susceptible to dilution by biodiffusion, because the thicker flood bed had a higher inventory of ^7Be (Figure 2-7). For the case that used a thick active layer (Model run 8), physical mixing during resuspension events mixed the available ^7Be inventory fairly uniformly over the top 2.5cm (Figure 2-8D).

Thorium-234 Profiles: The ^{234}Th profile for the standard model also began as a 0.75cm thick layer of high activity that was then mixed down to 2cm, and decayed with time (Figure 2-4F). Unlike the ^7Be , however, resuspension events repeatedly enriched the ^{234}Th inventory of the bed. The resuspension events in the standard model maintained a 1cm layer of high ^{234}Th activity. However, for the model run that did not include resuspension (Model run 4), ^{234}Th decayed very quickly due to its short half-life (Figure 2-6). For the case where a high biodiffusion coefficient was used (Model run 3), the

mixing process increased the penetration depth of ^{234}Th to more than 4cm deep (Figure 2-5). Model run 7 imposed a thicker flood deposit, creating a thicker surface layer of high ^{234}Th (Figure 2-7). The model run that assumed a thick active layer (Model run 8) produced a 2.5cm layer of very high ^{234}Th activity (Figure 2-8).

2.6.3 Synthesis of Event Bed Tracer Metrics

Event bed layers are often categorized using the penetration depth, surface activity, and bed inventory of tracers. These metrics were described and analyzed for the radioisotopes ^7Be and ^{234}Th in this model. The penetration depth and surface activity help determine whether an event bed was deposited recently, while the bed inventory gives a longer record of sedimentary processes. The penetration depth can give an indication of the thickness of an event layer, but with time, physical and biological mixing can increase the penetration depth (e.g. Model runs 3, 8). Surface activity is highest upon initial deposition and then decreases due to decay and dilution. High surface activities and uniform or only moderately lower activities below the surface indicate an event bed (e.g. Figure 2-4F, H), even if some dilution has occurred. The bed inventory indicates the relative inputs of tracers into the seabed in the recent past.

The utility of a radioisotope to identify an event layer is highly dependent on the half-life of the tracer, mixing within the seabed, erosion, and the detector used. Under weak mixing conditions, an event layer may be detected based on geochronology for months after deposition, for as long as 4-5 half-lives of ^7Be and ^{234}Th (e.g. Model run 2). However, under strong mixing conditions, an event layer could be indistinguishable on

the order of weeks (e.g. Model run 3), and could look like the product of continuous deposition. Erosion can also remove a part or the entire signal of an event bed. The three metrics listed above are very helpful in determining event bed layers, but detection of an event bed can be limited in time by short half-lives of tracers and mixing within the seabed.

2.7 Summary and Future Work

An exciting capability has been added to the CSTMS, the ability to account for reactive terms to represent tracers including particulate matter and porewater geochemistry. This capability enhances the utility of the model for many important issues within marine sciences including contaminant transport, geochemical cycling, and harmful algal blooms. This chapter highlighted the application of a model for calculating geochronological profiles in the sediment bed and explained the approach used to represent short half-life radioisotopes ^7Be and ^{234}Th . We implemented this in a one-dimensional (vertical) model of sediment suspension and the seabed to provide a proof-of-concept example of the model application that used idealized flood and storm scenarios. The sensitivity of calculated vertical profiles of radioisotopic tracers to the biodiffusion coefficient and resuspension intensity were demonstrated for a model application that included deposition of a thin flood bed and later physical reworking by resuspension. Analysis of the model runs showed:

- (1) In the standard model, flood deposition was evidenced by a layer having a fining upward grain size profile and high activities of ^7Be and ^{234}Th . This event bed was

reworked by bioturbation and resuspension which attenuated the fining upward signal. Within 5 half-lives, the ^7Be and ^{234}Th decayed below their detection limit.

- (2) The intensity of bioturbation impacted the persistence of the flood event bed. When bioturbation was neglected, the flood event bed persisted for longer, maintaining the fining upward grain size profile as well as a discrete layer of high radioisotope activity. Using a high bioturbation coefficient of $25 \text{ cm}^2 \text{ yr}^{-1}$, however, the flood event bed would be quickly destroyed as the grain size signal was attenuated, and the ^7Be and ^{234}Th mixed into the bed which diluted the activity of both radioisotopes near the sediment surface.
- (3) The intensity of resuspension impacted the enrichment of ^{234}Th into the bed. For the case that did not include resuspension, there was no enrichment of ^{234}Th after the initial flood deposit. As resuspension intensity and sediment availability increased, the amount of sediment resuspended from the bed increased, providing more enrichment of ^{234}Th . Resuspension could produce extremely intense physical mixing in the sediment surface layer, which enhanced the fining upward grain size signal in a storm event bed that had nearly uniform radioisotope activities.
- (4) The thickness of the initial flood deposit impacted the persistence of the flood event bed. The thinner flood layer initially deposited less fine and medium sediment and ^7Be than the standard model, providing less fine sediment at the surface so that bed armor limited later storm erosion. For the case of a thicker flood deposit, the availability of more fine and medium sediment increased resuspension depths so that the flood layer persisted longer in the record.

Now that the sediment transport model has been enhanced to include reactive tracers, it can be used to explore the behavior of geochronological tracers in coastal environments and test hypotheses that have been devised to explain observed patterns. For example, future model applications could include (1) evaluating the behavior of a system under more realistic resuspension scenarios by utilizing timeseries of waves and currents, (2) considering cross-shelf and along-shelf patterns of geochronological tracers using two- or three-dimensional models, and (3) accounting for effects such as grain size-dependent sorption and variations in the activities of source sediment.

Tables

Table 2-1: Model Sensitivity Test Parameters

Sensitivity tests and parameters for each model run. The active layer thickness was limited to 5mm in runs 1-7, but reached 1.8 cm in run 8.

Run	Biodiffusion Coefficient (cm ² yr ⁻¹)	Peak Bed Stress (Pa)	Peak Eroded Depth (cm)	Flood Layer Thickness (cm)
1 (Standard Model)	1	2.7	0.46	0.75
2	0	2.7	0.4	0.75
3	25	2.7	0.46	0.75
4	1	0	0	0.75
5	1	6	0.56	0.75
6	1	2.7	0.4	0.38
7	1	2.7	0.61	1.51
8	1	2.7	0.71	0.75

Table 2-2: Standard Model and Sensitivity Test Results

Surface activities, bed inventories, penetration depths and detection timescale after deposition (detection limit=0.1 dpm/g) for ^7Be and ^{234}Th for all model runs. See text for methods used to calculate these values, and Table 2-1 for conditions used in each model run. Days 63, 90, and 200 chosen for comparison to represent times when no sediment was resuspended, but cover a range of half-lives since time of deposition of ^7Be .

	Day	Run 1	Run 2	Run 3	Run 4	Run 5	Run 6	Run 7	Run 8
^7Be Surface Activity (dpm/g)	63	1.3	1.64	0.47	1.37	1.25	0.68	2.06	1.22
	90	0.85	1.16	0.28	0.9	0.82	0.44	1.39	0.8
	200	0.17	0.28	0.05	0.18	0.16	0.09	0.29	0.16
^7Be Bed Inventory (dpm/cm ²)	63	0.89	0.89	0.89	0.89	0.89	0.45	1.78	0.89
	90	0.63	0.63	0.63	0.63	0.63	0.31	1.25	0.63
	200	0.15	0.15	0.15	0.15	0.15	0.08	0.3	0.15
^7Be Penetration Depth (cm)	63	1.92	1.21	5.16	1.84	1.95	1.58	2.61	3.24
	90	1.95	1.09	5.25	1.87	1.98	1.58	2.64	3.23
	200	1.38	1.02	0	1.33	1.41	0	2.18	0.46
^7Be Detection Timescale		4.5	5.4	2.9	4.6	4.5	3.7	5.3	3.8
^{234}Th Surface Activity (dpm/g)	35	3.4	3.51	2.57	1.27	3.55	2.99	3.88	3.72
	90	3.52	3.6	2.7	0.23	3.66	3.21	3.9	3.75
	200	0.42	0.51	0.2	0.01	0.45	0.39	0.48	0.51
^{234}Th Bed Inventory (dpm/cm ²)	35	2.03	1.87	3	0.76	2.22	1.73	2.81	4.53
	90	2.18	1.91	3.44	0.16	2.41	1.94	2.72	4.69
	200	0.31	0.27	0.49	0.01	0.35	0.28	0.37	0.66
^{234}Th Penetration Depth (cm)	35	1.78	1.09	4.64	1.48	1.86	1.59	2.24	3.35
	90	1.94	1.08	5.56	1.21	1.99	1.9	2.23	3.49
	200	1.7	1.04	4.93	0	1.83	1.59	1.88	3.21
^{234}Th Detection Timescale		5.2	5.7	4	5.1	5.3	5.1	5.4	5.5

Figures

Figure 2-1: Comparison of Observed ^7Be Activity and Modeled Sediment Deposition
Examples of (A) typical observational data, ^7Be activity, and (B) model estimates on the Waipaoa River shelf, New Zealand (Kniskern *et al.*, 2012; Moriarty *et al.*, 2012).

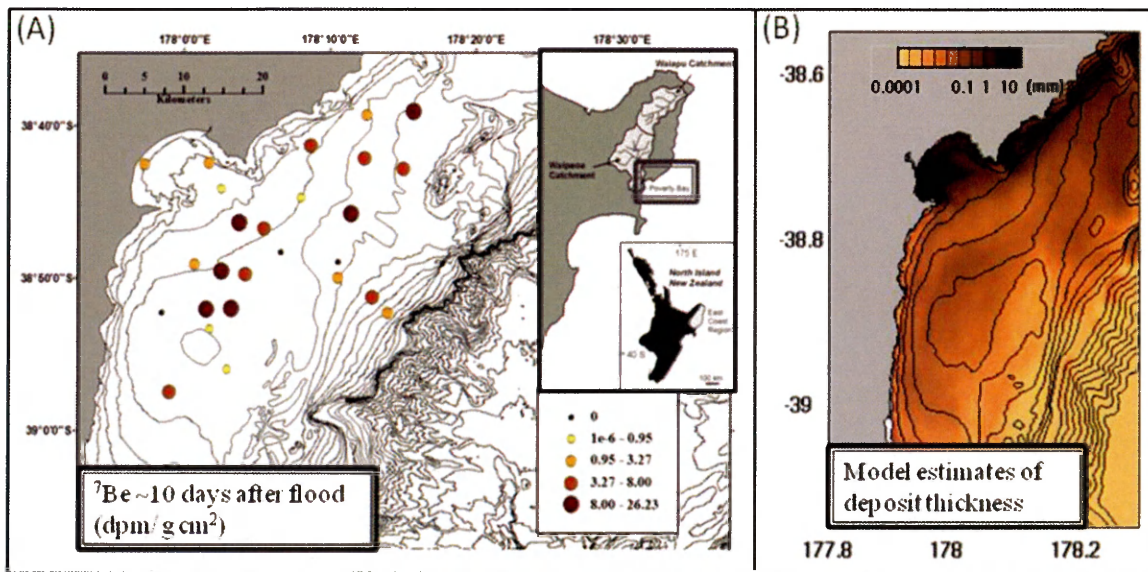


Figure 2-2: One-dimensional Model Illustration

(A) One-dimensional sediment bed model illustration (Warner *et al.*, 2008). Water column layers (blue and white) overlie seabed layers (brown) of variable thickness. (B) Schematic of the combined CSTMS sediment transport and geochronology model.

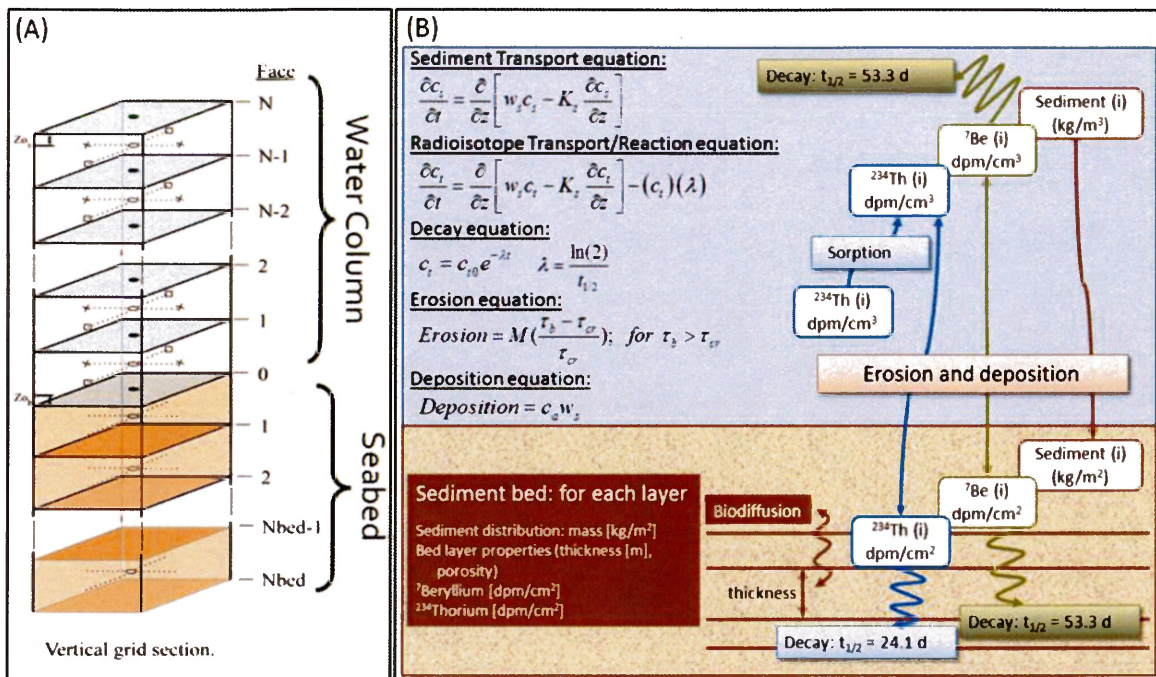


Figure 2-3: Standard Model Timeseries

Time series of (A) bed stress, (B) depth-integrated suspended sediment concentrations (see legend), (C) sediment bed thickness relative to the initial bed, (D) radioisotope bed inventories, and (E) radioisotope surface activities for the one-dimensional standard model. This shows the first 200 days of the 365 day model run; conditions were quiescent between days 130 and 365. Vertical lines mark days 63, 90, and 200 of the model run referenced in Table 2-2.

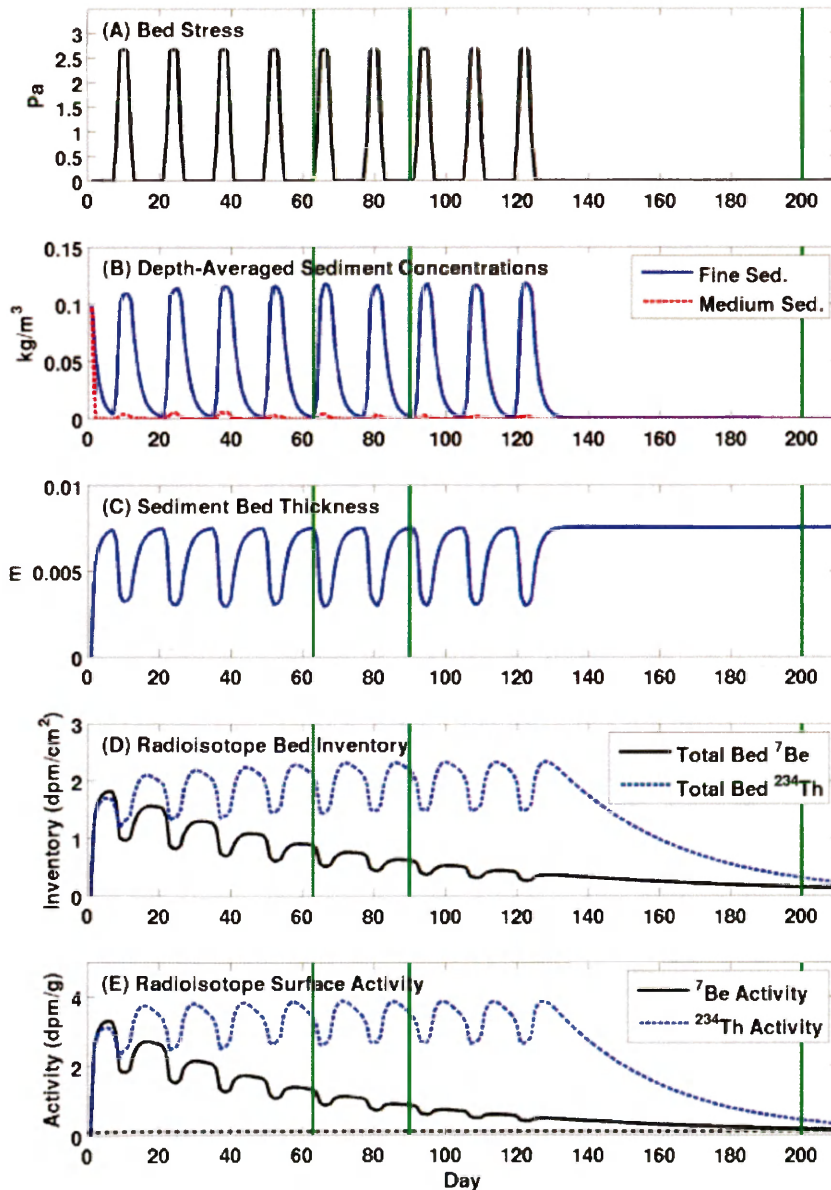


Figure 2-4: Profiles for the Standard Model

Vertical profiles of sediment bed grain size distributions (A-E) and radioisotope activities (F-J) on days 7, 25, 49, 140, and 240 for the standard model. Day 7 shows the initial flood deposit, day 25 was the peak of a resuspension event, day 49 was the peak of a deposition event, and days 140 and 240 show profiles during the quiescent period that followed resuspension events. The solid black lines represent the bed surface, the thick dotted lines represent three centimeters deep in the bed and the thin dotted lines show the interfaces between individual bed layers. The initial bed height is defined as $z_{bed} = 0$.

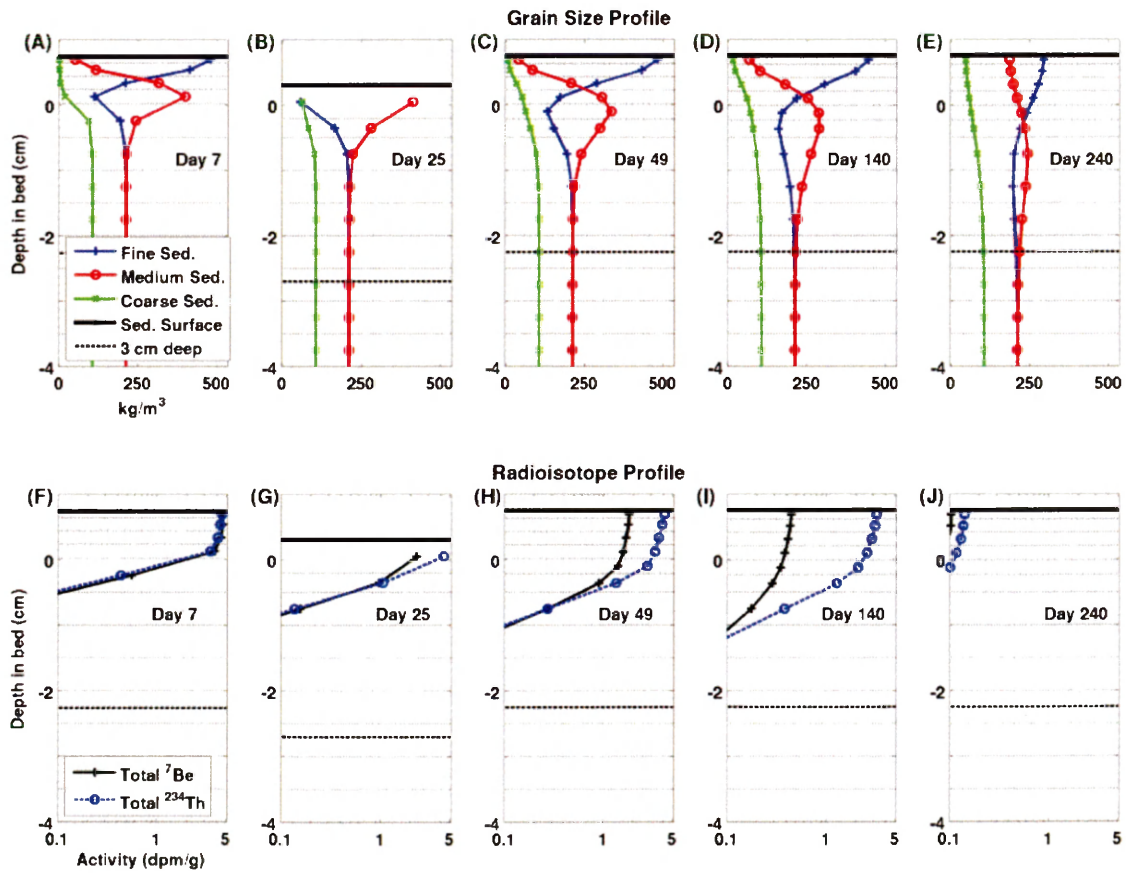


Figure 2-5: Profiles Varying by the Biodiffusion Coefficient (D_b)

Grain size distributions (A-C) and radioisotope profiles (D-F) calculated that (A,D) neglected biodiffusion (Model run 2), (B,E) used $D_{b,max}=1\text{ cm}^2\text{ yr}^{-1}$ (standard model, Model run 1), and (C,F) used $D_{b,max}=25\text{ cm}^2\text{ yr}^{-1}$ (Model run 3). Top row of grain size distribution shows results on day 100 while bottom row shows day 240. Top row of radioisotope profiles show results on day 20 while bottom row shows day 100. Horizontal lines are as described in Figure 2-4, the sediment-water interface is 0 cm.

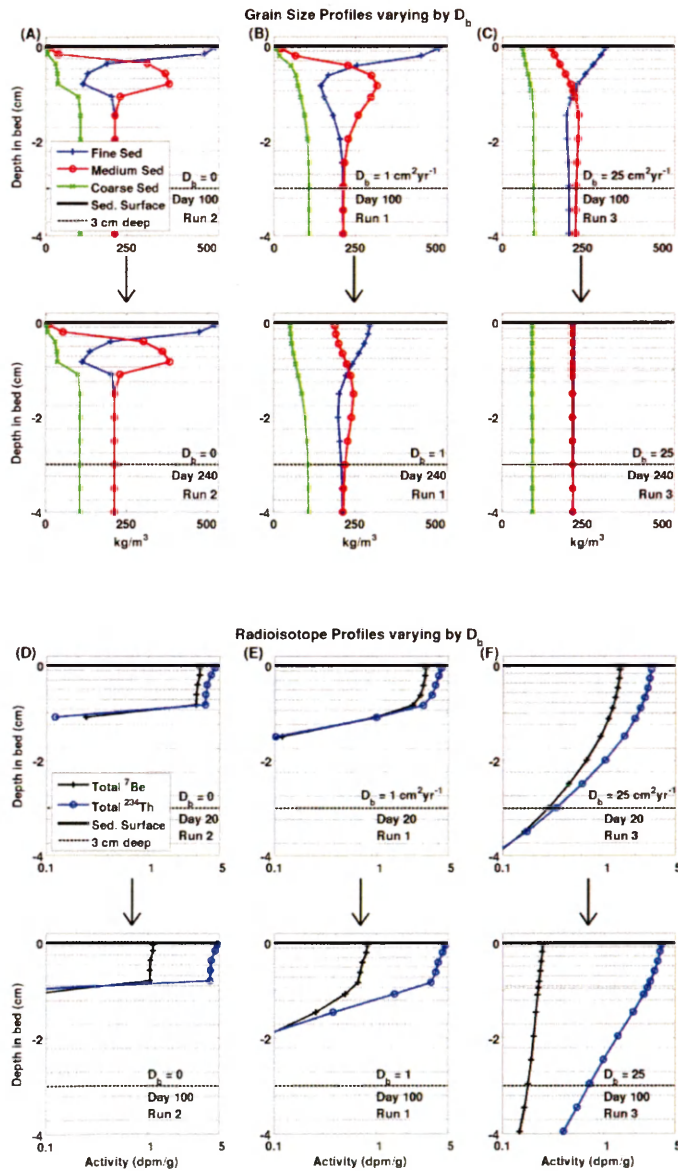


Figure 2-6: Profiles Varying by Resuspension Intensity

Grain size distributions (A-C) and radioisotope profiles (D-F) that (A,D) had no resuspension (Model run 4), (B,E) had a resuspension depth of 0.46 cm (standard model, Model run 1), and (C,F) had a resuspension depth of 0.6 cm (Model run 5). Top row of each panel shows results on day 20, after the first resuspension event while bottom row shows day 100 after several resuspension events. Horizontal lines are as described in Figure 2-4, the sediment-water interface is 0 cm.

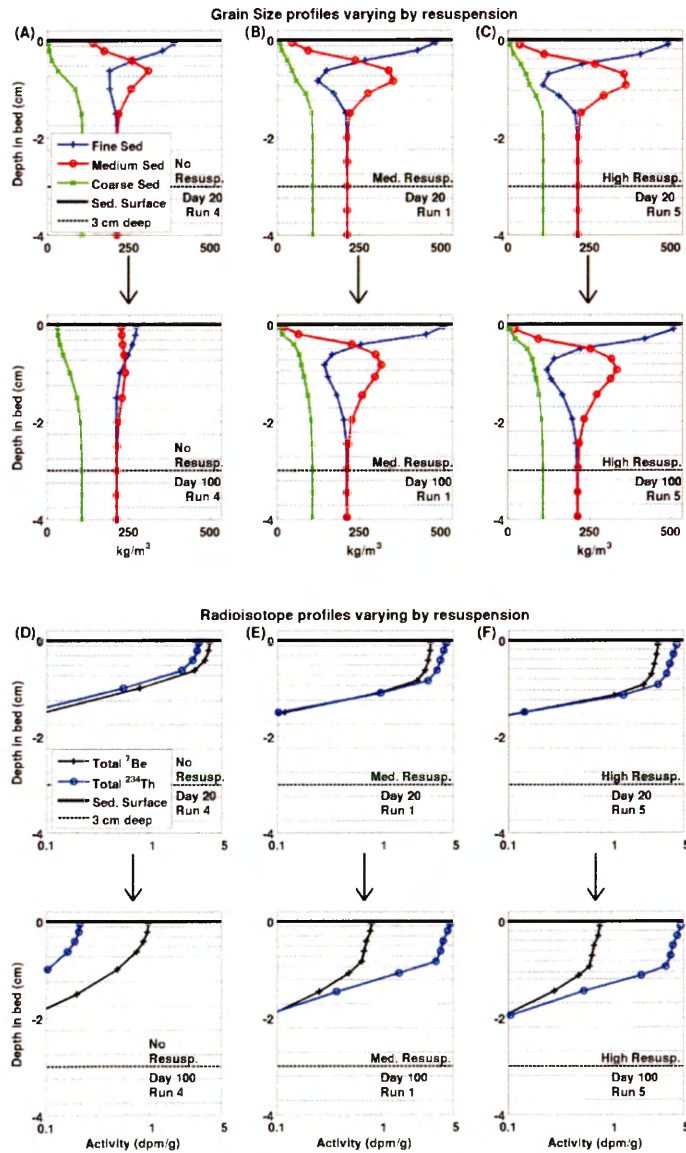


Figure 2-7: Profiles Varying by Flood Deposit Thickness

Grain size distributions (A-C) and radioisotope profiles (D-F) that (A,D) had a flood deposit thickness of 0.38 cm (Model run 6), (B,E) had a flood deposit thickness of 0.75 cm (standard model, Model run 1), and (C,F) had a flood deposit thickness of 1.5 cm (Model run 7). Top row of each panel shows results on day 20, after the first resuspension event, while bottom row shows day 100. Horizontal lines are as described in Figure 2-4; however, in this figure the thick dotted lines are the original sediment-water interface. The sediment-water interface is 0 cm.

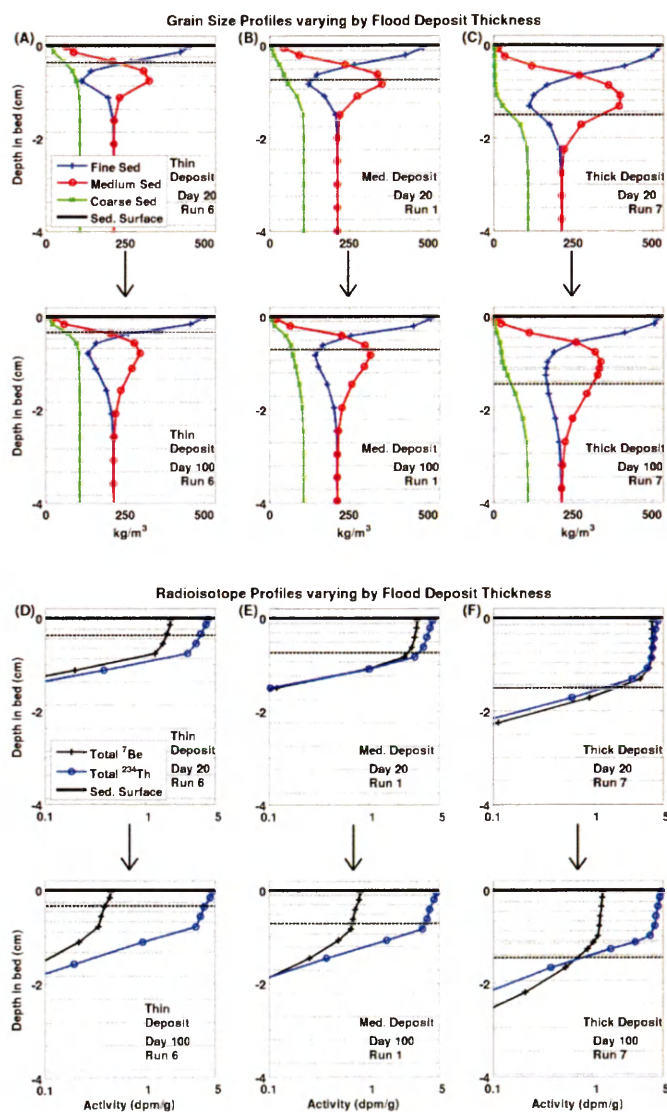
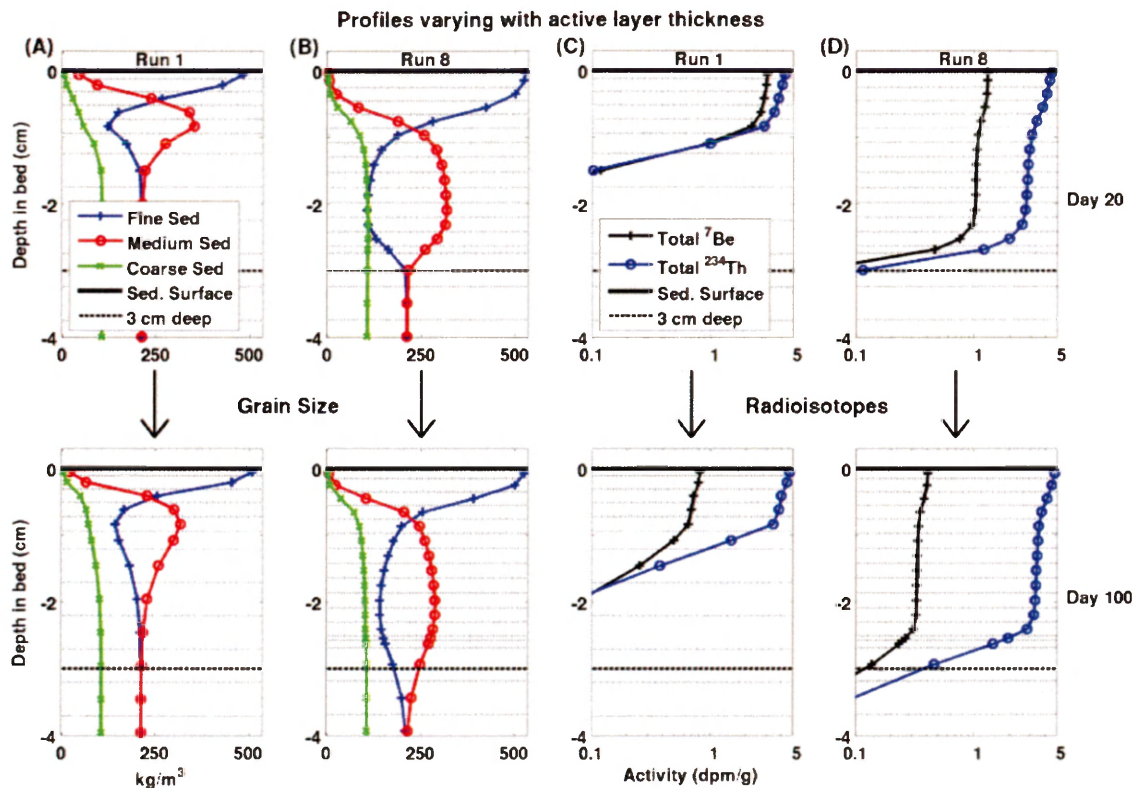


Figure 2-8: Profiles Varying by the Active Layer Thickness

Grain size (A-B) and radioisotope (C-D) profiles calculated for Model run 1 (A,C) and Model run 8 (B,D) on days 20 (top) and 100 (bottom). Model run 1 was the standard model, and Model run 8 had a thick active layer. Day 20 marks the point after the first resuspension event and day 100 marks the point after seven resuspension events. Black horizontal lines are as described in Figure 2-4, the sediment-water interface is 0 cm.



CHAPTER 3: Comparative Study of Modeled and Observed Radioisotope Profiles

3.1 Abstract

Sediment transport models that represent flood and storm sedimentation for coastal areas typically estimate grain size patterns and deposit thicknesses and are therefore disconnected from field data that rely on short half-life radioisotope tracers to infer event bed character. Interpreting field data based on radioisotopes presents challenges that stem from the tracers' source terms, as well as confounding sediment transport processes including suspended transport and physical and biological mixing. We use a numerical sediment model capable of representing ^7Be and ^{234}Th profiles in the seabed to develop a quantitative tool that can be used to reconcile model estimates with observational studies, and interpret field studies. A one-dimensional (vertical) model that includes two sediment classes and reactive tracers to represent ^7Be and ^{234}Th was configured to represent a 50-m deep site offshore of the Mississippi delta and subjected to periods of realistic flood deposition and storm resuspension. The model estimates were then compared to field observations from the northern Gulf of Mexico from April and October, 2000. The model reproduced radioisotopic profiles that were similar to field observations, but the simulated profiles of ^7Be and ^{234}Th could be directly related to the flood and storm sequences used as model input. The model-estimated profiles were sensitive to the timing of ^7Be input, phasing of wave and current energy, and

bioturbation. Riverine deposition increased the activities and inventories of both radioisotopes, while resuspension increased the activity and inventory of ^{234}Th only. Riverine deposition and resuspension typically produced fining upwards layers of grain size. Erosion events removed radioisotopes from the bed surface, and winnowed the more easily suspended fine sediment from the bed.

3.2 Introduction and Motivation

The geologic record contains many examples of “event beds” including storm beds that record erosion and subsequent deposition during energetic conditions, and flood beds that preserve a layer of rapid deposition of riverine material (Wheatcroft and Drake, 2003). An event bed is deposited during a short interval of time and differs from the ambient sediment (Wheatcroft, 1990). Immediately upon deposition, an event bed can be subjected to a number of processes, including chemical diagenetic processes, bioturbation, and physical reworking such as resuspension by energetic waves and currents or burial by subsequent sediment deposition. The degree to which an event bed may be preserved varies with the intensity of bioturbation, the thickness of the surface mixed layer, the thickness of the deposited layer, the sediment accumulation rate, and episodicity of deposition and reworking (Nittrouer and Sternberg, 1981; Wheatcroft, 1990; Wheatcroft and Drake, 2003). The surface mixed layer is the layer adjacent to the sediment-water interface wherein biological and physical mixing of sediment occurs (Wheatcroft and Drake, 2003). Bioturbation, defined as modification of the seabed or displacement of sediment particles by organisms, can destroy the signal of a layer

particularly when the mixed layer is thick or bioturbation is intense (Wheatcroft *et al.*, 1990). Conversely, the thicker the deposited layer, the greater chance it has to have some portion preserved. An event layer has an increased chance for preservation after it has been buried below the depth of the surface mixed layer (Wheatcroft, 1990). More rapid accumulation and frequent episodic deposition also improves the chances of a layer being preserved (Wheatcroft and Drake, 2003).

Small mountainous river systems often drain active margins, for example the Eel River in northern California, and the Waipaoa River on the North Island of New Zealand. Mud beds have been found on the continental shelves offshore of these examples where the seabed contains terrestrially derived sediment. Deposition of sediment on these mud beds is highly dependent on delivery by floods. If thick episodic flood beds are deposited frequently, there is an increased chance that a portion of a flood event layer will be preserved and not be destroyed by bioturbation or mixing (Wheatcroft and Drake, 2003).

Conversely, large rivers such as the Mississippi and Po River often drain passive margins. Floods on these systems can persist for weeks or months, and they typically carry a high sediment load commensurate with their large freshwater discharge. Sediment accumulation offshore of these rivers may therefore be somewhat continuous throughout the year or wet season. Because of this, a discrete flood event layer is typically not found near large rivers. Deposition offshore of these large rivers is typically evidenced by high radioisotope bed inventories and high porosity fine-grained sediments at the seabed surface (Corbett *et al.*, 2004).

A storm bed can be formed when significant amounts of sediment are mobilized (Wiberg, 2000), and is diagnostic of energetic flow conditions with little or no apparent input of new sediment. It may appear as a fining upward layer overlaying a coarse lag layer. The lag layer represents an erosional surface created during the increasing and peak phases of the storm, while the fining upward sequence represents redeposition of material as conditions became less energetic (Reed *et al.*, 1999; Wiberg, 2000).

Bioturbation results from a number of different processes, including organism locomotion on the seabed surface and deposit feeding, which dominates the biological mixing in the seabed (Wheatcroft *et al.*, 1990). Bioturbation due to a variety of animal activities is nearly ubiquitous in marine sediments (Wheatcroft and Drake, 2003).

Bioturbation is often quantified using a biodiffusion coefficient, D_b . In marine environments, D_b varies considerably depending on water depth, geographical location, and properties of the tracer used to infer it, and values in the literature range from 10^{-2} to $10^2 \text{ cm}^2 \text{ y}^{-1}$ (Boudreau, 1994; Wheatcroft *et al.*, 2007). These values can be constrained for continental shelves around the world to typically $10\text{-}100 \text{ cm}^2 \text{ y}^{-1}$ (Wheatcroft and Drake, 2003). As described later, short half-life radioisotope activity profiles provide a means of estimating a biodiffusion coefficient for a particular site.

Radionuclides that are highly particle-reactive, such as Beryllium-7 (^7Be), Thorium-234 (^{234}Th), and Lead-210 (^{210}Pb), have been quite useful as tracers of particle transport, particularly sediment deposition, resuspension, and mixing (Baskaran and Santschi, 1993). Radioisotopic tracers having short half-lives ($t_{1/2}$), such as ^7Be and ^{234}Th , have been widely used by marine geologists to characterize sediment transport

pathways over short time scales (days-months). The half-lives of ^7Be and ^{234}Th are 53.3 days and 24.1 days, respectively. Lead-210, having a longer half-life of 22.3 years, has also been used to determine sediment accumulation over time scales of decades to a century.

Beryllium-7 is formed in the atmosphere and delivered to the Earth's surface by wet and dry deposition. In the coastal ocean, especially in close proximity to a river, ^7Be provides a tracer for identifying riverine sediment (Baskaran *et al.*, 1997; Sommerfield *et al.*, 1999). Its association with riverine sediment makes ^7Be highly useful for characterizing sediment mixing and depositional processes on continental shelves. Canuel *et al.*, (1990) compared new and residual ^7Be inventories within the seabed at an 8 m site in a semi-enclosed coastal marine basin on the North Carolina continental shelf to determine whether sediment deposition or erosion had occurred in recent months.

Thorium-234 is a short-lived radioisotope produced in the water column by the in-situ decay of its parent, Uranium-238, which is conservative in seawater. Thorium-234 is particle reactive and is a tracer of sediment resuspension in saline water. The short half-life of ^{234}Th is ideal for studying fast biologically and physically mediated processes over short time-scales (Waples *et al.*, 2006). This radioisotope has also been widely used in a variety of environments to study transport of sediment and organic matter, particle cycling, and sediment dynamics (Waples *et al.*, 2006). For example, Aller and Cochran, (1976) studied the mixing and horizontal flux of ^{234}Th in the sediment bed in Long Island Sound.

Profiles of short-lived radioisotopes such as ^7Be and ^{234}Th can be used to estimate steady-state sediment accumulation rates or to quantify bioturbation within the seabed. Under dominantly depositional conditions, McKee *et al.*, (1983) estimated the steady-state sediment accumulation rate (S) using ^{234}Th profiles and the following equation:

$$S = \frac{\lambda z}{\ln(A_0 / A_z)} \quad (1)$$

where A_0 was the activity of the radionuclide near the sediment surface, A_z was the activity of the radionuclide at depth z , and λ was the decay constant of the radionuclide ($\ln(2)/t_{1/2}$). If mixing was present, the result from Equation 1 would overestimate the true accumulation rate. Conversely, for a location where mixing overwhelms accumulation, ^7Be was used to quantify bioturbation with a biodiffusion coefficient, D_b (e.g. Aller and Cochran, 1976; Nittrouer *et al.*, 1984):

$$D_b = \lambda \left[\frac{z}{\ln(A_0 / A_z)} \right]^2 \quad (2)$$

Equation 2 would be appropriate where sediment accumulation was negligible compared to vertical mixing, i.e. $S^2 \ll 4D_b\lambda$. An Advection-Diffusion Equation should be applied when biodiffusion, sediment accumulation and radioactive decay are all significant (Nittrouer *et al.*, 1984):

$$S = \frac{\lambda z}{\ln(A_0 / A_z)} - \frac{D_b}{z} (\ln(A_0 / A_z)) \quad (3)$$

Equation 3 adjusts the accumulation rate that would result from Equation 1 by adjusting for mixing by using an estimated or assumed biodiffusion coefficient for the particular environment studied.

Patterns of grain size on the seabed provide another way to identify event beds. Flood deposits may appear as a fine grained layer that overlies coarser layers of ambient sediment. On the Eel Shelf, Drake (1999) identified a flood layer containing predominantly small particles ($<20\mu\text{m}$), with less than 10% sand. This layer also coarsened slightly with depth in the sediment bed, with the explanation being that the largest particles discharged by the flood settled more quickly. After initial deposition, processes of erosion, bioturbation and deposition of coarser sediment can also modify a flood layer over time. Over a 14 month period, Drake (1999) found that bioturbation and introduction of coarse shelf sediment increased the thickness of the apparent flood layer from 1 to 4cm and caused the seabed surface to become inversely graded (i.e. coarsened upward) compared to the normal fining upward grading seen in the initial flood layer.

X-radiographic images show the relative bulk density of sediment within the seabed, and can also be useful for identifying flood layers, estimating their thicknesses, and evaluating the qualitative influence of biological or physical mixing in the seabed. A sediment layer that is unconsolidated and has a higher water content would be easily distinguishable from an underlying consolidated sediment layer because it would appear as a less dense layer overlying a dense layer. Layers having reduced density, along with the presence of laminations and/or absence of bioturbation and biological organisms suggest recent deposition of flood sediment. Signals that depend on layers seen in X-radiographs are more quickly destroyed by bioturbation than those that are defined by grain size (Wheatcroft and Drake, 2003) and therefore these signals may have a limited time to be recognized within X-radiographs.

Sediment erosion is challenging to characterize from the sediment record. While deposition obviously adds sediment to the seabed, erosion removes sediment and while it may leave a coarsened lag layer, provides little evidence that can be used to estimate the amount of erosion that has occurred. However, some studies have quantified erosion using measurements of the ^7Be inventory at the beginning and end of a time period. The measured ^7Be inventory is separated into residual and new components, while correcting for radioisotope decay (Canuel *et al.*, 1990; Palinkas *et al.*, 2010). If the new inventory at the end of time period is less than the original inventory at the beginning of the time period, then erosion has occurred, and the amount of sediment removed can be calculated and used to estimate the thickness of the eroded layer.

A number of tripod based measurements have been used to determine suspended sediment concentrations and seabed response to deposition and erosion. Suspended sediment concentrations can be measured using pumped water samples, but can also be measured in-situ by acoustic and optical instruments that can be left in the water for weeks or months at a time. These instruments include, but aren't limited to; LISST (Laser In-Situ Scattering and Transmissometry), OBS (Optical Backscatter Sensor), and ADV (Acoustic Doppler Velocimeter) (e.g. Fugate and Friedrichs, 2002). Typically in conjunction with a means of extrapolating these point measurements of sediment concentration to a depth-integrated volume of sediment suspended, these measurements can be used to infer resuspension depths (Wiberg *et al.*, 1994). Bed altimetry has also been used over short timescales to estimate changes in the height of the sediment - water interface. Acoustic altimeters have been used on bottom tripods in conjunction with

other acoustic or optical instruments, such as those listed above. Acoustic altimeters can take measurements on the order of minutes to hours and therefore can resolve erosion and deposition for short term resuspension events (Palinkas *et al.*, 2010).

Numerical sediment transport models provide another way to estimate resuspension, erosion, and deposition of sediment on continental shelves. Models traditionally solve the equations for conservation of mass of suspended sediment, and then relate suspended sediment flux convergences and divergences to deposition and erosion of sediment (Harris and Wiberg, 2001; Warner *et al.*, 2008). Very rarely, however, have sediment transport models included terms in the sediment bed model to account for bioturbation (see Harris and Wiberg, 1997), and the models typically estimate sediment grain size distributions, but not other sediment properties like radioisotope profiles. For example, Xu *et al.*, (2011) developed a three-dimensional numerical sediment transport model for the Gulf of Mexico and used it to estimate depositional thicknesses of Mississippi River sediment on the continental shelf. By way of model validation, Xu *et al.*, (2011) compared these estimates of sediment deposition to evidence derived from radioisotopic studies from ^7Be and ^{210}Pb . However, because the model did not directly model radioisotopes, these comparisons were difficult to interpret.

Previous attempts to explore the issues of bioturbation and radioisotope activity using numerical models include a one-dimensional (vertical) sedimentation-bioturbation model (Bentley and Sheremet, 2003) and a two-dimensional (horizontal) gravity flow model (Ma *et al.*, 2010). Bentley and Sheremet, (2003) presented a model for preservation of sedimentary fabric under deposition and bioturbation, but their model

assumed negligible physical mixing. The authors defined and analyzed the “preservation quotient”, the fraction of the original unit volume that retained its primary depositional fabric, for both depth-constant and depth-dependent bioturbation of sediments. Ma *et al.*, (2010) used a two-dimensional model to represent depth-integrated gravity-driven sediment transport and resultant deposition on the Waiapu shelf, New Zealand. The deposit thickness after ten discrete time segments was multiplied by a decay factor to estimate a relative ^7Be activity within the continental shelf flood deposit. The authors then compared this relative activity to ^7Be observations on the shelf to demonstrate that the model reproduced the observed depositional patterns.

Neither of these modeling efforts directly estimated the transport and behavior of radioisotopes, however. The objective of this study is to directly account for reactive tracers within a sediment transport model to provide a method for estimating the distribution of radionuclides within coastal sediment that will facilitate a direct comparison between the model and field data. As a case study, I use the model to represent a location offshore of the birdfoot delta of the Mississippi River where profiles of short – lived radioisotopes have previously been analyzed.

3.3 Example from the Gulf of Mexico

I apply the numerical model to evaluate transport processes operating offshore of the Mississippi Delta. As a basis for the case study, we consider conditions at a 50 m deep site offshore of the Southwest Pass of the Mississippi River, termed the ‘near river’ site by Corbett *et al.*, (2004) (Figure 3-1). This site is highly influenced on a yearly basis

by freshwater and sediment discharge from the Mississippi River, is impacted by wave reworking throughout the majority of the year, and the sediment bed consists of predominantly mud. Corbett *et al.*, (2004) obtained radioisotope activity profiles of ^7Be and ^{234}Th with depth in the sediment bed at this site for April and October, 2000 (Figure 3-2). Analysis of sediment cores indicated that bioturbation was not an important mixing mechanism at this site, based on X-radiograph data and lack of macro-fauna obtained during core collection.

Corbett *et al.*, (2004) related differences in the sediment bed profiles and inferred depositional rates from each sampling period to seasonal variation in conditions in the northern Gulf of Mexico. Deposition rates based on ^7Be profiles were estimated to be 1.5 cm/month in April, 2000 and 3.0 cm/month in October, 2000. The time period from April to October was characterized as a period having initially high river discharge which decreased with time, a high amount of sediment deposition, but low wave energy (Figure 3-3A, B). In October, 2000, high inventories of ^7Be were attributed to spring and summer sediment deposition and ^{234}Th inventories were explained by increased wave energy at the end of the time period (Figure 3-2B). In contrast, the period from around October to April was characterized by initially low river discharge which began to increase in December, and a high amount of wave energy (Figure 3-4A, B). Inventories of ^7Be and high surface activities in April, 2000 reflected recent river sediment deposition, but the activity deeper in the bed was most likely relict from the previous season (Figure 3-2A). The April profiles had relatively high inventories of ^{234}Th attributed to resuspension from large waves during the winter and fluvial sediment

deposition in the early spring. Estimated errors in Figure 3-2 for ^7Be were approximately 10-20% for the near surface samples and approximately 50-75% for the deeper samples. Estimated errors in Figure 3-2 for ^{234}Th were approximately 5-10% for the near surface samples and approximately 25-50% for the deeper samples (Corbett, personal communication, April 2014).

In this paper, we use a numerical model that includes both sediment transport and geochronology to reproduce the observed radioisotopic profiles. More so than with field data, the model-generated profiles can be directly related to the known forcing conditions such as river discharge, erosion rates, and bioturbation.

3.4 Methods

The Community Sediment Transport Modeling System (CSTMS) provides a sediment-transport module within the Regional Ocean Modeling System (ROMS), (Warner *et al.*, 2008). The CSTMS calculates the transport of a user – specified number of sediment classes that are treated as particulate tracers and exchange particulate mass between the water column and the sediment bed via erosion and deposition (Warner *et al.*, 2008). To this, we have added reactive tracers to store the concentrations of geochemical constituents that are associated with a sediment class (see Chapter 2). For this study, these reactive tracers represent short-lived radioisotopes ^7Be and ^{234}Th so that the model can calculate the sediment activities of each radioisotope.

As described in Sherwood *et al.*, (in prep.), the model included biodiffusion that mixed particulate matter across bed layers assuming that the diffusive flux was

proportional to the concentration gradient with the constant of proportionality being the biodiffusion coefficient, D_b . The model assumed that the intensity of biodiffusion was largest near the sediment – water interface, and $D_b = D_{b,max}$ for $z_{b,k} < Z_{b,max}$, where the model input parameter $Z_{b,max}$ specified the vertical scale of the mixed layer. The biodiffusion coefficient then decayed linearly until it reached a small value specified as $D_{b,min}$, at depths below twice $Z_{b,max}$.

A one-dimensional (vertical) model that represented sediment transport and radioisotope activities was implemented to represent a 50 meter deep site on the Mississippi River shelf offshore of Southwest Pass, the main distributary of the Mississippi River (Figure 3-1). The modeled time periods represented conditions that preceded Corbett *et al.*,’s (2004) sampling periods. Wave timeseries for October 1999 through October 2000 were obtained from the National Oceanic and Atmospheric Administration’s National Data Buoy Center (NOAA NDBC). Hourly significant wave height and dominant wave period data were downloaded for the closest buoys to the study site, buoys 42040 and 42007, both located east of the Mississippi Birdfoot Delta. A constant wind stress of 15 m/s was applied in order to force the currents in the model for the duration of both model runs.

The hydrodynamic model used 30 layers with uniform thickness to represent the 50 meter deep water column, while the sediment bed model used 40 layers that were each initially 0.5 centimeter thick. Over time, the thickness of individual seabed layers varied depending on erosion and deposition, but a constant number of layers (40) were maintained. When deposition caused the surface layer thickness to exceed more than 0.5

cm, it was split into thinner layers and the bottom two layers were joined. When erosion removed the surface layer, the bottom layer was split into two layers following Sherwood *et al.*, (in prep.).

This model used two sediment grain sizes to represent mud. The finer sediment class represented micro-flocs and was assigned a grain diameter of 0.015 mm. The medium sediment class represented macro-flocs and had a grain diameter of 0.063 mm. The fine and medium sizes had settling velocities of 0.1 and 1.0 mm/s and had critical shear stresses of 0.03 and 0.08 Pa, respectively. The model treated these sediment types as “non-cohesive” in that it held the critical shear stresses and settling velocities constant, thus neglecting aggregation, particle breakup, consolidation and swelling. The sediment grains had a density of 2650 kg m⁻³ and the porosity of the sediment bed was 0.8. The bulk density of the sediment bed was reasonable at 1350 kg m⁻³. The erosion rate parameter, M (units of kg m⁻² s⁻¹), relates the erosion rate, E (units of kg m⁻² s⁻¹), to the excess shear stress through the Partheniades equation:

$$E = M \frac{\tau_b - \tau_{cr}}{\tau_{cr}}. \quad (4)$$

The value of M was chosen to equal 5x10⁻⁵ kg m⁻² s⁻¹, so that the model produced erodibility curves of M vs. τ_b that were consistent with Gust Erosion Microcosm experiments conducted in the vicinity of the Mississippi delta by Xu *et al.*, (in prep.).

The model accounted for two short-lived radioisotopes, ⁷Be and ²³⁴Th, and their initial bed profiles were based on those from Corbett *et al.*, (2004; see Figure 3-2). As the model proceeded, there was a continuous source for ⁷Be from newly delivered river sediment. The model assumed that ⁷Be decayed in both the water column and on the

seabed, with a decay constant of $\lambda = 0.013 \text{ day}^{-1}$, and that ^{234}Th on the seabed decayed with a decay constant of 0.029 day^{-1} . For suspended material, however, the model assumed that the water column always had sufficient ^{234}Th to maintain a constant activity of ^{234}Th of 95 dpm/g on suspended sediment. The water column tracer for ^{234}Th was therefore reset to maintain a constant activity on suspended material. This supplied ^{234}Th to the bed during cycles of sediment resuspension and deposition.

Penetration depth has been used to estimate the thickness of an event bed, but can be impacted both not only by the original thickness of the event bed, but also biodiffusion and physical mixing. As the radioisotopic signal decays, the penetration depth associated with an event bed may contract with time. In analyzing model results, the penetration depth (cm) was defined as the depth at which the modeled tracer activity equaled a detection limit of 0.1 dpm/g. It was calculated by finding the sediment bed layers whose activities bracketed the detection limit, and then linearly interpolating the modeled activities to find the depth at which the activity would fall below 0.1 dpm/g.

The surface activity of radioisotopes provides a proxy for inferring recent deposition or resuspension for ^7Be and ^{234}Th , respectively, and is modified by biodiffusion as well as decay (Sommerfield *et al.*, 1999; Corbett *et al.*, 2004). In analyzing model results, surface activities (dpm/g) were estimated as the average activity of the top centimeter of the bed.

Bed inventories of these tracers account for fluvial deposition and resuspension activity over longer timescales than the surface activity, but are modified by radioisotopic decay (Corbett *et al.*, 2004). Bed inventory would be unmodified by biodiffusion,

assuming that the sediment core's length exceeded the tracer's penetration depth. To analyze model results, bed inventory (dpm/cm²) was estimated as the depth-integrated tracer activity within the sediment bed.

Mixing of both sediment and radioisotopic profiles in the sediment bed included biodiffusion. The equation used for the linear decay of the biodiffusion coefficient was

$$D_{b,k} \begin{cases} D_{b,k} = D_{b,max} & z_{b,k} \leq Z_{b,max} \\ D_{b,k} = D_{b,min} + (2Z_{b,max} - z_{b,k}) \frac{(D_{b,max} - D_{b,min})}{Z_{b,max}} & Z_{b,max} < z_{b,k} \leq 2Z_{b,max} \\ D_{b,k} = D_{b,min} & z_{b,k} > 2Z_{b,max} \end{cases} \quad (5)$$

where $D_{b,k}$ represented a biodiffusion coefficient for bed layer k at depth $z_{b,k}$. Note that the coordinate system for the sediment bed model assumed that z_b represented the depth in the sediment bed, so that $z_b = 0$ at the sediment – water interface, and increased with depth. The following parameterizations were chosen for Equation 5. The thickness of the mixed layer was set using $Z_{b,max} = 3$ cm, so that the biodiffusion coefficient (D_b) in this model was set to a maximum value ($D_{b,max}$) in the top 3 cm of the sediment bed, and decreased to a background value below 6 cm. A range of values for $D_{b,max}$ were used to determine which provided profiles that best matched the observations from Corbett *et al.*, (2004).

One challenge with using a one-dimensional (vertical) model of sediment transport was that they typically account for only locally resuspended sediment. This means that though the sediment experiences periods of erosion and deposition, the model conserves sediment mass and at the end of the model run, any eroded material returns to the bed, because the one-dimensional model neglects horizontal flux convergences and

divergences that lead to net erosion or deposition. The study location receives a net of ~1 – 3 cm of new sediment per month, however, and during times of the year appears to supply sediment to downstream locations (Corbett *et al.*, 2007).

A source term was therefore added to represent Mississippi River sediment delivered to the 50 meter deep site. Sediment was added to the model as a surface tracer flux (m/s) at the water surface. As this sediment settled, the seabed became thicker with time. The timing of the surface tracer flux followed that of the observed river sediment discharge at Tarbert Landing, MS, obtained from the U.S. Geological Survey. The flux was scaled so that the accumulation rates (cm month^{-1}) produced modeled radioisotope profiles that matched the profiles from Corbett *et al.*, (2004). Because the surface flux represented fluvial material, it was assumed to carry an activity of 20 dpm/g of ^7Be in the calm model and an activity of 3 dpm/g of ^7Be in the storm model. As described in Chapter 2, the model accomplished this by also adding a surface tracer flux ($\text{dpm/m}^2/\text{s}$) representing ^7Be . The new sediment was assigned a ^{234}Th activity of 95 dpm/g as it settled through the water column.

The one-dimensional model was also modified to include an “erosional” term that operated during times of elevated bed shear stress. To account for removal of sediment from the 50 m site, roughly 50-75% of the suspended material was removed from the model when the bed shear stress exceeded 0.1 Pa. Like the sediment source term, sediment removal was handled using a surface tracer flux. When bed shear stresses did not exceed 0.1 Pa, sediment could be suspended, but it all would be retained in the model grid.

Two standard model scenarios were run; the Standard Calm Period Model (or calm model) and the Standard Storm Period Model (or storm model). Figures 3-3 and 3-4 show the timeseries used as input for these two scenarios, and some of the model – calculated values. Both scenarios included continuous deposition based on Mississippi River discharge, and erosion (sediment removal) under high bed stresses. Though both Standard Models included biodiffusion, different diffusion coefficients were used in order to limit the ^{234}Th penetration depth in the storm model. The calm model represented April to October, 2000, and therefore used river discharge and wave heights measured for that time period (Figure 3-3A, B). The calm model assumed $D_{b,max} = 1 \text{ cm}^2 \text{ yr}^{-1}$. The storm model represented October, 1999 to April, 2000, and used sediment discharge and wave heights measured for that time period (Figure 3-4A, B), but assumed a lower $D_{b,max}$ of $0.5 \text{ cm}^2 \text{ yr}^{-1}$.

Producing profiles similar to those found by Corbett *et al.*, (2004), required that the model find a balance between deposition, biodiffusion and erosion. Because the data from October, 2000 only had ^{234}Th observations for the very surface sample, it was fairly straightforward to match the ^7Be and ^{234}Th profiles from the calm model to those observed by Corbett and colleagues in October, 2000. The main choices made to match the calm model profiles were the parameterization of biodiffusion, the deposition rate used, and the activity of new sediment.

However, the storm model needed to match both the ^7Be and ^{234}Th profiles for April, 2000. Because ^{234}Th has a shorter half-life than ^7Be , it had a shallower penetration depth. Both the biodiffusion coefficient and sediment deposition rate were constrained

by the observed penetration depth of 6 cm for ^{234}Th . Too much sediment deposition or a value for D_b on the order of $25 \text{ cm}^2 \text{ yr}^{-1}$ and the model produced a deeper penetration of ^{234}Th that did not match the observed profile. Sediment erosion was constrained by the observed penetration depth of 10 cm for ^7Be . Too much erosion and the model produced a shallower penetration of ^7Be preventing the modeled profile from matching the observed profile. With some experimentation, it was determined that for the Standard Storm Model, the lower D_b value of $0.5 \text{ cm}^2 \text{ yr}^{-1}$, roughly 7 cm of sediment deposition, and roughly 2 cm of sediment erosion provide results that matched both the observed ^7Be and ^{234}Th profiles.

Additional model runs were completed that varied the biodiffusion coefficient (indicated by $D_{b,max}$) and flood thickness. By comparing results of the standard models to these model runs, we evaluated the sensitivity of penetration depth, surface activity, and bed inventory of each tracer to biodiffusion, resuspension, and flood thickness.

3.5 Results

This section describes the results of the models that represented the calm and storm periods. By imposing a sediment deposition and erosion, and using an input wave timeseries, and an appropriate biodiffusion coefficient, the one-dimensional models produced profiles similar to field observations from Corbett *et al.*, (2004).

3.5.1 Standard Calm Model Run

The Standard Calm Model was run for seven months to represent April, 2000 to October, 2000 (Figure 3-3). During this time, the sediment rating curve at Tarbert Landing indicated that 4.02×10^{10} kg of sediment was transported down-river. Wave heights varied between 0.2 and 2.1 m and averaged 0.73 m; waves were energetic enough to erode sediment at the 50-m site only during four episodes that accounted for about 2% of the time (Figure 3-3B, C). The surface tracer flux for sediment was scaled so that a total of 4.6 cm of sediment was deposited (Figure 3-3F). The timing of sediment supply followed that of the discharge curve, while episodic sediment removals coincided with wave resuspension events (Figures 3-3A, B, D).

The initial grain size profile was uniform with depth, but as deposition and resuspension occurred, the bed developed layers showing gradations in grain size. At the end of the model run, the grain size distribution was well mixed in most of the modeled sediment bed, except at the sediment surface and a layer around 4.6 cm deep, where medium sediment was slightly more prevalent than the finer sediment (Figure 3-5). This layer corresponded to the initial sediment surface for the model run, which became graded during two resuspension and erosion events that occurred in the first 10 days of the model run. This storm bed persisted for the seven months of the model run because burial by new sediment outpaced bioturbation.

The sediment bed was initialized to have the radioisotope activity profiles found in April, 2000 by Corbett *et al.*, (2004) and the profiles then evolved with sediment deposition and erosion. The final radioisotope profiles were similar to the profiles

observed in October, 2000 (Figure 3-6B). They differed from the initial isotopic profiles in that the ^7Be surface activity increased through the model run from 1.1 to 5.6 dpm/g, while the penetration depth of ^7Be decreased. The calculated profiles were insensitive to the initial radioisotope profiles; the ^7Be activity was low and decayed quickly; while the ^{234}Th profile responded even more quickly because of its shorter half-life.

Figure 3-7 shows timeseries of the surface activities and bed inventories calculated for both radionuclides. The surface activity of ^7Be increased quickly from 1.1 at the beginning of the model run, to 14.1 dpm/g at day 24 in response to high riverine sediment deposition (Figure 3-7A). After this, it decreased slightly until another input of riverine sediment occurred around day 98, when the surface activity increased to 13.7 dpm/g. River input was low throughout the rest of the model run, so surface activity decayed to 5.6 dpm/g. The peaks in ^7Be surface activity were associated with riverine sediment deposition, while the decreases reflected erosion, radioisotopic decay, and biodiffusion that mixed the higher activity surficial sediment downward. The ^{234}Th surface activity followed a similar pattern, but generally had a surface activity about 4 to 5 times greater than ^7Be because the input activity of ^{234}Th was about 5 times greater than ^7Be (Figure 3-7).

The bed inventories calculated for both ^7Be and ^{234}Th followed the trend of their respective surface activities (Figure 3-7), as deposition at the sediment surface was the source for both radioisotopes to the seabed. The bed inventories of ^7Be and ^{234}Th were 12.1 and 65.7 dpm/cm² on day 30, increased to 19.7 and 83.2 dpm/cm² on day 110, and decreased to 7.7 and 17.1 dpm/cm² at the end of the model run.

River sediment deposition added both radioisotopes to the bed, resuspension episodes replenished only the ^{234}Th , and both were removed from the bed during erosion. We examined the ratio of ^7Be to ^{234}Th to see if it provided an indication of recent erosion or flood deposition (Figure 3-8). For the case considered, the ratio of ^7Be to ^{234}Th increased through the model run because deposition was more prevalent than resuspension and ^{234}Th decayed faster than ^7Be . High river sediment discharge, such as after day 80, decreased the $^7\text{Be}:$ ^{234}Th ratio of both surface activity and bed inventory, because the ^{234}Th activities of the new sediment was assumed higher than its ^7Be activity, 95 dpm/g compared to 20 dpm/g, respectively, so deposition delivered a greater amount of ^{234}Th than ^7Be to the bed. Resuspension events, such as those on days 185 and 192, also decreased the $^7\text{Be}:$ ^{234}Th ratio because ^{234}Th activity was replenished on the grains that were suspended. When sediment was eroded from the bed during resuspension events, such as on days 170 and 210, the $^7\text{Be}:$ ^{234}Th ratio increased, because ^{234}Th has a shorter half-life and a greater percentage of the total ^{234}Th was associated with sediment near the seabed surface.

The penetration depths of ^7Be and ^{234}Th responded to the timing of sediment input (Figure 3-9). The initial penetration depth of ^7Be was about 10 cm, then decreased to 9cm as the signal decayed. The initial penetration depth of ^{234}Th was about 6 cm. Around day 100, the penetration depth of ^7Be and ^{234}Th increased to 10.5cm, and 8 cm, respectively, in response to a large sediment input. After day 100, river discharge was low and decay and biodiffusion gradually decreased the penetration depths of ^7Be and ^{234}Th to 6.3 cm, and 5.8 cm, respectively, by the end of the model run.

3.5.2 Standard Storm Model Run

The Standard Storm Model covered seven months from October, 1999 to April, 2000, during which time, data from Tarbert Landing indicated that 3.98×10^{10} kg of sediment was transported down-river. Fluvial input occurred mainly during the second half of the model run (Figure 3-4A). Wave heights averaged 1.09 m, and were energetic enough to erode sediment at the 50-m site during 22 episodes that accounted for about 10% of the time (Figure 3-4B, C). The surface tracer flux for sediment was scaled so that the timing followed that of the sediment discharge curve, with the net amount of sediment deposited being 4.8 cm, and most of it occurring during the second half of the model run.

The initial grain size profile was uniform with depth, but as deposition and resuspension occurred, layers showing gradations in sediment bed grain size developed. At the end of the model run, the grain size distribution was somewhat mixed close to the sediment - water interface, but there was a thick layer from 2.5 to 6.5 cm deep where medium sediment was more prevalent than the finer sediment (Figure 3-10). This layer roughly represented the initial sediment surface for the model run, and became a graded layer because of a number of resuspension and erosion events coupled with little river sediment input in the first 140 days of the model run. Storm layers that were created by larger wave events, such as occurred on Day 120 were preserved in the grain size signature because fine sediment was winnowed from the bed due to high bed stresses. This event caused the 0.5 cm thick graded layer from 4.2 to 4.7 cm deep in the final sediment bed (Figure 3-10E), located just above the initial sediment – water interface.

Though the model represented October, 1999 – April, 2000, the sediment bed was initialized to have the radioisotope activity profiles found in October, 2000 by Corbett *et al.*, (2004), because observations from October 1999 were not available. The final radioisotope profiles were similar to the profiles observed in April, 2000 (Figure 3-11). They differed from the initial isotopic profiles in that the ^7Be surface activity decreased through the model run from 4.9 to 2.3 dpm/g, while the ^{234}Th surface activity increased from 39 to 69 dpm/g. The calculated profiles were somewhat sensitive to the initial ^7Be profile which had a high activity in the top 4 cm of the sediment bed and remained above the detection limit throughout the model run, as evidenced by the ^7Be signal from 6 to 8 cm deep in the final profile (Figure 3-11). The calculated profile was less sensitive to the initial ^{234}Th profile, because it has a shorter half-life.

Figure 3-12 shows timeseries of the surface activities and bed inventories calculated for both radionuclides. The surface activity of ^7Be decreased from 4.9 dpm/g at the start of the model to 1.8 dpm/g on day 80 during which time fluvial input was low. Then, the deposition of riverine sediment increased and the ^7Be surface activity increased slightly to 2.2 dpm/g by day 145 (Figure 3-12). Due to continued deposition of fluvial sediment between days 145 and the end of the model run, the ^7Be surface activity increased to 2.3 dpm/g. The ^{234}Th surface activity increased with minor variations due to resuspension and riverine sediment deposition from 39 to 84 dpm/g on day 157, and decreased to 69 dpm/g at the end of the model run due to erosion, decay, and decreasing riverine sediment deposition after day 190. The bed inventories of both ^7Be and ^{234}Th followed the trend of their respective surface activities (Figure 3-12). The bed

inventories of ^7Be and ^{234}Th were 7.7 and 20.5 dpm/cm² at the beginning of the model run, were 4.1 and 93.0 dpm/cm² on day 166 and decreased to 3.9 and 73.0 dpm/cm² at the end of the model run.

River sediment deposition added both radioisotopes to the bed, and the ratio of $^7\text{Be}:$ ^{234}Th decreased throughout the model run (Figure 3-8). Because the initial bed inventory of ^{234}Th was low due to limited data from Corbett *et al.*, (2004), the initial $^7\text{Be}:$ ^{234}Th ratio was relatively high. The ratio increased when sediment and ^{234}Th were eroded from the bed, such as on days 7 and 15, but the ratio decreased when resuspension occurred to replenish ^{234}Th in the seabed.

The initial penetration depth of ^7Be was about 6cm, stayed fairly constant until day 90 because river input was minimal during this time (Figure 3-13). Later, when fluvial input increased, the penetration depth expanded, reaching 8.5cm at the end of the model run. The initial penetration depth of ^{234}Th was 1cm due to limited data in the initial profile and increased to 6cm by the end of the model run due to river sediment deposition and biodiffusion.

3.5.3 Deposition Rates

We can calculate the deposition rates for the numerical model by integrating the surface tracer flux with time, or calculating the rate of change in sediment bed thickness. Accounting for the cumulative deposition and erosion imposed in the model, the net amount of sediment deposited on the bed was 4.6 cm and 4.8 cm for the seven-month long calm and storm models, respectively, which equate to average net deposition rates of

0.66 cm month⁻¹ and 0.69 cm month⁻¹. Over the course of the model runs, the short-term erosion and deposition rates varied, however. To examine erosion and deposition rates on shorter timescales, a moving average of ten days was applied to the instantaneous values for both model runs. The calm model experienced two depositional pulses in the first half of the model run, after which deposition slowed. The storm model started as erosional, and then deposition generally increased with model time, reflective of higher river discharge. Averaged over ten-day timescales, erosion rates reached as high as 1 cm month⁻¹, and deposition rates as high as 3 cm month⁻¹ (Figure 3-14).

Profiles of short-lived radioisotopes like ⁷Be and ²³⁴Th are often used to estimate deposition rates in coastal environments, using Equations 1 and 3. In field situations, however, it is difficult to evaluate the reliability of these estimates. Within the model, however, we can compare the “true” deposition rates to the “apparent” values obtained by analyzing the geochronological profiles. For comparison to the “apparent” accumulation rates, the modeled deposition rates were averaged over the last 100 days of the model runs, during which time the calm and storm models supplied 0.17 and 1.21 cm month⁻¹ of sediment to the bed, respectively (Table 3-1). This represented a time scale equal to about two half-lives of ⁷Be.

These “actual deposition rates” for the two time periods were compared to the apparent deposition rates derived from the modeled profiles using Equation 1 which neglected biodiffusion, and Equation 3 which had an additional term to account for biodiffusion. To apply Equations 1 and 3, logarithmic regressions were fit to the final model profiles. This regression only used those radioisotope activities greater than the

detection limit of 0.1 dpm/g. The “theoretical logarithmic activity” for each activity value was calculated using the depth of that value and the slope and intercept of the regression line. The inverse logarithm was taken for each theoretical logarithmic activity value; A_0 and A_z in Equations 1 and 3 were the theoretical activities at the surface and at depth, and z was the difference in the depth of these two values.

Based on the final model profiles of ^7Be and ^{234}Th (Figure 3-6b), the apparent deposition rates estimated for the standard calm model were $0.69 \text{ cm month}^{-1}$ and $0.87 \text{ cm month}^{-1}$ respectively, using Equation 1, and were $0.65 \text{ cm month}^{-1}$ and $0.78 \text{ cm month}^{-1}$, respectively, using Equation 3 (Table 3-1). For the standard storm model, application of Equation 1 to the final modeled profiles (Figure 3-11b) yielded apparent deposition rates of 1.37 and $1.04 \text{ cm month}^{-1}$ for ^7Be and ^{234}Th , respectively; application of Equation 3 to the final modeled profiles yielded apparent deposition rates of 1.36 and $1.01 \text{ cm month}^{-1}$ for ^7Be and ^{234}Th , respectively (Table 3-1). Comparing the values obtained using Equation 1 to those from Equation 3 showed that for this model run, knowledge of the bioturbation coefficient and consideration of bioturbation in estimating the accumulation rates reduced the deposition rates by as much as 12%.

We expected that the apparent deposition rates for both the calm and the storm models would be similar to the true deposition rates averaged over a few half-lives of the tracers. This was true of the storm model, where the ^7Be and ^{234}Th derived apparent deposition rates bracketed the actual deposition rates averaged over the last 100 days of the model run (Table 3-1). For the calm model, however, the apparent deposition rate of ^7Be exceeded the modeled deposition in the last 100 days of the model run, due to the

persistence of a large depositional pulse around day 100. The apparent deposition rate of ^{234}Th in the calm model was even larger than that estimated for ^7Be . Some of the difference in apparent deposition rates of the two tracers, compared to each other and to the actual modeled deposition rates, may be explained by the fact that the model experienced episodic deposition at day 100, and periods of episodic erosion and resuspension at days 170 and 210. Also, Equations 1 and 3 assume that sediment accumulation occurs at a fairly steady rate, yet the actual deposition in the model experienced episodes of both sediment deposition and erosion.

3.6 Discussion

Beryllium-7 and Thorium-234 have different sources to the continental shelf, and therefore are impacted by different processes. A one – dimensional sediment transport model that included both of these radioisotopes produced geochronological profiles similar to those observed in a field study. A series of sensitivity tests were then considered, to evaluate the degree that biodiffusion, resuspension, and flood thickness impact the radioisotopic profiles.

3.6.1 Sensitivity to Bioturbation

To test the sensitivity of the modeled profiles to the intensity of bioturbation, the storm and calm models were each repeated using different values of the biodiffusion coefficient (D_b). The standard calm and storm models used $D_b=1$ and $D_b=0.5 \text{ cm}^2 \text{ yr}^{-1}$, respectively, and the sensitivity runs included implementations that neglected

biodiffusion ($D_b = 0 \text{ cm}^2 \text{ yr}^{-1}$), and ones that used a larger coefficient ($D_b = 25 \text{ cm}^2 \text{ yr}^{-1}$) similar to values cited for many continental shelves (Wheatcroft and Drake, 2003).

When bioturbation was neglected, the surface activity of both radioisotopes in the standard calm model was slightly higher, and the penetration depth was shallower, because there was no biodiffusion in the bed (Figure 3-15). Because the standard storm model used a very low D_b , neglecting biodiffusion only caused a minor difference in the activity profile at depth below the initial sediment - water interface (Figure 3-16).

Use of the larger biodiffusion coefficient decreased the surface activity, but increased the penetration depth for both radioisotopes by mixing the high-activity surface layers deeper into the bed (Figures 3-15, 3-16). Increasing the biodiffusion coefficient did not change the bed inventory of ^7Be , but generally increased the bed inventory of ^{234}Th because it mixed sediment from deep in the bed that had lower activities of ^{234}Th to the sediment surface where it could be resuspended, and then pick up more ^{234}Th in the water column.

3.6.2 Sensitivity to Flood Thickness

Next, the storm and calm models were rerun, using lower and higher flood deposition thicknesses. These model runs indicated the relative importance of resuspension intensity and flood deposition. The case using a greater flood thickness illustrated a case where deposition overwhelmed physical mixing by resuspension. Conversely, the case using a lesser flood thickness illustrated the situation where physical mixing by resuspension overwhelmed flood deposition. Because deposition was imposed

during times of high river discharge, the amount of deposition for the sensitivity cases differed from the standard model runs. For the calm model, the net sediment deposition was 5.8 and 3.2 cm for high and low flood thicknesses, respectively, while the standard calm model deposited 4.6 cm of sediment (Figure 3-17). For the storm model, the total sediment deposition was 6.7 and 3.1 cm for high and low flood thicknesses, respectively, while the standard storm model deposited 4.8 cm of sediment (Figure 3-18).

The flood thickness did not have a large effect on the surface activity, but both total inventories and penetration depth varied directly with the flood thickness. More deposition increased the penetration depth while less deposition decreased the penetration depth of both radioisotopes; net sediment deposition is the primary control on penetration depth. Increased sediment deposition increased radioisotope inventories because more sediment, and the associated radioisotope activity, was added to the bed. Reduced deposition decreased radioisotope inventories because less radioisotope activity was added when sediment was deposited.

3.6.3 Application to Mississippi Delta Field Site

The target of this study was to reproduce observed radioisotope profiles from Corbett *et al.*, (2004); therefore, the sediment deposition, erosion, and input radioisotope activity had to be coordinated in order to simulate the penetration depth and activity profile of both radioisotopes. Sediment deposition was related to the Mississippi River sediment discharge curve, but sediment erosion had to be estimated based on the wave

and bed stress timeseries. The input radioisotope activities were chosen based on both the radioisotope surface activities and the shape of the observed activity profiles.

For the standard calm model, the initial ^7Be surface activity from the observed profile in April, 2000 was 1 dpm/g, and increased to 5 dpm/g by October, 2000. Nearly all the sediment deposition was in the first half of the model run, and ^7Be underwent a high amount of decay between deposition and the end of the model run. Therefore a high input activity of 20 dpm/g was chosen for this model run to achieve a final surface activity of roughly 5 dpm/g and match the final ^7Be profile. The surface activity for ^{234}Th was high in the initial and final observed profiles; a high value of 95 dpm/g was chosen for the water column activity of ^{234}Th in order to match the high surface activity in October, 2000. Using these values for radioisotope activity as well as a balance between deposition and erosion to replicate the penetration depth of ^7Be , the observed profiles from October, 2000 were reproduced by the calm model.

For the standard storm model, the final ^7Be surface activity in April, 2000 was much lower than the final surface activity in October, 2000. Nearly all the sediment deposition was in the second half of the model run, and ^7Be did not decay very much from the time of deposition to the end of the model run. Therefore, a low input activity of 3 dpm/g for ^7Be was chosen to achieve a similar profile to that observed in April, 2000. The ^{234}Th activity in the water column was identical to that in the calm model, as the April, 2000 profile had a high ^{234}Th surface activity. The quantity of sediment deposition and erosion were determined through experimentation in order to correspond to the correct penetration depth for both radioisotopes.

3.7 Conclusions and Future Work

Future efforts with the sediment transport geochronological model include adding the capabilities to a full three-dimensional model, such as that developed by Moriarty for the Waipaoa River Shelf, New Zealand or a northern Gulf of Mexico continental shelf model.

It would be useful to add size-dependent sorption of the radioisotopes ^7Be and ^{234}Th , as well as running the model within a cohesive bed configuration. Because fine-grained particles have a greater surface area than larger particles, they tend to adsorb more particle reactive elements such as ^{234}Th or ^7Be (Feng *et al.*, 1999). Including size-dependence in the model would give a more accurate representation of the sorption and transport of radioisotopes on different particle sizes in the coastal ocean.

A one-dimensional numerical sediment transport model within ROMS was used to evaluate the response of radioisotope profiles to variations in riverine sediment input, storm intensity, and bioturbation. Reactive radioisotope tracers, ^7Be and ^{234}Th , have been added into the one-dimensional sediment transport model to interpret deposition of river derived sediment and sediment resuspension, respectively. Corbett *et al.*, (2004) analyzed sediment cores from a 50 meter site near the Southwest Pass of the Mississippi River in April and October, 2000. Using calm and storm models, it was possible to reproduce the profiles measured by Corbett and colleagues. The modeled profiles were very similar to the observed profiles and this capability will be able to be used in the future to reproduce field data. This capability can also be added to more complex

numerical sediment transport models in order to get a more widespread estimation of radioisotope activity and inventory on continental shelves.

While this model did a good job at reproducing field observed profiles, it simplified realistic oceanic processes that could be represented in more complex three-dimensional models. Although the model accounted for erosion from the seabed by removing sediment from the model when a bed stress threshold was exceeded, the percent of sediment in suspension eroded was not correlated to bed stress. In a more realistic model, the eroded amount would depend on flux divergences that would respond both to spatial gradients in the waves and currents. This model also could not account for addition of non-local sediment supplied by erosion from shallower areas of the shelf. Instead, for this study, we based the net depositional amounts on the river sediment discharge curve and deposition estimates.

Our model results indicated that surface activity was diagnostic of recent processes; riverine deposition increased ^7Be surface activity and both riverine deposition and resuspension increased the surface activity of ^{234}Th , while erosion decreased the surface activity of both radioisotopes. Bed inventory was diagnostic of more long term processes, but was decreased over short-time scales by sediment erosion and was increased by sediment discharge pulses. Penetration depths of both radioisotopes were representative of the initial profile early in the model run, but were impacted by sediment deposition and bioturbation later in the model run.

Tables

Table 3-1: Sediment Deposition Rates

Deposition rates for the standard calm and storm models; the actual model deposition rates, the actual model deposition rate over the last 100 days of the model run, and the apparent model deposition rates calculated from the radioisotope profiles using Equation 1 and Equation 3.

	Average model deposition rate (cm month ⁻¹)	Model deposition rate over last 100 days (cm month ⁻¹)		Apparent model deposition rate, Equation 1 (cm month ⁻¹)	Apparent model deposition rate, Equation 3 (cm month ⁻¹)
Standard Calm Model	0.66	0.17	⁷ Be	0.69	0.65
			²³⁴ Th	0.87	0.78
Standard Storm Model	0.69	1.21	⁷ Be	1.37	1.36
			²³⁴ Th	1.04	1.01

Figures

Figure 3-1: Study Site Map

Map of Study Area showing the Mississippi birdfoot delta (shaded) and bathymetry (black lines, contours labeled in meters water depth). The red triangle marks the 50 meter deep site represented in our model and reoccupied by Corbett *et al.*, (2004). Figure modified from Corbett *et al.*, (2004).

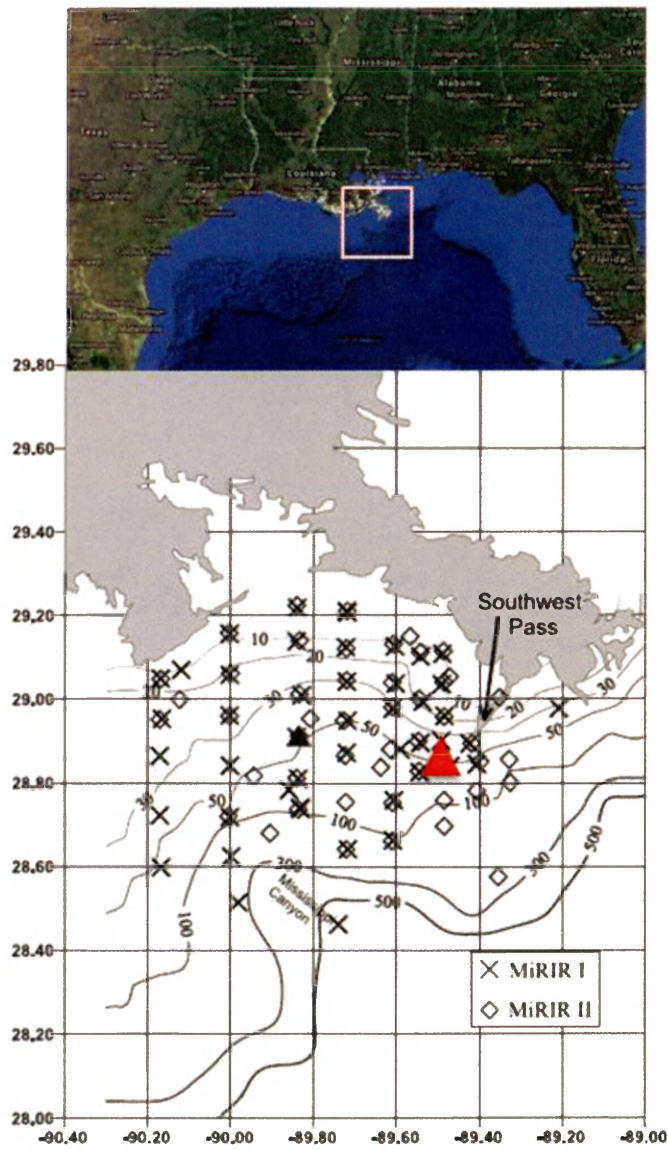


Figure 3-2: Radioisotope Profiles from Corbett *et al.*, (2004)

Radioisotope profiles for April, 2000 (MiRIR 1) and October, 2000 (MiRIR 2). Circles denote ^7Be activity and squares denote ^{234}Th activity (dpm/g). Estimated errors for ^7Be were approximately 10-20% for the near surface samples and approximately 50-75% for the deeper samples. Estimated errors for ^{234}Th were approximately 5-10% for the near surface samples and approximately 25-50% for the deeper samples (Corbett, personal communication, April 2014). Figure from Corbett *et al.*, (2004).

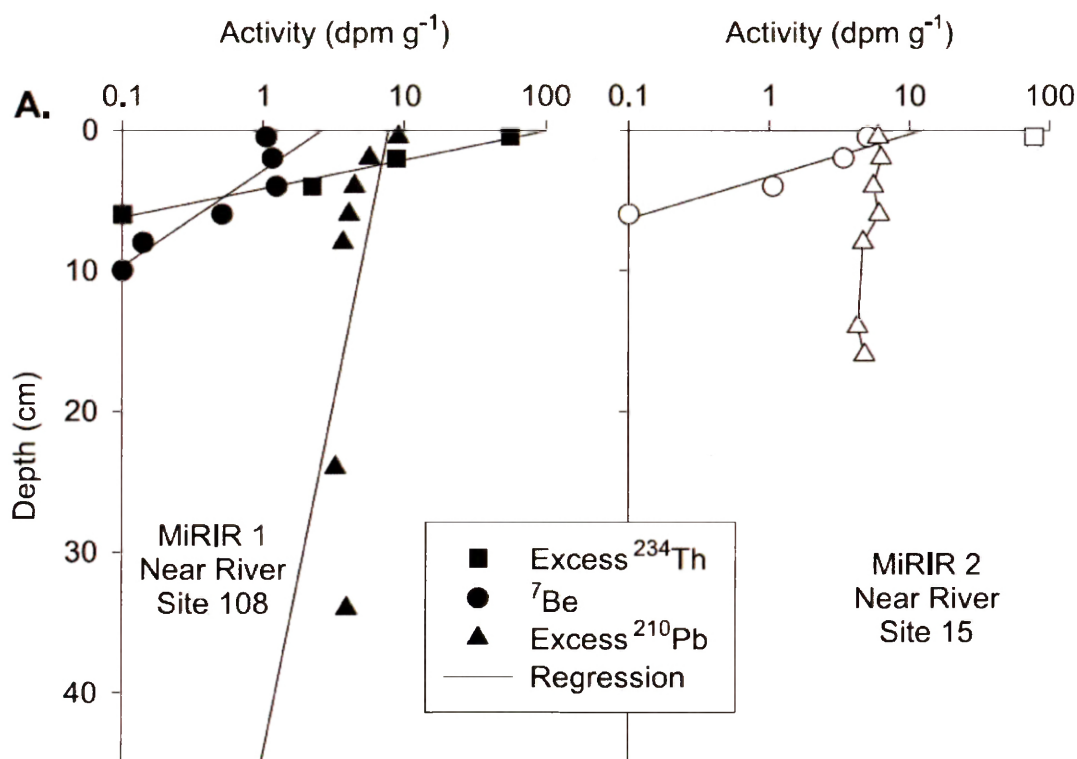


Figure 3-3: Calm Model Timeseries

Time series for the standard calm model showing model inputs (A) Mississippi River sediment discharge (United States Geological Survey), and (B) significant wave height (NOAA NDBC). Also shown are model – calculated values (C) bed stress, (D) cumulative surface tracer flux, integrated with time, (E) depth-averaged suspended sediment concentrations and (F) sediment bed height.

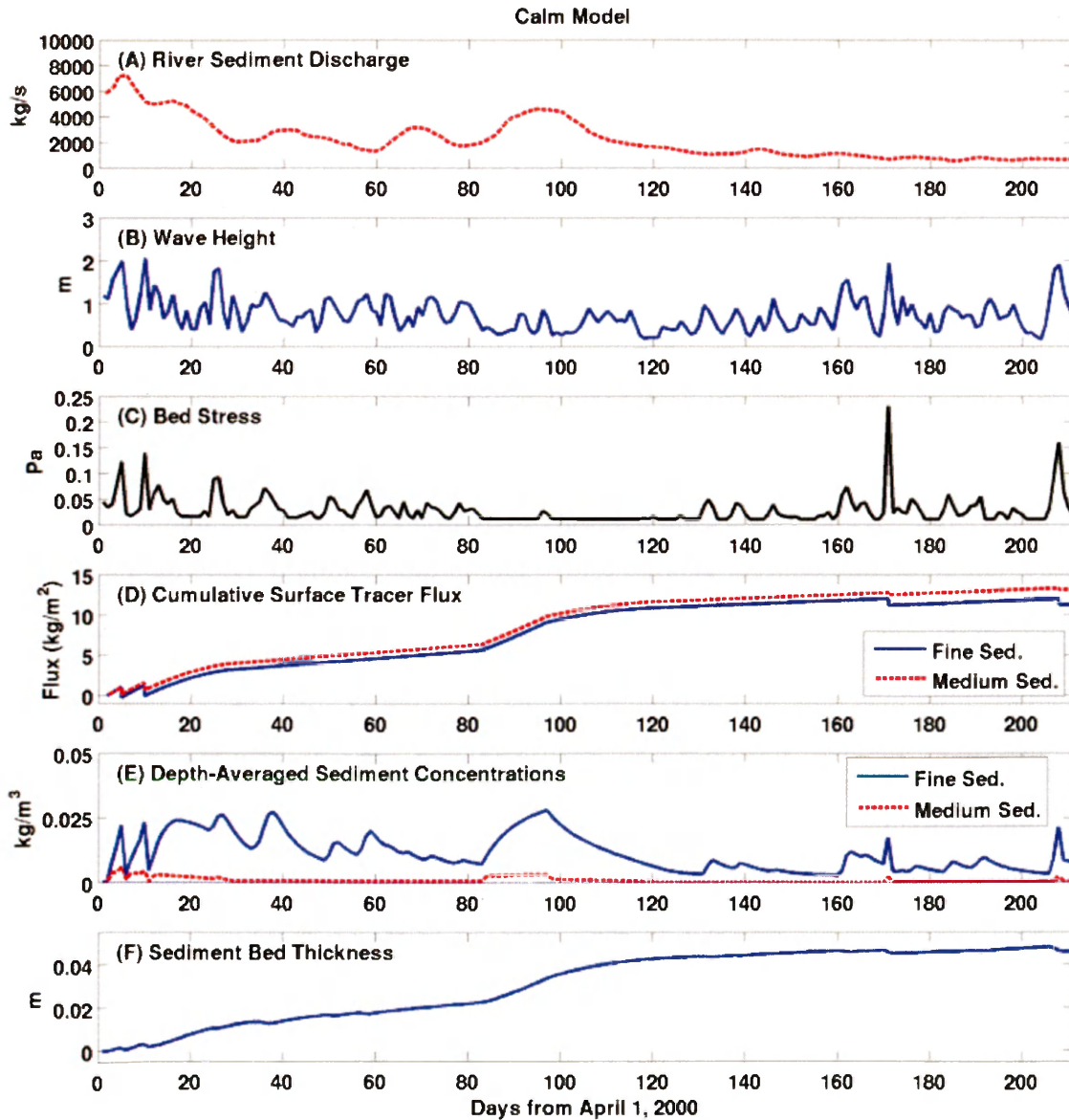


Figure 3-4: Storm Model Timeseries

Time series for the standard storm model showing model inputs (A) Mississippi River sediment discharge (United States Geological Survey), and (B) significant wave height (NOAA NDBC). Also shown are model – calculated values (C) bed stress, (D) cumulative surface tracer flux, integrated with time, (E) depth-averaged suspended sediment concentrations and (F) sediment bed height.

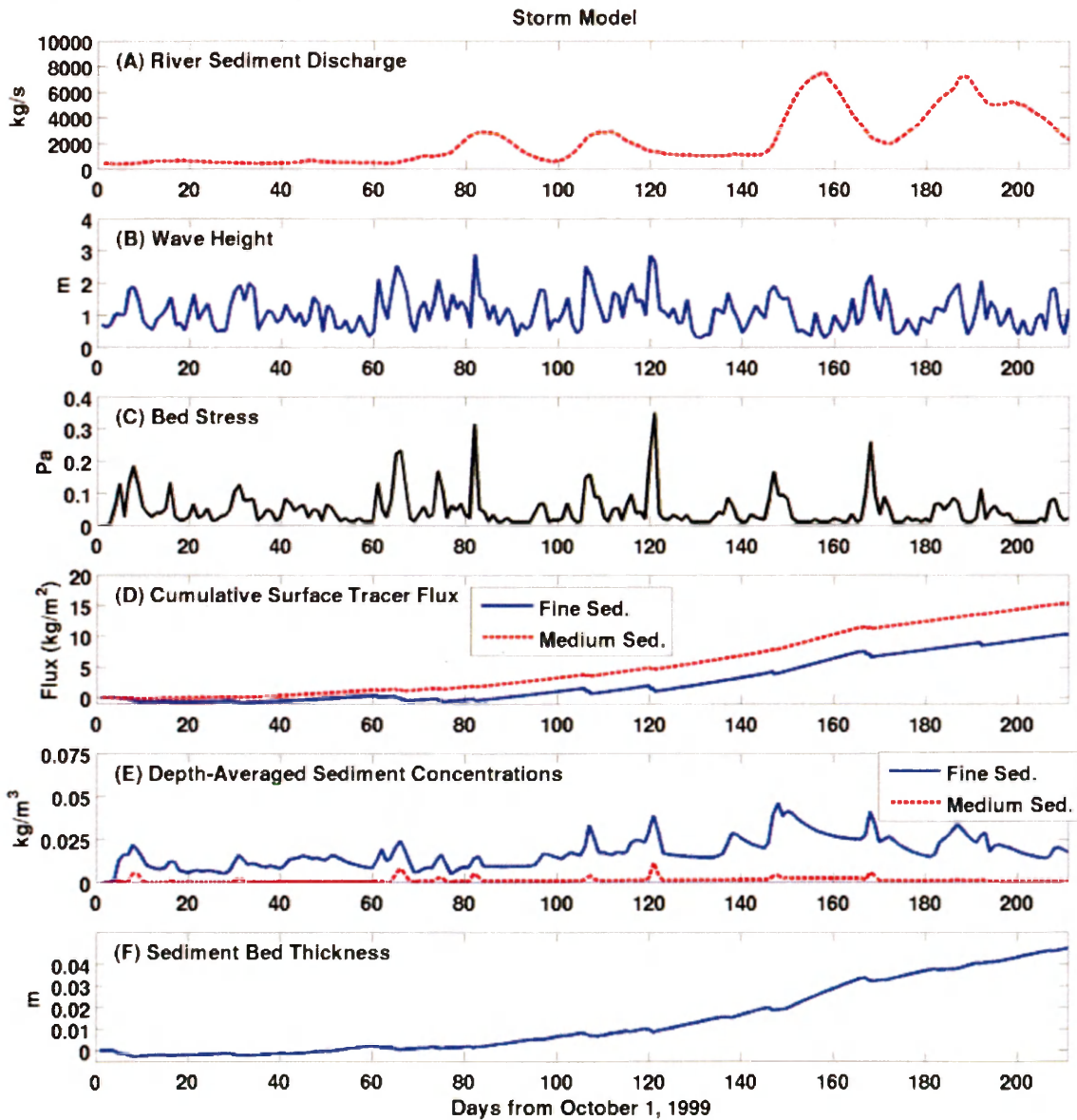


Figure 3-5: Calm Model Grain Size and Radioisotope Profiles

Profiles of grain size and radioisotope activity calculated for five different days during the Standard Calm Model. Grain size panels (A-E) show seabed concentrations (kg/m^3) for the two sediment types, while radioisotope panels (F – J) show calculated activities (dpm/g). On each profile, the depth in the bed is shown relative to instantaneous sediment – water interface, shown by the thick black line at $z_{bed} = 0$. The dashed black line marks the location of the initial sediment - water interface.

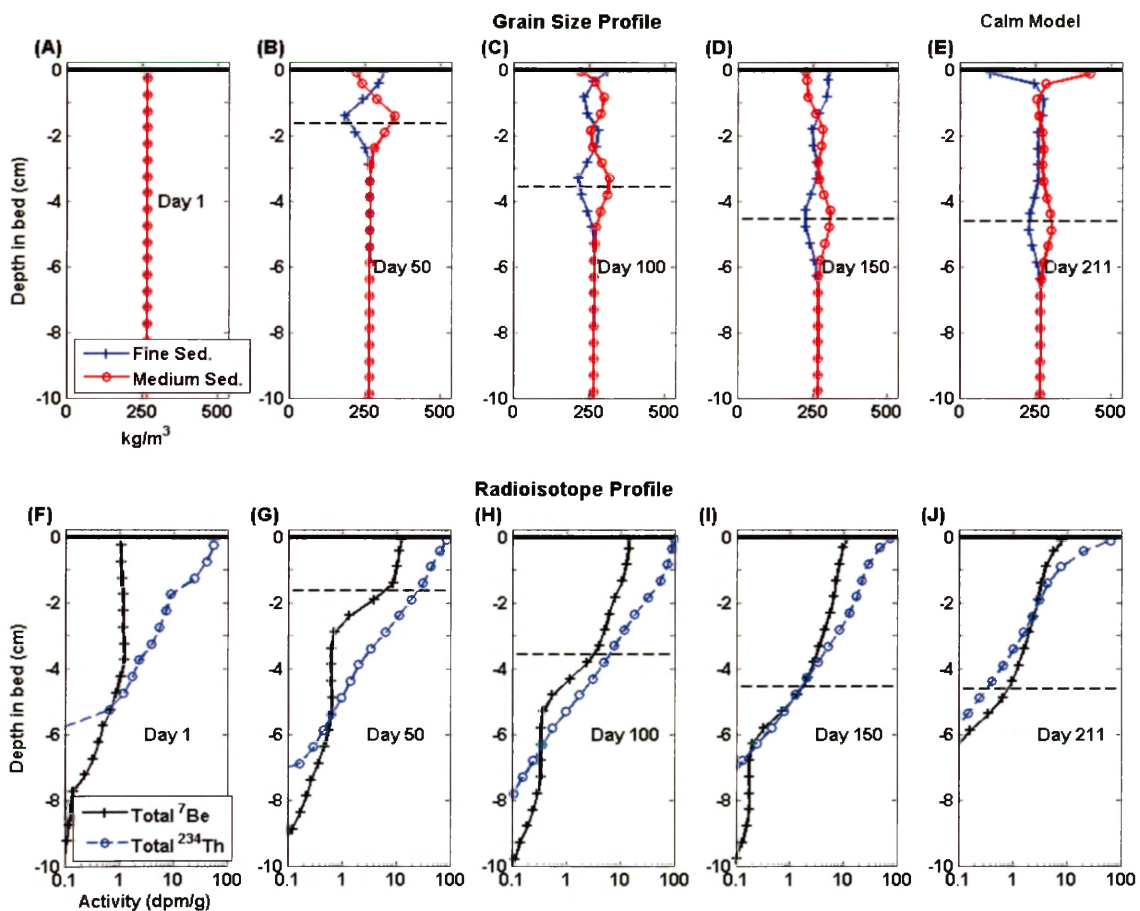


Figure 3-6: Calm Model Comparison with Observations

Comparison of model estimated profiles to those from Corbett *et al.*, (2004) for the Standard Calm Model. The initial profiles are shown on the left and the final profiles after seven months of model time are shown on the right. The thick black line shows the final sediment - water interface, and the dashed black line marks the level of the model's initial sediment - water interface.

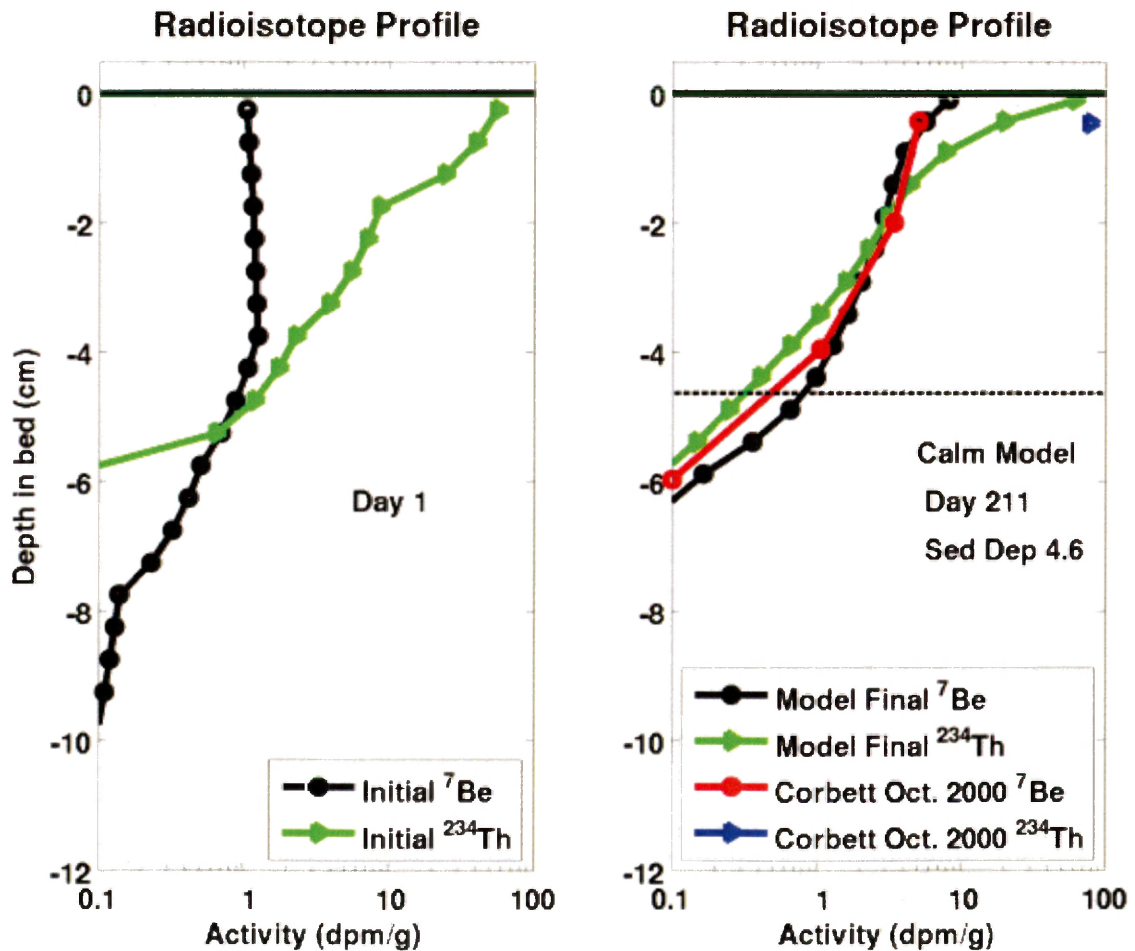


Figure 3-7: Calm Model Timeseries of Bed Inventory and Surface Activity
 Timeseries of radioisotopic bed inventory and surface activity for (A) ^7Be and (B) ^{234}Th for the Standard Calm Model. Bed inventory is shown as a solid black line and surface activity is shown as a dashed blue line.

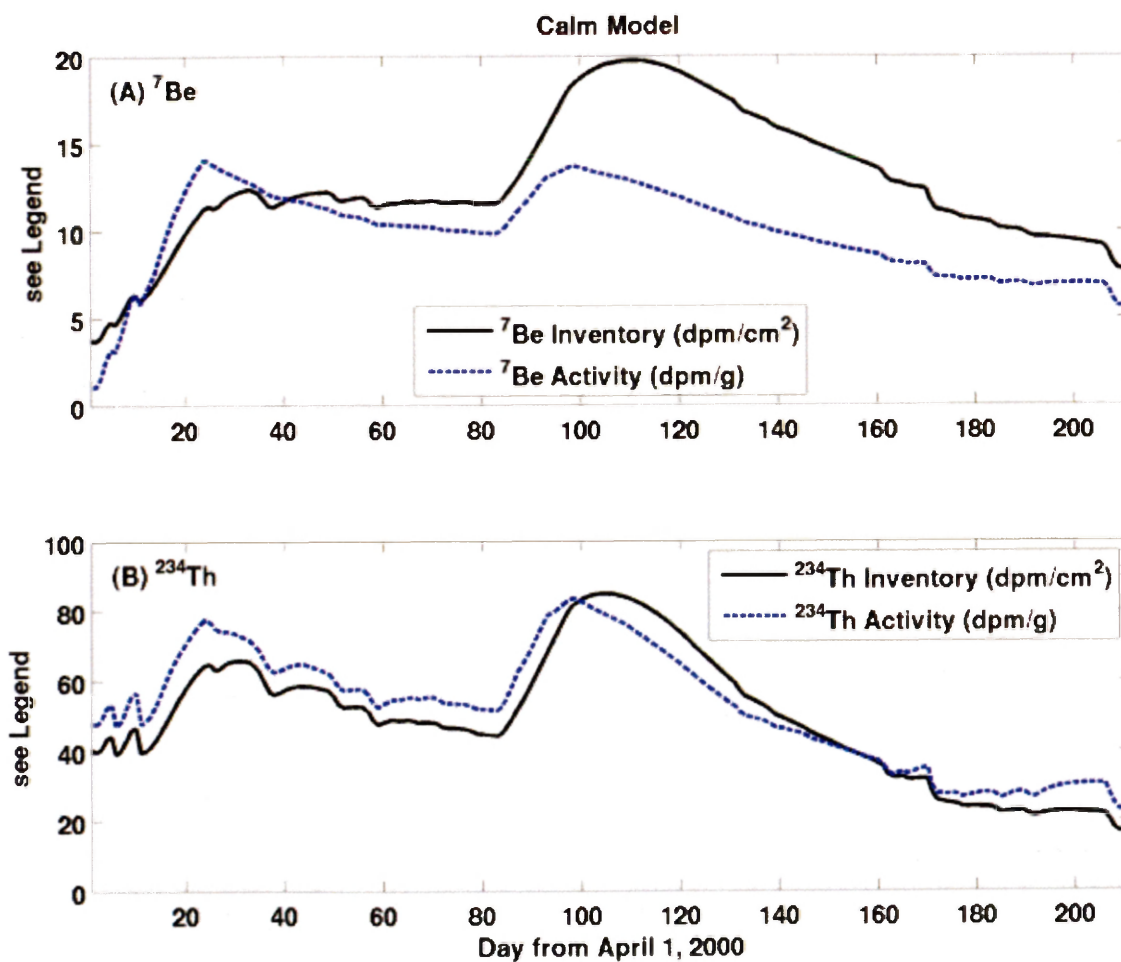


Figure 3-8: $^7\text{Be}:$ ^{234}Th Ratio for Bed Inventory and Surface Activity

Timeseries of the $^7\text{Be}:$ ^{234}Th ratios for the standard calm model (top) and the standard storm model (bottom). The ratio of bed inventories is shown by the solid black lines and the ratio of surface activities is shown by the dashed blue line.

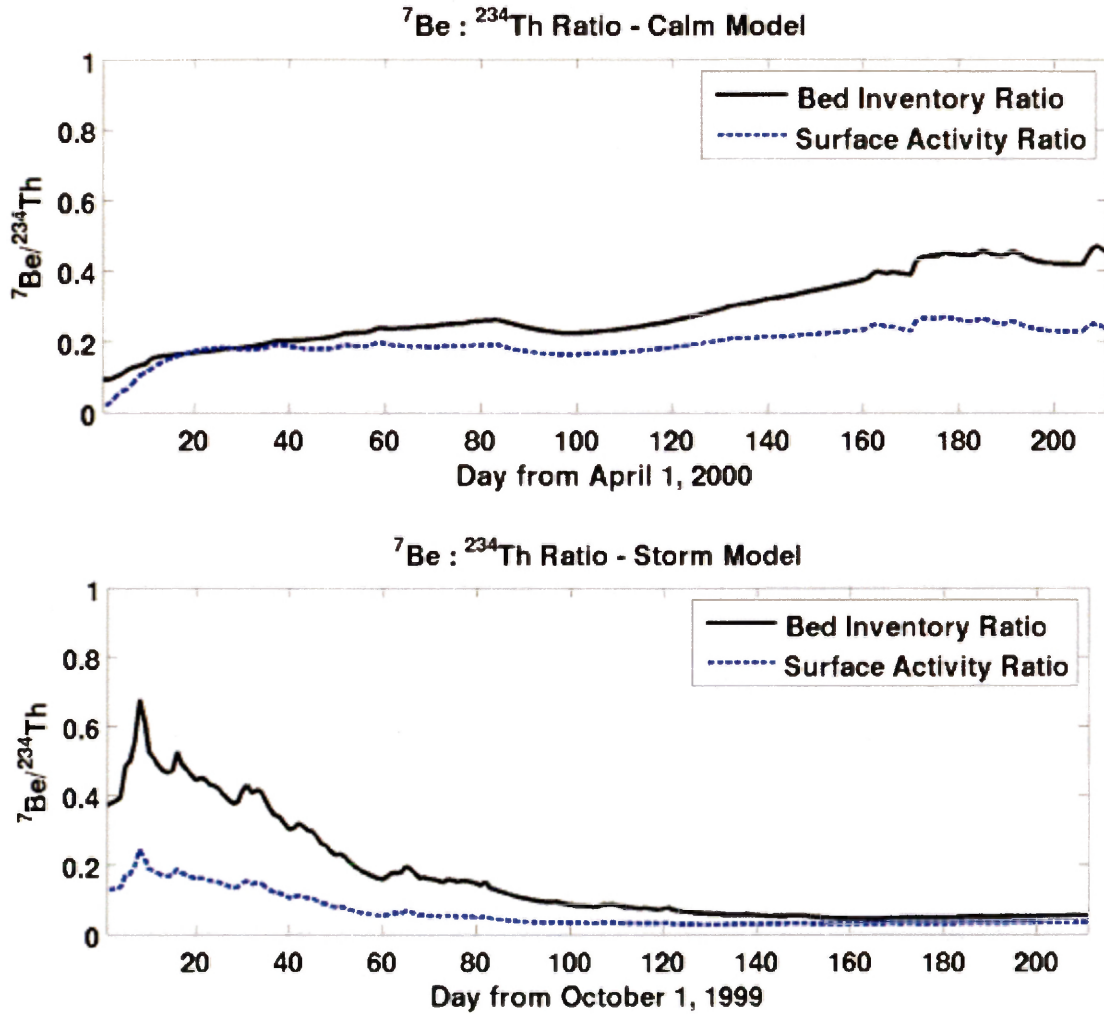


Figure 3-9. Calm Model Penetration Depth

Penetration depth of ^7Be and ^{234}Th for the standard calm model; ^7Be is shown by the solid black line and ^{234}Th is shown by the dashed blue line.

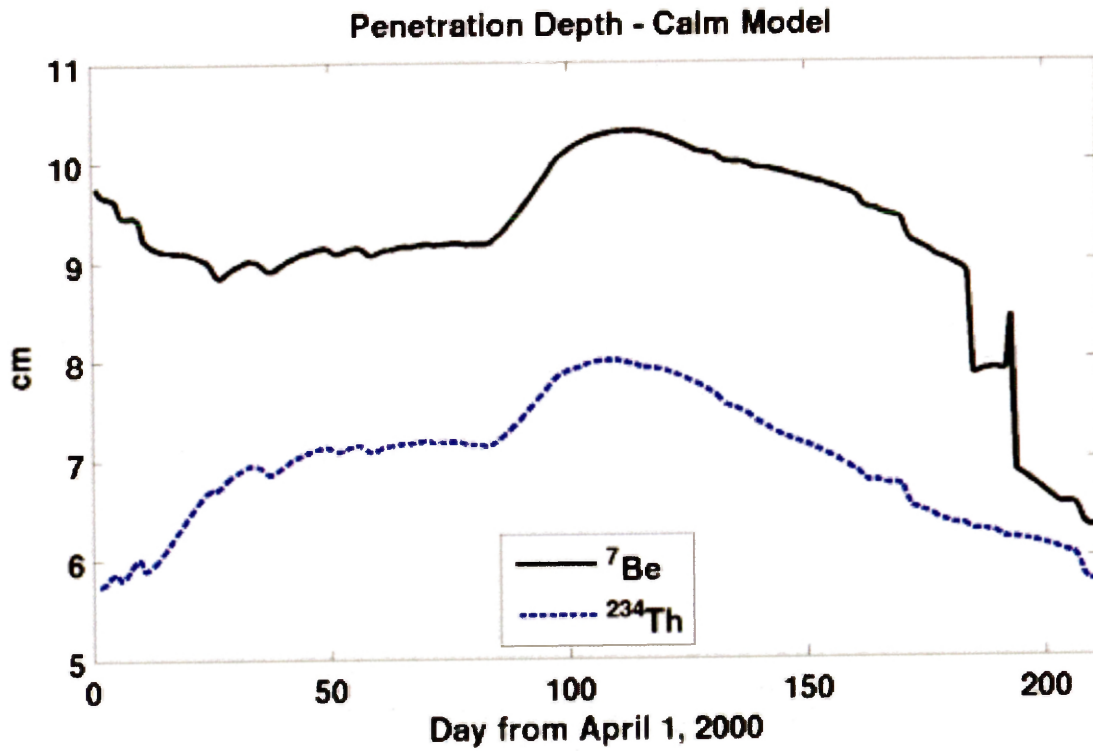


Figure 3-10: Storm Model Grain Size and Radioisotope Profiles

Profiles of grain size and radioisotope activity calculated for five different days during the Standard Storm Model. Grain size panels (A-E) show seabed concentrations (kg/m^3) for the two sediment types, while radioisotope panels (F – J) show calculated activities (dpm/g). On each profile, the depth in the bed is shown relative to instantaneous sediment – water interface, shown by the thick black line at $z_{bed} = 0$. The dashed black line marks the location of the initial sediment - water interface.

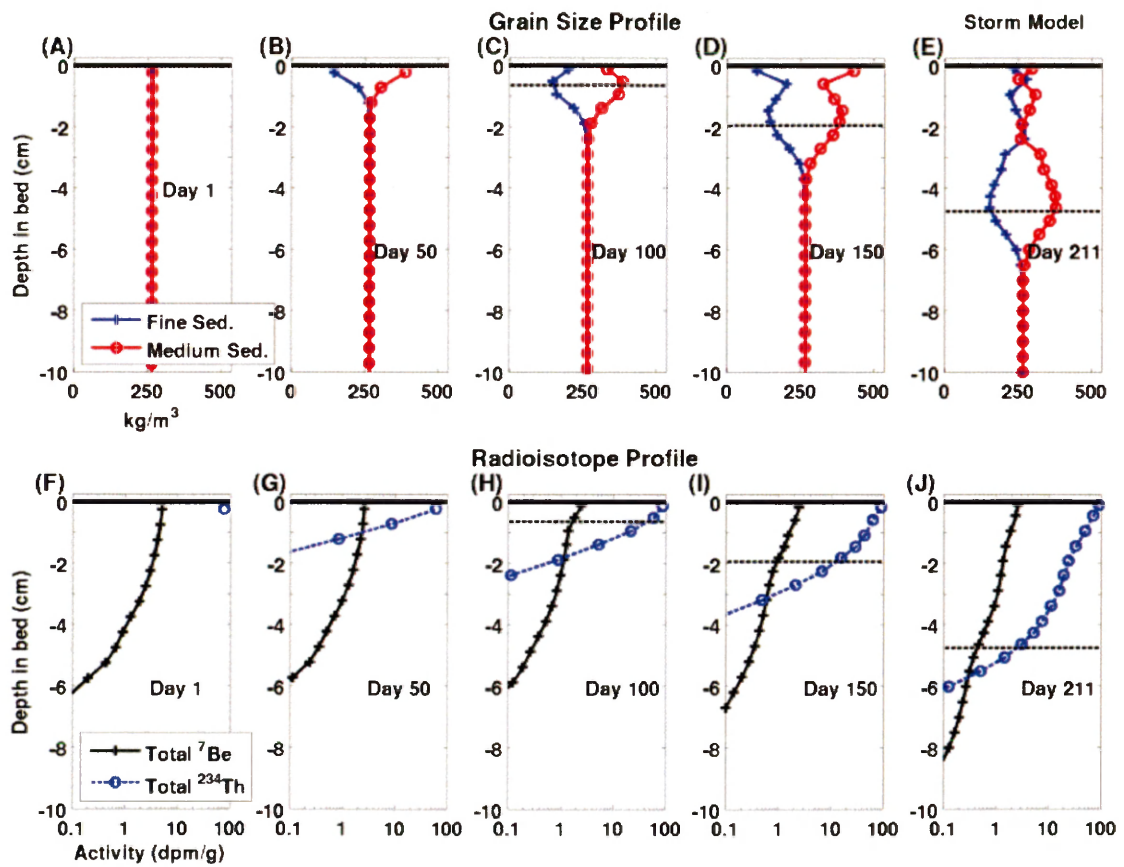


Figure 3-11: Storm Model Comparison with Observations

Comparison of model estimated profiles to those from Corbett *et al.*, (2004) for the Standard Storm Model. The initial profiles are shown on the left and the final profiles after seven months of model time are shown on the right. The thick black line shows the final sediment - water interface, and the dashed black line marks the level of the model's initial sediment - water interface.

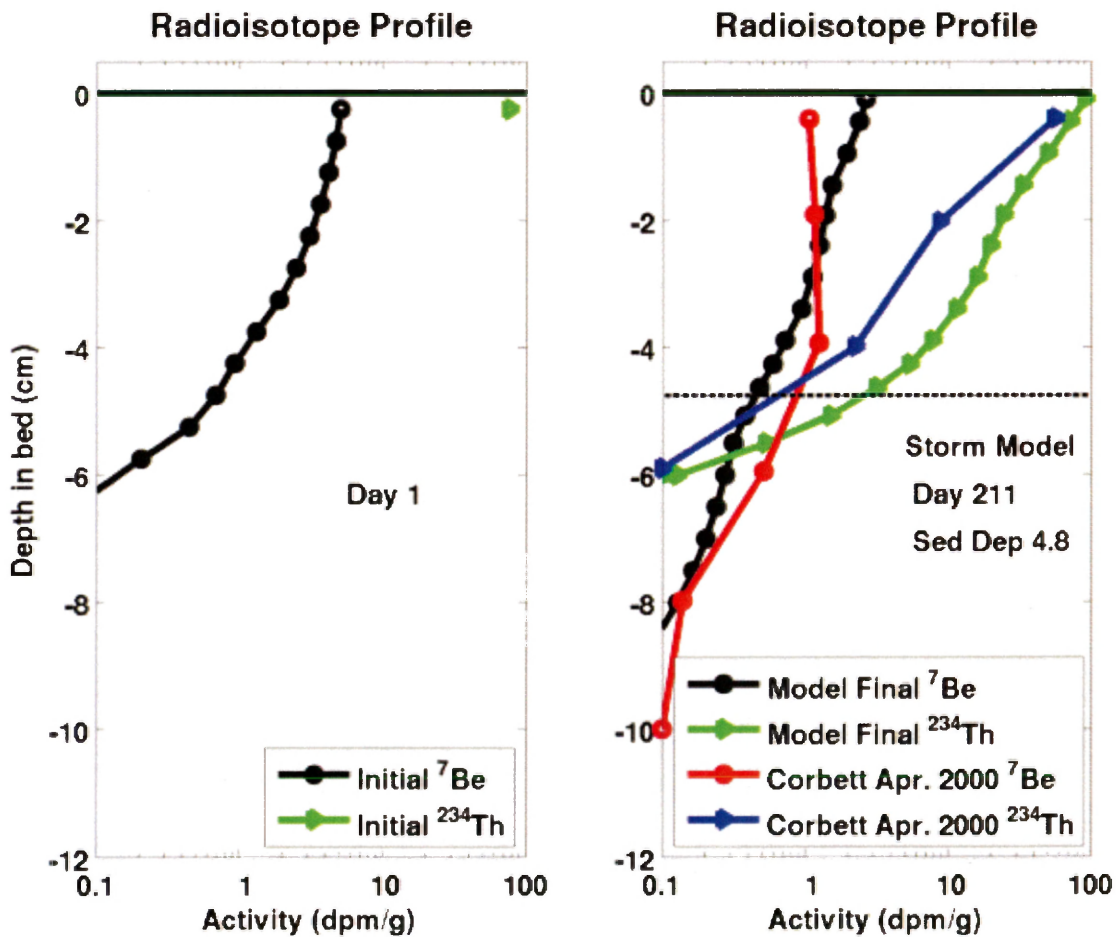


Figure 3-12: Storm Model Timeseries of Bed Inventory and Surface Activity
 Timeseries of radioisotopic bed inventory and surface activity for (A) ^7Be and (B) ^{234}Th for the Standard Storm Model. Bed inventory is shown as a solid black line and surface activity is shown as a dashed blue line.

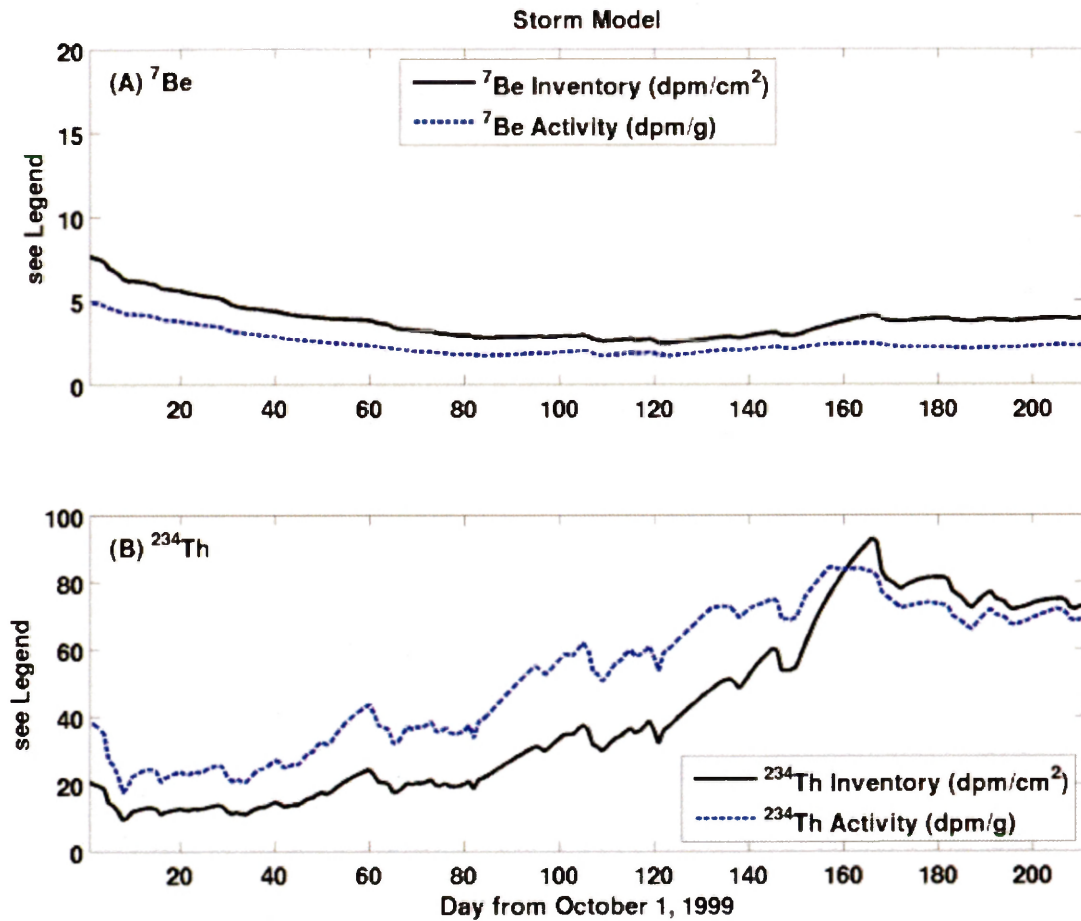


Figure 3-13. Storm Model Penetration Depth

Penetration depth of ^7Be and ^{234}Th for the standard storm model; ^7Be is shown by the solid black line and ^{234}Th is shown by the dashed blue line.

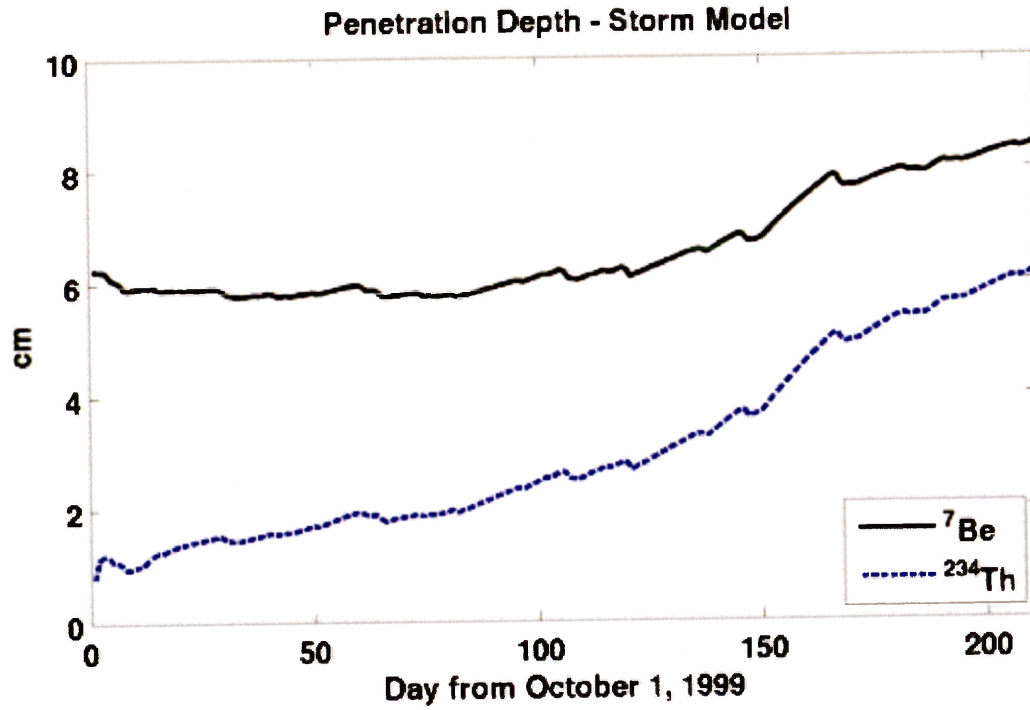


Figure 3-14. Model Deposition Rates

The model sediment deposition rates over the seven months of the calm model (top) and the storm model (bottom). A ten-day moving average was applied to both the calm and storm model values.

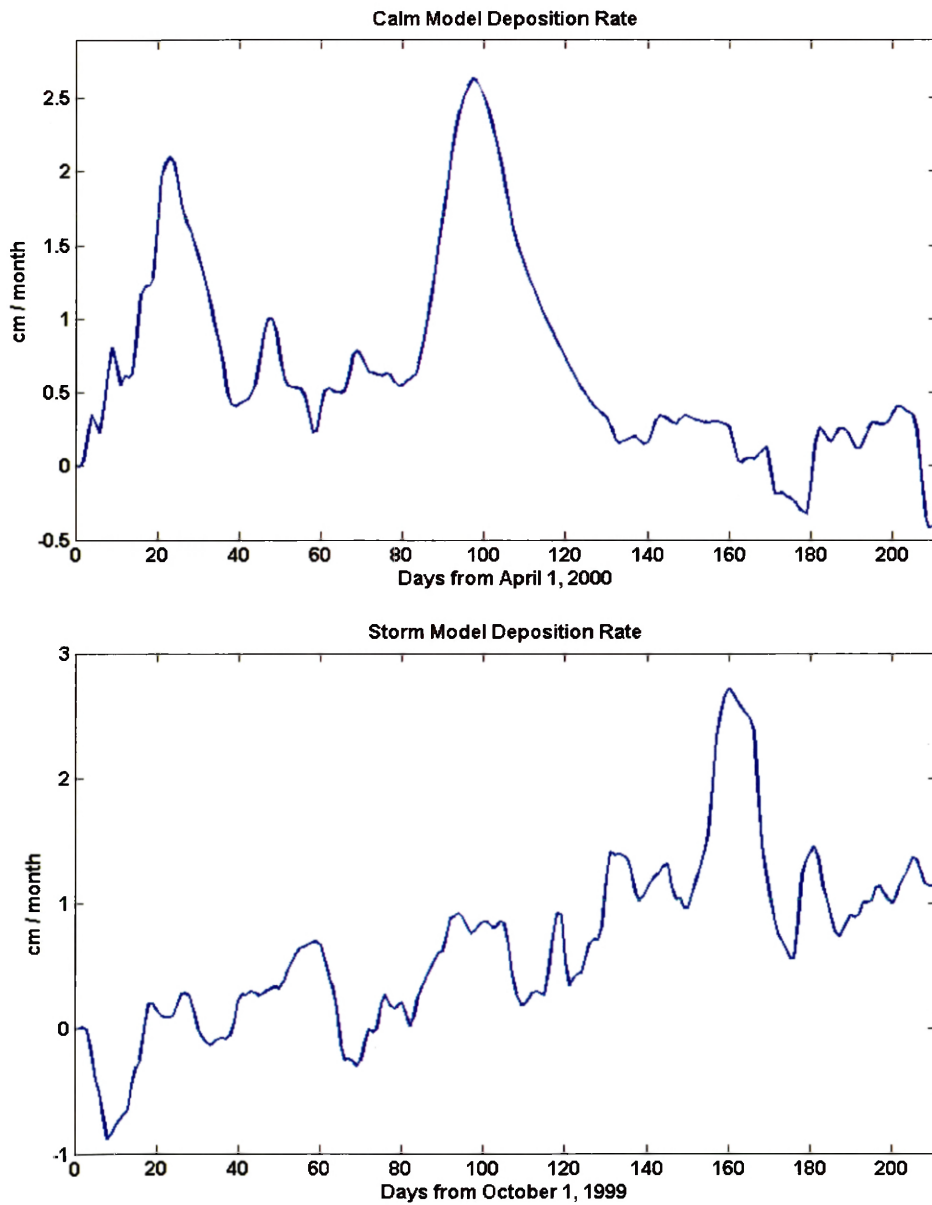


Figure 3-15. Calm Model Sensitivity to D_b

The final profiles for the calm model after seven months of model time are shown on the left for a ^7Be and on the right for ^{234}Th . The cases shown used a medium biodiffusion coefficient, $D_b=1\text{cm}^2\text{yr}^{-1}$, a high biodiffusion coefficient, $D_b=25\text{cm}^2\text{y}^{-1}$, and neglected biodiffusion. Also shown is Corbett *et al.*, 's (2004) profile from October, 2000. The thick black line shows the sediment – water interface and the dashed black line marks the level of the model's initial sediment – water interface.

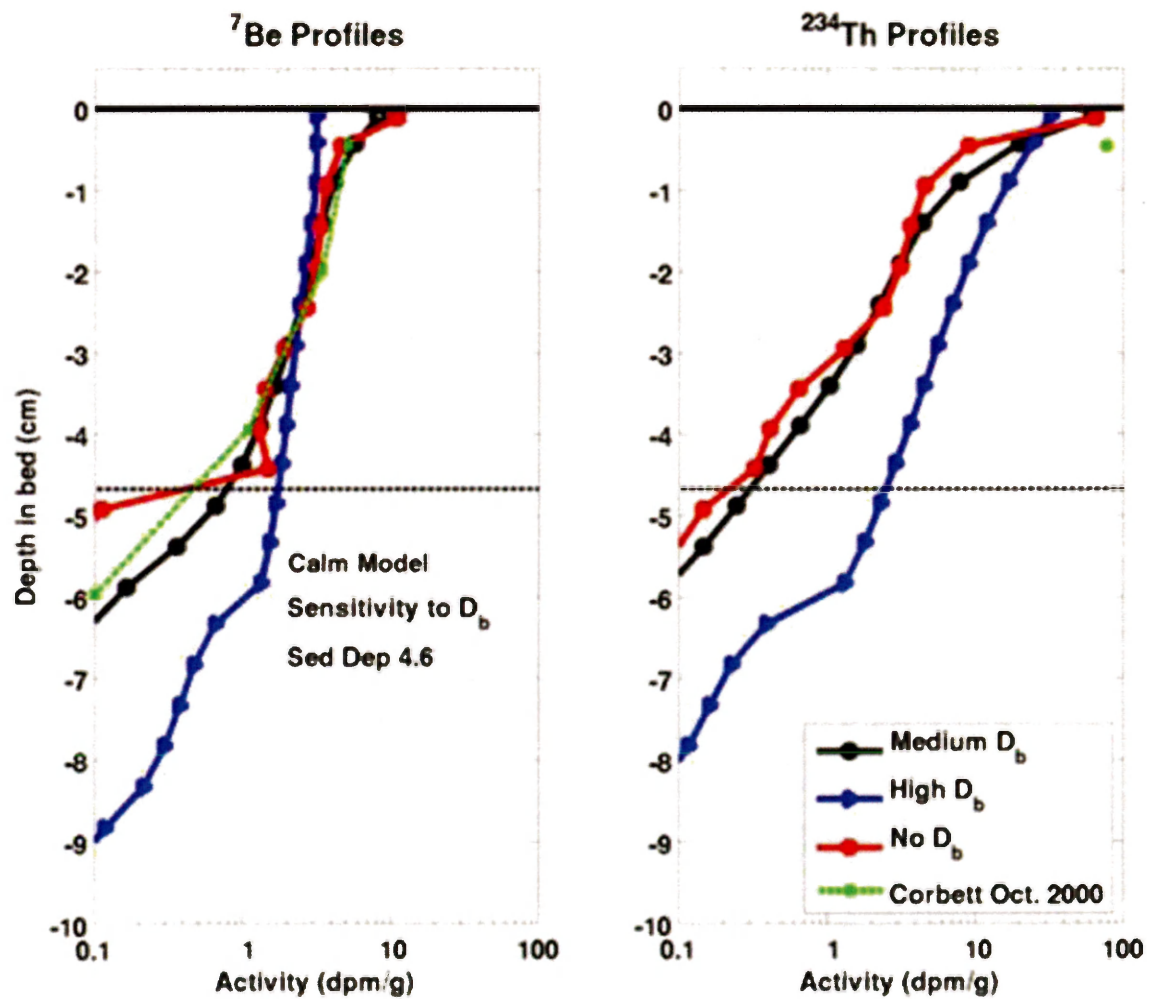


Figure 3-16. Storm Model Sensitivity to D_b

The final profiles for the storm model after seven months of model time are shown on the left for a ^7Be and on the right for ^{234}Th . The cases shown used a medium biodiffusion coefficient, $D_b=1\text{cm}^2\text{yr}^{-1}$, a high biodiffusion coefficient, $D_b=25\text{cm}^2\text{y}^{-1}$, and neglected biodiffusion. Also shown is Corbett *et al.*,’s (2004) profile from April, 2000. The thick black line shows the sediment – water interface and the dashed black line marks the level of the model’s initial sediment – water interface.

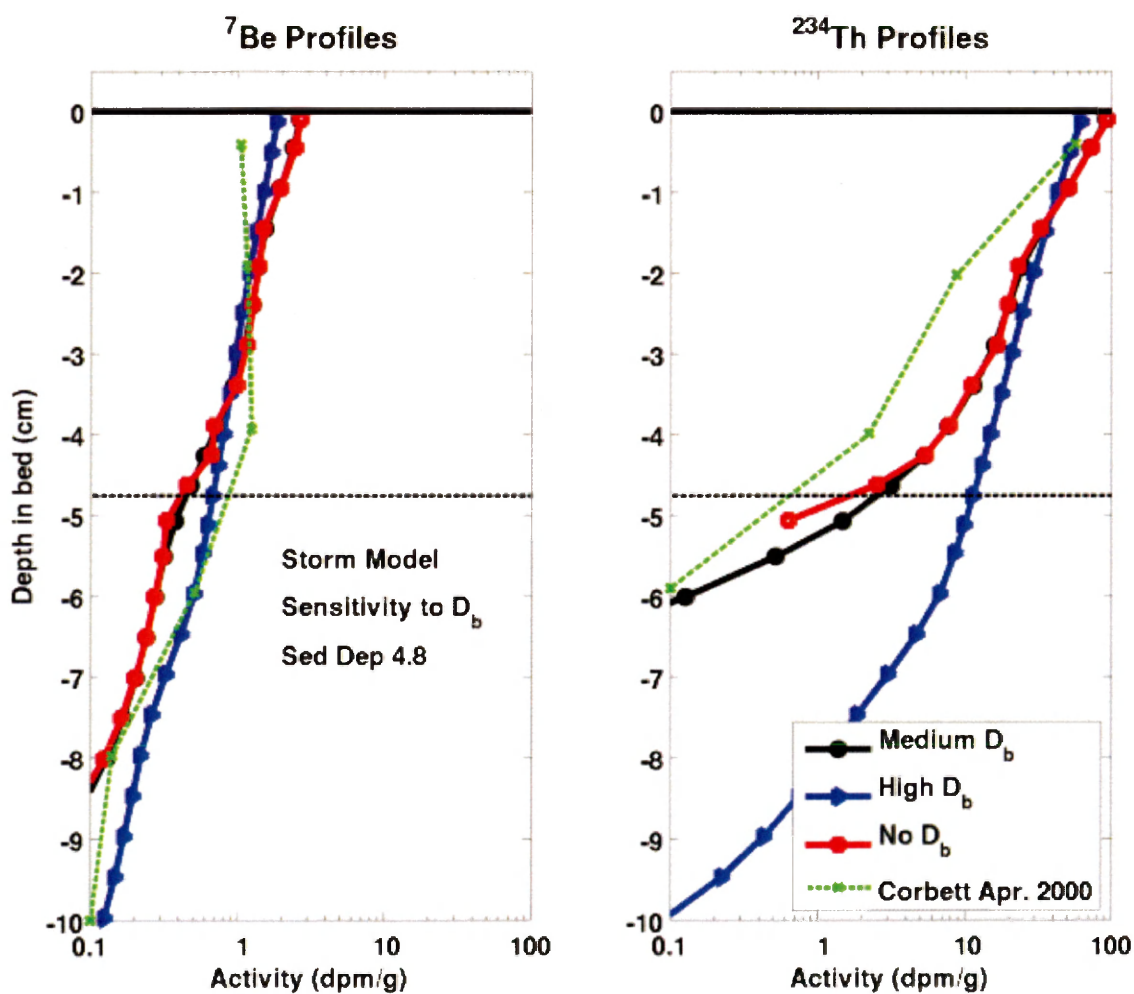


Figure 3-17: Calm Model Sensitivity to Deposition

The final profiles for the calm model after seven months of model time are shown on the left for a ^7Be and on the right for ^{234}Th . The cases shown are the standard model, a high deposition case, and a high erosion case. Also shown is Corbett *et al.*'s (2004) profile from October, 2000. The thick black line shows the sediment – water interface.

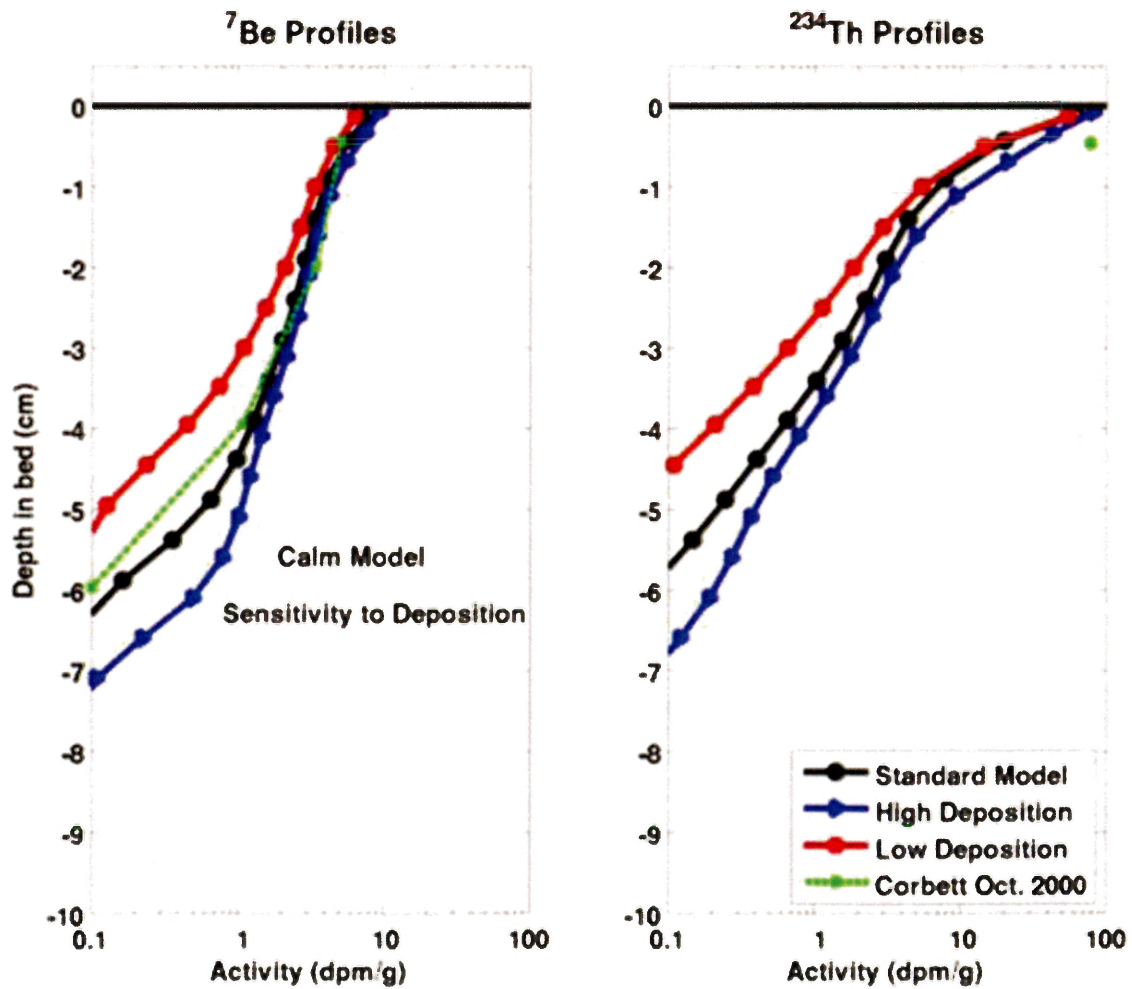
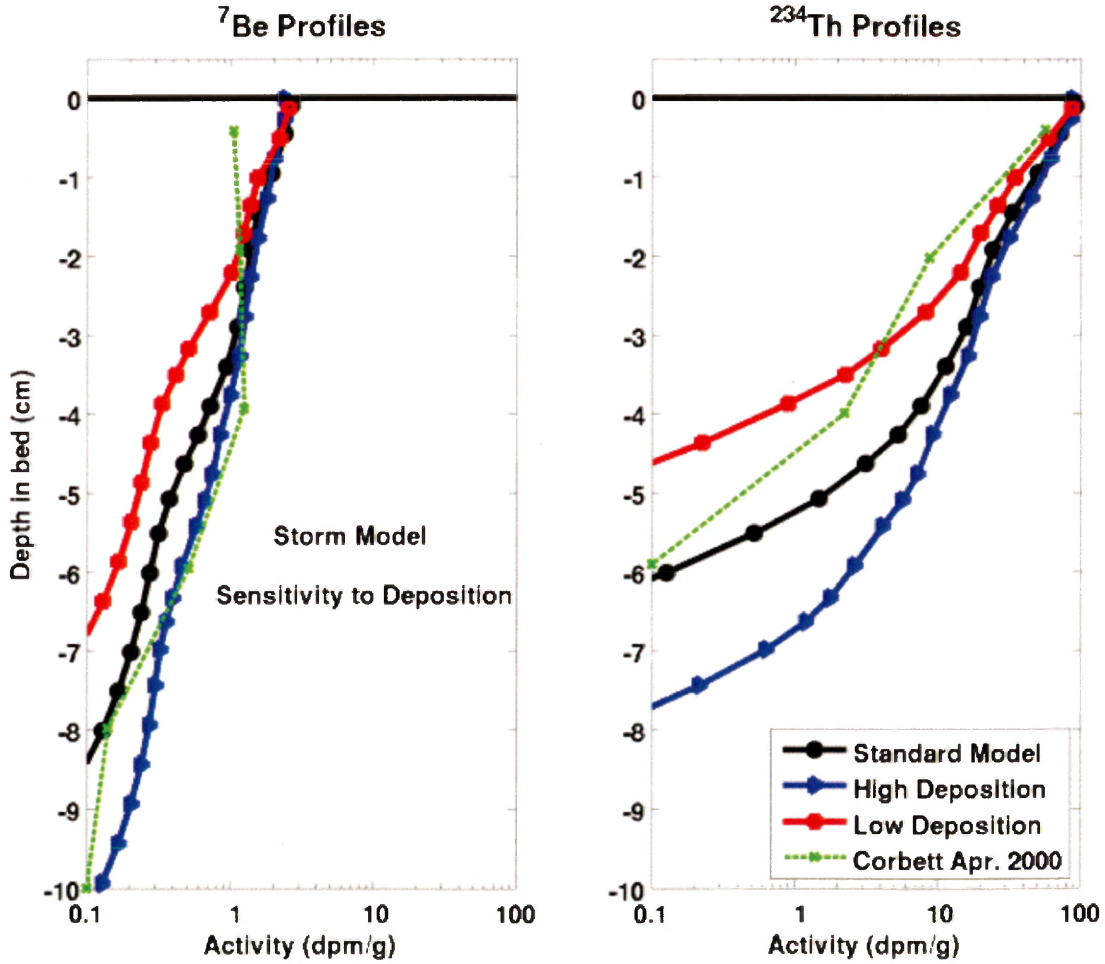


Figure 3-18: Storm Model Sensitivity to Deposition

The final profiles for the storm model after seven months of model time are shown on the left for a ^7Be and on the right for ^{234}Th . The cases shown are the standard model, a high deposition case, and a high erosion case. Also shown is Corbett *et al.*, 's (2004) profile from October, 2000. The thick black line shows the sediment – water interface.



CHAPTER 4: Summary and Future Directions

This thesis describes the development and application of a novel numerical model that resolves both sediment transport and geochronological tracers. The numerical model was written as an extension of the Community Sediment Transport Modeling System (CSTMS) within the Regional Ocean Modeling System (ROMS). The models presented in the thesis considered flood and storm deposition, and used both grain size and geochronological tracers as the markers for event beds. When using radioisotopes, event beds were identified based on the penetration depths and surface activities of the vertical profiles of geochronological tracers. Two short-lived radioisotopes were resolved in the model, both of which have half-lives on the order of a few months; ^7Be provided a tracer for flood deposition, while ^{234}Th provided evidence of recent resuspension.

Chapter 2 of the thesis described the model itself in detail and presented an application of the model to an idealized timeseries of storm forcing. The “standard model” for this was designed to analyze the effect of a low biodiffusion coefficient, medium resuspension intensity and medium flood thickness on grain size and radioisotopic profiles of ^7Be and ^{234}Th over a year long period using idealized wave forcing. Sensitivity tests were designed to analyze the effects of varying the intensity of bioturbation by using biodiffusion coefficients that ranged from 0 to $25 \text{ cm}^2 \text{ yr}^{-1}$; varying the intensity of storm resuspension; and changing the initial flood deposit thicknesses.

The modeled flood deposits were evident as layers having a fining upward grain size profile and high radioisotope activities of both ^7Be and ^{234}Th . Biodiffusion and resuspension both mixed the surface sediments on the bed to impact the preservation of a detectable flood event bed. Resuspension also acted to enrich the bed in ^{234}Th . Based on both penetration depth and surface activities, the thick flood event bed was preserved longer than a thin flood event bed.

Chapter 3 described a case study examining the one-dimensional model within the context of field observations from the Mississippi delta region. Corbett *et al.*, (2004) analyzed radioisotope activity in the northern Gulf of Mexico offshore of the Mississippi River. Sediment cores were taken at 50 meters depth in April and October, 2000 and analyzed for ^7Be and ^{234}Th activity with depth in the seabed. Chapter 3 analyzed models that represented two time periods; the “Standard Calm Model” was run from April, 2000 to October, 2000 to capture the time of year predominated by low wave energy and river sediment discharge; while the “Standard Storm Model” was run from October, 1999 to April, 2000 to capture the time of year predominated by wave reworking. Both models used as input wave data from nearby buoys and the Mississippi River sediment discharge curve from Tarbert Landing. The one-dimensional model reproduced the radioisotope profiles measured by Corbett *et al.*, (2004) in April and October, 2000 offshore of the Southwest Pass of the Mississippi River. Calculated profiles of ^7Be and ^{234}Th were sensitive to the timing and amount of deposition of riverine sediment, and ^{234}Th was also sensitive to the amount of resuspension. Surface activity was impacted by recent

deposition and the radioisotope input activity and penetration depth was impacted by the initial profile, the total amount of sediment deposition and the bioturbation coefficient.

The modeling approach presented in this thesis lent itself to consideration of event bed preservability, and to examining the sensitivity of event bed characteristics to deposition, resuspension, and reworking processes, but neglected some important processes. For example, the version of the CSTMS used as our framework (Warner *et al.*, 2008) assumes that sediment behaves non-cohesively, because the critical shear stress and settling velocity are assigned as input, and remain constant. Because radioisotopic tracers are typically most useful in muds, however, the reactive tracers should also be implemented in the version of the CSTMS that accounts for cohesive sediment behavior, such as the consolidation and swelling model discussed in Rinehimer *et al.*, (2008). Additionally, the model presented here assumed that fluvial sediment and suspended sediment had constant, prescribed activities of ^7Be and ^{234}Th , respectively. Actually, the ^7Be activity of fluvial discharged sediment can vary depending on time of year and storage time in a river's drainage basin (Olsen *et al.*, 1986; Palinkas *et al.*, 2005), and ^{234}Th concentrations vary with salinity in river influenced shelves and in estuaries (Waples *et al.*, 2006). Later applications of the model might consider how variations in the activity of ^7Be and ^{234}Th in fluvially discharged sediment and within regions of freshwater influence impact flood and storm event bed characteristics. Also, our study considered only two radioisotopes, but the modeling framework developed could be useful for evaluating the sediment profiles expected for other geochronological tracers.

The next obvious step to take with the sediment transport-geochronological model, however, is to apply the approach to an established three-dimensional sediment transport model. Because the one-dimensional model does not directly resolve horizontal flux convergence and divergence, the timeseries for net erosion and deposition had to be applied in a somewhat ad hoc manner for the model results in Chapter 3. Within a three-dimensional sediment transport model, however, timeseries of sediment bed erosion and deposition would be calculated directly based on convergences and divergences in sediment flux. For example, Xu *et al.*, (2011) used a three-dimensional sediment-transport model to estimate fluvial sediment deposition and storm reworking for the northern Gulf of Mexico continental shelf offshore of the Mississippi and Atchafalaya Rivers. Addition of geochronological tracers to a similar model would provide a means of directly comparing model estimates to field observations, and for evaluating model parameterizations of values like bioturbation coefficients.

Implementation of the coupled geochronological – sediment transport model within the northern Gulf of Mexico would provide an interesting study area because the Mississippi River system is the largest river in the United States, discharges 2×10^{14} g of sediment annually, and drains 47% of the contiguous United States (Meade and Parker, 1985; Meade, 1996). The Mississippi serves as a prototype large river system in that its discharge events tend to persist for weeks or months at a time, and much of its proximal shelf is wide. Interestingly, the main discharge mouth of the Mississippi River, the Southwest Pass, empties onto a very narrow portion of the shelf and directly conveys into Mississippi Canyon (Wright and Coleman, 1974; Corbett *et al.*, 2006).

To contrast with the Gulf of Mexico, future research should also apply the coupled geochronological – sediment transport model to active margins, where small mountainous rivers deposit episodic flood layers that may have high potentials for preservation (Wheatcroft and Drake, 2003). Sites that have established sediment transport models include; the Waipaoa River shelf, New Zealand (Moriarty *et al.*, in revision) and the Eel River shelf, California (Harris *et al.*, 2005). Use of the coupled model to represent a continental shelf offshore of a small mountainous river would allow for consideration of factors that influence preservation potential of event beds there.

Application of the coupled sediment transport – geochronological model also lends itself to resolving the transport of contaminants that are associated with sediment. An example of this is on the Palos Verdes shelf, CA. This site is highly contaminated with DDT and PCBs due to wastewater discharge from chemical manufacturing in Los Angeles, CA (Lee *et al.*, 2002). On the shelf, the affected layer of sediment varies in thickness from 5 cm to greater than 60 cm (Eganhouse *et al.*, 2000). This contaminated site poses a risk to benthic organisms as well as many fish species that feed near the sediment bed or are exposed to these chemicals through the food chain. The numerical models developed for the Palos Verdes shelf, like Sherwood *et al.*, (2002), would benefit from directly resolving the suspended transport of the contaminant, sorption and desorption processes in the water column (i.e. Wiberg and Harris, 2002), and biodiffusion in the seabed. The methods described in Chapter 2 could be modified to account for these processes within the CSTMS and provide a tool useful for study of contaminants in

the marine environment to evaluate how contaminated sediments may be transported on the continental shelf and slope or buried by other sediments.

A continuing challenge in developing increasingly comprehensive numerical models is the need to choose a growing set of model parameters. Data assimilation techniques (Moore *et al.*, 2004) could be useful for optimizing the parameters such as the bioturbation coefficient, sediment deposition rate, and radioisotope activity input. This could enable a more direct method for estimating values for the model parameters, whereas the standard practice now is to do repeated model runs using a range of parameters, and then choose the parameter set that best matches available data such as measured radioisotope profiles.

Resolving geochronological tracers within a sediment-transport model is a novel approach. There has been extensive study of short-lived radioisotopes in the field to identify flood and storm event beds, characterize accumulation rates over a variety of timescales, and estimate bioturbation coefficients. Meanwhile, sediment-transport models have been applied in a variety of environments, coupled to ROMS as well as other modeling systems. But these sediment transport models calculated grain size, and not erosion and deposition. Linking the two together in our coupled model is an important step forward because it enables direct comparison between radioisotope observations from the field and sediment-transport simulations.

REFERENCES

- Aller, R.C. and J.K. Cochran, (1976). $^{234}\text{Th}/^{238}\text{U}$ Disequilibrium in near-shore sediment: Particle reworking and diagenetic time scales. *Earth and Planetary Science Letters*, 29, 37-50.
- Allison, M.A., G.C. Kineke, E.S. Gordon, and M.A. Goni, (2000). Development and reworking of a seasonal flood deposit on the inner continental shelf off the Atchafalaya River. *Continental Shelf Research*, 20, 2267–2294.
- Baskaran, M. and P.H. Santschi, (1993). The role of particles and colloids in the transport of radionuclides in coastal environments of Texas. *Marine Chemistry*, 43, 95-114.
- Baskaran, M., M. Ravichandran, and T.S. Bianchi, (1997). Cycling of ^7Be and ^{210}Pb in a high DOC, shallow, turbid estuary of south-east Texas. *Estuarine, Coastal and Shelf Science*, 45, 165-176.
- Bentley, S.J., T.R. Keen, C.A. Blain and W.C. Vaughan, (2002). The origin and preservation of a major hurricane event bed in the northern Gulf of Mexico: Hurricane Camille, 1969. *Marine Geology*, 186, 423-446.
- Bentley, S.J. and C.A. Nittrouer, (2003). Emplacement, modification, and preservation of event strata on a flood-dominated continental shelf: Eel shelf, Northern California. *Continental Shelf Research*, 23, 1465-1493.
- Bentley, S.J. and A. Sheremet, (2003). New model for the emplacement, bioturbation and preservation of fine-scaled sedimentary strata. *Geology*, 31, 725-728.

- Bever, A.J., C.K. Harris, C.R. Sherwood, and R.P. Signell, (2009). Deposition and flux of sediment from the Po River, Italy: An idealized and wintertime numerical modeling study. *Marine Geology*, 260, 69-80.
- Boudreau, B.P. (1994). Is burial velocity a master parameter for bioturbation? *Geochimica et Cosmochimica Acta*, 58, 1243-1249.
- Canuel, E.A., C.S. Martens, and L.K. Benninger, (1990). Seasonal variations in ^7Be activity in the sediments of Cape Lookout Bight, North Carolina. *Geochimica et Cosmochimica Acta*, 54, 237-245.
- Corbett, D.R., B.A. McKee, and D. Duncan, (2004). An evaluation of mobile mud dynamics in the Mississippi River deltaic region. *Marine Geology*, 209, 91-112.
- Corbett, R., B. McKee, and M. Allison, (2006). Nature of decadal-scale sediment accumulation on the western shelf of the Mississippi River delta. *Continental Shelf Research*, 26, 2125-2140.
- Corbett, D.R., M. Dail and B.A. McKee, (2007). High-frequency time-series of the dynamic sedimentation processes on the western shelf of the Mississippi River Delta. *Continental Shelf Research*, 27, 1600-1615.
- Drake, D.E. (1999). Temporal and spatial variability of the sediment grain-size distribution on the Eel shelf: the flood layer of 1995. *Marine Geology*, 154, 169-182.
- Drake, D.E. and D.A. Cacchione, (1985) Seasonal variation in sediment transport on the Russian River shelf, California. *Continental Shelf Research*, 4, 495-514.

- Eganhouse, R.P., J. Pontolillo, and T.J. Leiker, (2000). Diagenetic fate of organic contaminants on the Palos Verdes Shelf, California. *Marine Chemistry*, 70, 289-315.
- Feng, H., J.K. Cochran, and D.J. Hirschberg, (1999). ^{234}Th and ^7Be as tracers for the transport and dynamics of suspended particles in a partially mixed estuary. *Geochimica et Cosmochimica Acta*, 63, 2487-2505.
- Fennel, K., J. Wilkin, J. Levin, J. Moisan, J. O'Reilly, and D. Haidvogel, (2006). Nitrogen cycling in the Middle Atlantic Bight: Results from a three-dimensional model and implications for the North Atlantic nitrogen budget. *Global Biogeochemical Cycles*, 20, GB3007.
- Fennel, K., J. Hu, A. Laurent, M. Marta-Almeida, and R. Hetland, (2013). Sensitivity of hypoxia predictions for the northern Gulf of Mexico to sediment oxygen consumption and model nesting. *Journal of Geophysical Research Oceans*, 118, doi:10.1002/jgrc.20077.
- Frey, R.W. and S.G. Pemberton, (1990). Bioturbate Texture or Ichnofabric? *Palaios*, 5, 385-386.
- Fugate, D.C. and C.T. Friedrichs, (2002). Determining concentration and fall velocity of estuarine particle populations using ADV, OBS and LISST. *Continental Shelf Research*, 22, 1867-1886.
- Guillen, J., F. Bourrin, A. Palanques, X. Durrieu de Madron, P. Puig, and R. Buscail, (2006). Sediment dynamics during wet and dry storm events on the Tet inner shelf (SW Gulf of Lions). *Marine Geology*, 234, 129-142.

- Harris, C.K. and P.L. Wiberg, (1997). Approaches to quantifying long-term continental shelf sediment transport with an example from the northern California STRESS mid-shelf site. *Continental Shelf Research*, 17, 1389–1418.
- Harris, C.K. and P.L. Wiberg, (2001). A two-dimensional, time-dependent model of suspended sediment transport and bed reworking for continental shelves. *Computers & Geosciences*, 27, 675-690.
- Harris, C.K. and P.L. Wiberg, (2002). Across-shelf sediment transport: Interactions between suspended sediment and bed sediment. *Journal of Geophysical Research*, 107 (C1), 12.
- Harris, C.K., P.A. Traykovski, and W.R. Geyer, (2005). Flood dispersal and deposition by near-bed gravitational sediment flows and oceanographic transport: A numerical modeling study of the Eel River shelf, northern California. *Journal of Geophysical Research*, 110, C09025.
- Harris, C.K., C.R. Sherwood, R.P. Signell, A.J. Bever and J.C. Warner, (2008). Sediment dispersal in the northwestern Adriatic Sea. *Journal of Geophysical Research*, 113, C11S03.
- Harris, C.K., K. Fennel, R.D. Hetland, and R. Wilson, (2012). Coupling sediment transport to biogeochemical processes; effects of resuspension on oxygen consumption. *Ocean Sciences Meeting*, American Geophysical Union (AGU).
- Hetland, R.D. and S.F. DiMarco, (2008). How does the character of oxygen demand control the structure of hypoxia on the Texas-Louisiana continental shelf? *Journal of Marine Systems*, 70, 49-62.

- Kachel, N. and J.D. Smith, (1986). Geological impact of sediment transporting events on the Washington continental shelf, in *Shelf Sands and Sandstones*, edited by R.J. Knight and J.R. McLean, pp. 145-162, Canadian Society of Petroleum Geologists, Calgary, Alberta, 1986.
- Keen, T.R., S.J. Bentley, W.C. Vaughan, and C.A. Blain, (2004). The generation and preservation of multiple hurricane beds in the northern Gulf of Mexico. *Marine Geology*, 210, 79-105.
- Keen, T.R., Y. Furukawa, S.J. Bentley, R.L. Slingerland, W.J. Teague, J.D. Dykes and C.D. Rowley, (2006). Geological and oceanographic perspectives on event bed formation during Hurricane Katrina. *Geophysical Research Letters*, 33, L23614.
- Komar, P.D., R.H. Neudeck, and L.D. Kulm, (1972). Observations and significance of deep-water oscillatory ripple marks on the Oregon continental shelf. In: *Shelf Sediment Transport: Process and Pattern* (Eds D.J.P. Swift, D.B. Duane and O.H. Pilkey), pp. 601–624. Dowden, Hutchinson and Ross, Stroudsburg, PA.
- Lee, H.J., C.R. Sherwood, D.E. Drake, B.D. Edwards, F. Wong, and M. Hamer, (2002). Spatial and temporal distribution of contaminated, effluent-affected sediment on the Palos Verdes margin, southern California. *Continental Shelf Research*, 22, 859–880.
- Leithold, E.L. (1989). Depositional processes on an ancient and modern muddy shelf, northern California. *Sedimentology*, 36, 179-202.

- Ma, Y., C.T. Friedrichs, C.K. Harris, and L.D. Wright, (2010). Deposition by seasonal wave- and current-supported sediment gravity flows interacting with spatially varying bathymetry: Waiapu shelf, New Zealand. *Marine Geology*, 275, 199-211.
- McKee, B.A., C.A. Nittrouer, and D.J. DeMaster, (1983). Concepts of sediment deposition and accumulation applied to the continental shelf near the mouth of the Yangtze River. *Geology*, 11, 631-633.
- McKee, B.A., D.J. DeMaster, and C.A. Nittrouer, (1984). The use of $^{234}\text{Th}/^{238}\text{U}$ disequilibrium to examine the fate of particle-reactive species on the Yangtze continental shelf. *Earth and Planetary Science Letters*, 68, 431-442.
- Meade, R.H. (1996). River-sediment inputs to major deltas. In: Milliman, J., Haq, B. (Eds.), *Sea-Level Rise and Coastal Subsidence*. Kluwer Academic Publishing, London, pp. 63– 85.
- Meade, R., and R. Parker, (1985). Sediment in rivers of the United States. In: *National Water Summary 1984*. US Geological Survey, Water Supply Paper 2275, pp. 49– 60.
- Miller, M.C., I.N. McCave, and P.D. Komar, (1977). Threshold of sediment motion under unidirectional currents. *Sedimentology*, 24, 507-527.
- Moore, A.M., H.G. Arango, E. Di Lorenzo, B.D. Cornuelle, A.J. Miller, and D.J. Neilson, (2004). A comprehensive ocean prediction and analysis system based on the tangent linear and adjoint of a regional ocean model. *Ocean Modelling*, 7, 227-258.

- Moriarty, J.M., C.K. Harris, and M.G. Hadfield, (2014). A hydrodynamic and sediment transport model for the Waipaoa Shelf, New Zealand: Sensitivity of fluxes to spatially-varying erodibility and model nesting. *Journal of Marine Science and Engineering*, 2(2), 336-369; doi:10.3390/jmse2020336.
- Myrow, P.M. and Southard, J.B., (1996). Tempestite deposition. *Journal of Sedimentary Research*, Sect. A, 66, 875–887.
- Nittrouer, C.A., R.W. Sternberg, R. Carpenter, and J.T. Bennett, (1979). The use of ^{210}Pb geochronology as a sedimentological tool: application to the Washington continental shelf. *Marine Geology*, 31, 297–316.
- Nittrouer, C.A., and R.W. Sternberg, (1981). The formation of sedimentary strata in an allochthonous shelf environment: The Washington continental shelf. *Marine Geology*, 42, 201-232.
- Nittrouer, C.A., D.J. DeMaster, B.A. McKee, N.H. Cutshall, and I.L. Larson, (1984). The effect of sediment mixing on Pb-210 accumulation rates for the Washington continental shelf. *Marine Geology*, 54, 201-221.
- Nittrouer, C.A., D.J. DeMaster, S.A. Kuehl, B.A. McKee, and K.W. Thorbjarnarson, (1985). Some questions and answers about accumulation of fine-grained sediment in continental margin environments. *Geo-Marine Letters*, 4, 211–213.
- Nittrouer, C.A., and L.D. Wright, (1994). Transport of particles across continental shelves, *Reviews of Geophysics*, 32(1), 85–113.

- Olsen, C.R., I.L. Larsen, P.D. Lowry, N.H. Cutshall, and M.M. Nichols, (1986).
Geochemistry and Deposition of ^7Be in River-Estuarine and Coastal Waters.
Journal of Geophysical Research, 91, C1, 896-908.
- Palinkas, C.M., C.A. Nittrouer, R.A. Wheatcroft, and L. Langone, (2005). The use of ^7Be
to identify event and seasonal sedimentation near the Po River delta, Adriatic Sea.
Marine Geology, 222-223, 95-112.
- Palinkas, C.M., A.S. Ogston, and C.A. Nittrouer, (2010). Observations of event-scale
sedimentary dynamics with an instrumented bottom-boundary-layer tripod.
Marine Geology, 274, 151-164.
- Reed, C.W., A.W. Niedoroda, and D.J.P. Swift, (1999). Modeling sediment entrainment
and transport processes limited by bed armoring. *Marine Geology*, 154, 143-154.
- Reineck, H.-E. and I.B. Singh, (1972). Genesis of laminated sand and graded rhythmites
in storm-sand layers of shelf mud. *Sedimentology*, 18, 123–128.
- Richter, R. (1952). Fluidal-Textur in Sediment-Gesteinen und über Sedifluktion
überhaupt. Notizbl. Hess. Landesamtes Bodenforsch. Wiesbaden, 6, 67–81.
- Rinehimer, J.P., C.K. Harris, C.R. Sherwood, and L.P. Sanford, (2008). Estimating
cohesive sediment erosion and consolidation in a muddy, tidally-dominated
environment: model behavior and sensitivity. In *Estuarine and Coastal Modeling,*
Proceedings of the Tenth Conference, November 5–7, Newport, RI.
- Sanford, L.P. and J.P.-Y. Maa, (2001). A unified erosion formulation for fine sediments.
Marine Geology, 179, 9-23.

- Sherwood, C.R., B. Butman, D.A. Cacchione, D.E. Drake, T.F. Gross, R.W. Sternberg, P.L. Wiberg and A.J. Williams III, (1994). Sediment transport events on the northern California shelf during the 1990–1991 STRESS experiment. *Continental Shelf Research*, 14, 1063–1099.
- Sherwood, C.R., D.E. Drake, P.L. Wiberg, and R.A. Wheatcroft, (2002). Prediction of the fate of *p,p'*-DDE in sediment on the Palos Verdes shelf, California, USA. *Continental Shelf Research*, 22, 1025–1058.
- Sherwood, C.R., C.K. Harris, J.P. Rinehimer, A. Aretxabaleta, and B. Ferre, (In Prep.) Cohesive and mixed sediment bed model: Extension of the Community Sediment Transport Modeling System. In Prep. for *Journal of Marine Systems*.
- Sommerfield, C.K. and C.A. Nittrouer, (1999). Modern accumulation rates and a sediment budget for the Eel shelf: a flood-dominated depositional environment. *Marine Geology*, 154, 227-241.
- Sommerfield, C.K., C.A. Nittrouer, and C.R. Alexander, (1999). ⁷Be as a tracer of flood sedimentation on the northern California continental margin. *Continental Shelf Research*, 19, 225-361.
- Walsh, J.P., D.R. Corbett, D. Mallinson, M. Goni, M. Dail, C. Loewy, K. Marciniak, K. Ryan, C. Smith, A. Stevens, B. Sumners and T. Tesi, (2006). Mississippi Delta Mudflow Activity and 2005 Gulf Hurricanes. *EOS*, 87, 477-478.
- Waples, J.T., C. Benitez-Nelson, N. Savoye, M. Rutgers van der Loeff, M. Baskaran, and O. Gustafsson, (2006). An introduction to the application and future use of ²³⁴Th in aquatic systems. *Marine Chemistry*, 100, 166-189.

- Warner, J.C., C.R. Sherwood, R.P. Signell, C.K. Harris, and H.G. Arango, (2008).
Development of a three-dimensional, regional, coupled wave, current, and
sediment-transport model. *Computers & Geosciences*, 34, 1284-1306.
- Wheatcroft, R.A. (1990). Preservation potential of sedimentary event layers. *Geology*, 18,
843-845.
- Wheatcroft, R.A. (2000). Oceanic flood sedimentation: a new perspective. *Continental
Shelf Research*, 20, 2059-2066.
- Wheatcroft, R.A. (2006). Time-series measurements of macrobenthos abundance and
sediment bioturbation intensity on a flood-dominated shelf. *Progress in
Oceanography*, 71, 88-122.
- Wheatcroft, R.A., P.A. Jumars, C.R. Smith, and A.R.M. Nowell, (1990). A mechanistic
view of the particulate biodiffusion coefficient: Step lengths, rest periods and
transport directions. *Journal of Marine Research*, 48, 177-207.
- Wheatcroft, R.A. and D.E. Drake, (2003). Post-depositional alteration and preservation of
sedimentary event layers on continental margins, I. The role of episodic
sedimentation. *Marine Geology*, 199, 123-137.
- Wheatcroft R. A., et al., (2007). In *Continental-margin sedimentation: from sediment
transport to sequence stratigraphy*, Post-depositional alteration and preservation
of sedimentary strata, Eds Nittrouer C. A., Austin J. A., Field M. E., Kravitz J. H.,
Syvitski J. P. M., Wiberg P. L. (Blackwell, Malden, MA) International
Association of Sedimentologists Special Publication no. 37, pp 101–155.

- Wiberg, P.L. (2000). A perfect storm: the formation and preservation of storm beds on the continental shelf. *Oceanography*, 13, 93–99.
- Wiberg, P.L., D.E. Drake, and D.A. Cacchione, (1994). Sediment resuspension and bed armoring during high bottom stress events on the northern California inner continental shelf: measurements and predictions. *Continental Shelf Research*, 14, 1191–1219.
- Wiberg, P.L., and C.K. Harris, (2002). Desorption of *p,p'*-DDE from sediment during resuspension events on the Palos Verdes shelf, California: a modeling approach. *Continental Shelf Research*, 22, 1005–1023.
- Wright, L.D., and J.M. Coleman, (1974). Mississippi River mouth processes: effluent dynamics and morphologic development. *Journal of Geology*, 82, 751–778.
- Wright, L.D., and C.A. Nittrouer, (1995). Dispersal of river sediments in coastal seas—6 contrasting cases. *Estuaries* 18, 494–508.
- Xu, K., C.K. Harris, R.D. Hetland, and J.M. Kaihatu, (2011). Dispersal of Mississippi and Atchafalaya sediment on the Texas-Louisiana shelf: Model estimates for the year 1993. *Continental Shelf Research*, 31, 1558-1575.
- Xu, K, D.R. Corbett, J.P. Walsh, D. Young, K.B. Briggs, G.M. Cartwright, C.T. Friedrichs, C.K. Harris, R.C. Mickey, and S. Mitra, (In Prep). Seabed erodibility variations on the Louisiana continental shelf before and after the 2011 Mississippi River flood. In Prep. for *Estuarine, Coastal and Shelf Science*.

APPENDIX: Model Input Files

This appendix contains input files for the ROMS model runs described in Chapters Two and Three. The input text files, including `sedbiotoy.h`, `ocean_sedbiotoy.in` and `sediment_sedbio.in`, are included. These files, as well as NetCDF input files, NetCDF output files and model animations are contained on the attached CD:

Chapter 2:

Input Text Files:

- `ana_wwave.h` – Model wave forcing file
- `build.bash` – ROMS model compiling script
- `sedbiotoy.h` – ROMS C-preprocessing options file
- `ocean_sedbiotoy_001.in` – ROMS standard input parameters file
- `sediment_sedbio_lowDb.in` – ROMS sediment model parameters

Input NetCDF Files:

- `fre_sedbiotoy.nc` – NetCDF file providing forcing conditions
- `roms_sedbiotoy_grd.nc` – NetCDF file providing model grid
- `roms_sedbiotoy_ini_sed_med.nc` – NetCDF file providing initial conditions for the standard model

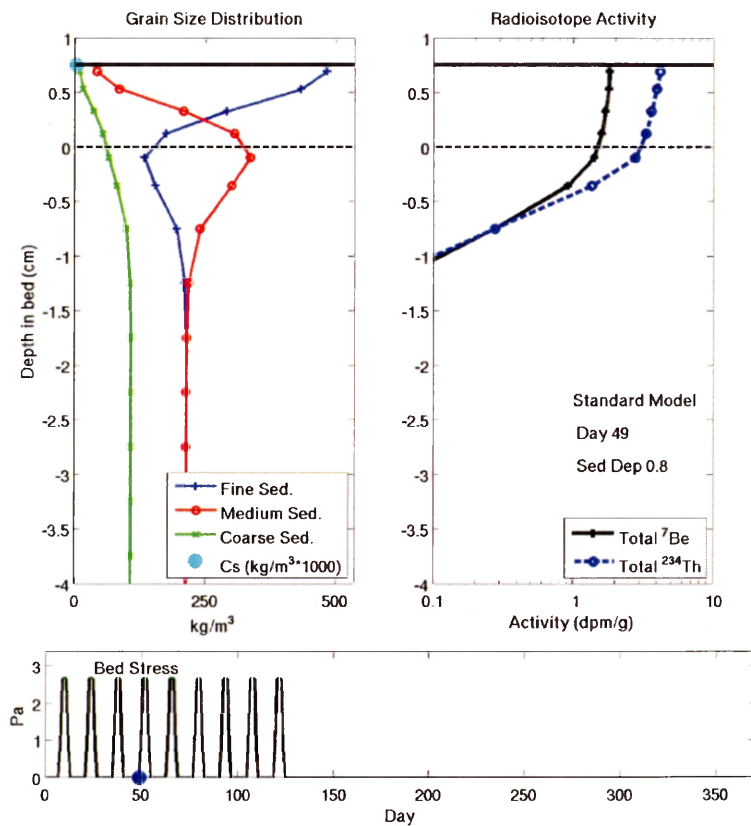
Output NetCDF Files:

- `his_sedbiotoy_001.nc` – Model output history file for the standard model
- `his_sedbiotoy_002.nc` – Model output history file for Model run 2
- `his_sedbiotoy_003.nc` – Model output history file for Model run 3
- `his_sedbiotoy_004.nc` – Model output history file for Model run 4
- `his_sedbiotoy_005.nc` – Model output history file for Model run 5
- `his_sedbiotoy_006.nc` – Model output history file for Model run 6
- `his_sedbiotoy_007.nc` – Model output history file for Model run 7
- `his_sedbiotoy_008.nc` – Model output history file for Model run 8

Model Animation:

`Ch2Standard.mp4` – Animation of the Standard Model presented in Section 2.5.1. See Figure A-1.

Figure A-1: One frame of the animation showing sediment bed calculations for the Standard Model. The left panel shows seabed concentrations for the three sediment types and near-bed suspended sediment concentrations. The right panel shows calculated radioisotope activities. On each profile, the depth in the bed is shown relative to instantaneous sediment – water interface, shown by the thick black line at $z_{bed} = 0$. The dashed black line marks the location of the initial sediment - water interface. The bottom panel shows the bed stress timeseries; the blue circle moves along the timeseries as the animation moves forward in time.



Chapter 3:

Input Text Files:

ana_stflux.h – Model surface tracer flux file
build.bash – ROMS model compiling script
sedbiotoy.h – ROMS C-preprocessing options file
ocean_sedbiotoy.in – ROMS standard input parameters file
sediment_sedbio.in – ROMS sediment model parameters

Input NetCDF Files:

frc_sedbiotoy_waves2.nc – NetCDF file providing physical forcing conditions
roms_sedbiotoy_grd.nc – NetCDF file providing model grid
roms_sedbiotoy_ini_sed_apr1.nc – NetCDF file providing initial conditions for the
standard calm model
roms_sedbiotoy_ini_sed_oct1.nc – NetCDF file providing initial conditions for the
standard storm model

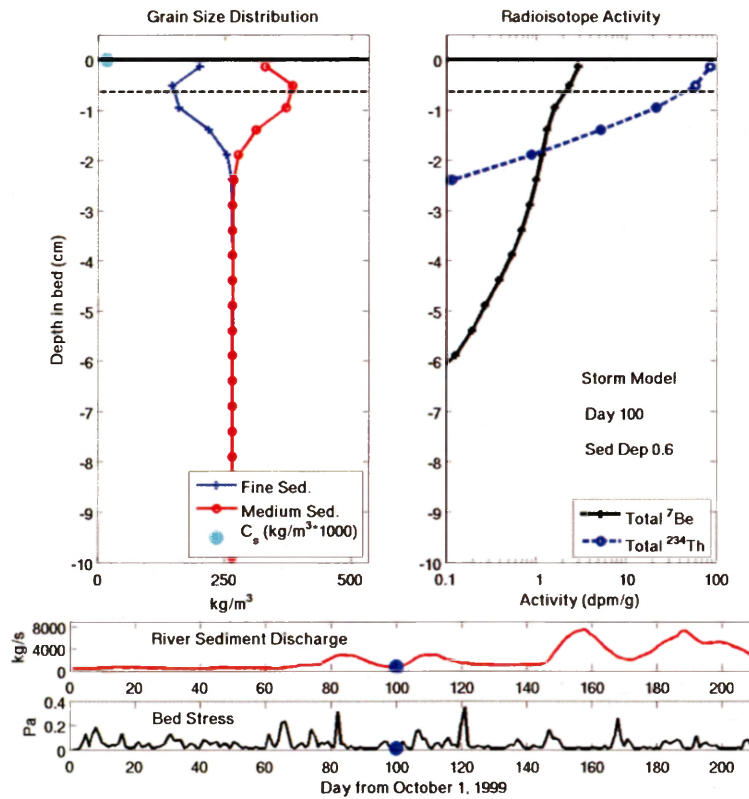
Output NetCDF Files:

his_sedbiotoy_012.nc – Model output history file for the standard calm model
his_sedbiotoy_013.nc – Model output history file for the high D_b calm model
his_sedbiotoy_014.nc – Model output history file for the low D_b calm model
his_sedbiotoy_015.nc – Model output history file for the high deposition calm model
his_sedbiotoy_021.nc – Model output history file for the low deposition calm model
his_sedbiotoy_016.nc – Model output history file for the standard storm model
his_sedbiotoy_017.nc – Model output history file for the high D_b storm model
his_sedbiotoy_018.nc – Model output history file for the low D_b storm model
his_sedbiotoy_019.nc – Model output history file for the high deposition storm model
his_sedbiotoy_020.nc – Model output history file for the low deposition storm model

Model Animations:

Ch3Calm.mp4 – Animation of the Standard Calm Model presented in Section
3.5.1. See Figure A-2.
Ch3Storm.mp4 – Animation of the Standard Storm Model presented in Section
3.5.2. See Figure A-2.

Figure A-2: One frame of the animation showing sediment bed calculations for the Standard Storm Model (Standard Calm Model animation is similar). The left panel shows seabed concentrations for the two sediment types and near-bed suspended sediment concentrations. The right panel shows calculated radioisotope activities. On each profile, the depth in the bed is shown relative to instantaneous sediment – water interface, shown by the thick black line at $z_{bed} = 0$. The dashed black line marks the location of the initial sediment - water interface. The bottom panel shows the river sediment discharge and bed stress timeseries; the blue circle moves along the timeseries as the animation moves forward in time.



sedbiotoy.h

```
/*
** One-dimensional (vertical) Sediment Biology Test.
*/
#define SG_4
#undef CONTINUOUS_DEP
#undef EPISODIC_DEP
#undef STORM
#define FLOOD
#undef ERO
#define DEP
#undef SEDBIO_COUP
#define SED_GEOCH
#define SEDGEO_TOY
#undef BIO_TOY
#define SED_BIODIFF
#define SEDTR_REACTIONS

#define UV_ADV
#undef UV_SADVECTION
#define UV_COR
#undef UV_QDRAG
/* define only one of the four following */
#undef UV_LOGDRAG
#undef MB_BBL
#undef SG_BBL
#define SSW_BBL
#define SSW_CALC_UB
#ifdef SG_BBL
# define SG_CALC_ZNOT
# undef SG_LOGINT
#endif
#ifdef MB_BBL
# define MB_CALC_ZNOT
# undef MB_ZOBIO
# undef MB_ZOBL
# undef MB_ZORIP
#endif
#ifdef SSW_BBL
# define SSW_CALC_ZNOT
# undef SSW_LOGINT
# undef SSW_ZORIP
#endif
#if defined MB_BBL || defined SG_BBL || defined SSW_BBL
# undef ANA_WWAVE
#endif
#define DJ_GRADPS
#define UV_VIS2
#define MIX_S_UV /* momentum mixing on s-surfaces */
#define TS_DIF2
#define MIX_GEO_TS /* tracer mixing on constant z surfaces */
#define TS_MPDATA
#undef TS_U3HADVECTION
#undef TS_C4VADVECTION
#define SOLAR_SOURCE
#define DIURNAL_SRFLUX
#define NONLIN_EOS
#define SALINITY
#define SPLINES
#undef TCLIMATOLOGY
```

```

#undef TCLM_NUDGING
#define AVERAGES
#define AVERAGES_FLUXES
#define AVERAGES_AKV
#define AVERAGES_AKT
#undef AVERAGES_AKS
#define SOLVE3D
#define EW_PERIODIC /*east-west periodic b.c.*/
#define NS_PERIODIC /* north-south periodic b.c.*/
#undef LMD_MIXING
#define MY25_MIXING
#undef GLS_MIXING
#ifdef MY25_MIXING
# define N2S2_HORAVG
# define KANTHA_CLAYSON
#endif
#ifdef GLS_MIXING
# define KANTHA_CLAYSON
# undef CANUTO_A
# define N2S2_HORAVG
#endif
#ifdef LMD_MIXING
# define LMD_RIMIX
# define LMD_CONVEC
# define LMD_SKPP
# define LMD_BKPP
# define LMD_NONLOCAL
#endif
#undef BIO_FENNEL
#undef OXYGEN
#ifdef BIO_FENNEL
# undef CARBON
# define DENITRIFICATION
# define BIO_SEDIMENT
# define DIAGNOSTICS_BIO
#endif
#undef ECOSIM
# define ANA_SPFLUX
# define ANA_BPFLUX
#define BULK_FLUXES
#ifdef BULK_FLUXES
# define EMINUSP
# undef LONGWAVE
# undef ANA_RAIN
#else
# define ANA_SMFLUX
# define ANA_STFLUX
#endif
#if defined BULK_FLUXES || defined ECOSIM
# undef ANA_CLOUD
# undef PAPA_CLM
#endif
#undef ANA_SSFLUX
#define ANA_BSFLUX
#define ANA_BTFLUX
# define ANA_STFLUX
# define ANA_SMFLUX
# undef TS_PSOURCE
# undef UV_PSOURCE
#define SEDIMENT

```

```
#ifdef SEDIMENT
#  define SUSPLOAD
#  undef RIVER_SEDIMENT
#  undef ANA_SEDIMENT
#endif
#define BODYFORCE
```

ocean_sedbiotoy.in

```
!
! ROMS/TOMS Standard Input parameters.
!
!svn $Id: ocean_bio_toy.in 29 2007-04-23 19:23:26Z arango $
!===== Hernan G. Arango =====
! Copyright (c) 2002-2007 The ROMS/TOMS Group
! Licensed under a MIT/X style license
! See License_ROMS.txt
!=====
!
! Input parameters can be entered in ANY order, provided that the parameter
! KEYWORD (usually, upper case) is typed correctly followed by "=" or "=="
! symbols. Any comment lines are allowed and must begin with an exclamation
! mark (!) in column one. Comments may appear to the right of a parameter
! specification to improve documentation. All comments will ignored during
! reading. Blank lines are also allowed and ignored. Continuation lines in
! a parameter specification are allowed and must be preceded by a backslash
! (\). In some instances, more than one value is required for a parameter.
! If fewer values are provided, the last value is assigned for the entire
! parameter array. The multiplication symbol (*), without blank spaces in
! between, is allowed for a parameter specification. For example, in a two
! grids nested application:
!
!     AKT_BAK == 2*1.0d-6  2*5.0d-6           ! m2/s
!
! indicates that the first two entries of array AKT_BAK, in fortran column-
! major order, will have the same value of "1.0d-6" for grid 1, whereas the
! next two entries will have the same value of "5.0d-6" for grid 2.
!
! In multiple levels of nesting and/or multiple connected domains step-ups,
! "Ngrids" entries are expected for some of these parameters. In such case,
! the order of the entries for a parameter is extremely important. It must
! follow the same order (1:Ngrids) as in the state variable declaration. The
! USER may follow the above guidelines for specifying his/her values. These
! parameters are marked by "==" plural symbol after the KEYWORD.
!
!=====
!
! Application title.
!
!     TITLE = ROMS3.0 sedbio_coup
!
! C-preprocessing Flag.
!
!     MyAppCPP = SEDBIOTOY
!
! Input variable information file name. This file needs to be processed
! first so all information arrays can be initialized properly.
!
!     VARNAME = ./External/varinfo.dat
!
! Grid dimension parameters. See notes below in the Glossary for how to set
! these parameters correctly.
!
!     Lm == 4           ! Number of I-direction INTERIOR RHO-points
!     Mm == 4           ! Number of J-direction INTERIOR RHO-points
!     N  == 30          ! Number of vertical levels
!
!     Nbed = 40         ! Number of sediment bed layers
```

```

        NAT = 2           ! Number of active tracers (usually, 2)
        NPT = 0           ! Number of inactive passive tracers
        NCS = 3           ! Number of cohesive (mud) sediment tracers
        NNS = 0           ! Number of non-cohesive (sand) sediment tracers

! Domain decomposition parameters for serial, distributed-memory or
! shared-memory configurations used to determine tile horizontal range
! indices (Istr,Iend) and (Jstr,Jend), [1:Ngrids].

        NtileI == 1           ! I-direction partition
        NtileJ == 1           ! J-direction partition

! Time-Stepping parameters.

        NTIMES == 67681      ! 210 days (Apr-Oct), first time step 34081
        DT == 540.0d0      ! 160 ts per day
        NDTFAST == 30

! Model iteration loops parameters.

        ERstr = 1
        ERend = 1
        Nouter = 1
        Ninner = 1
        Nintervals = 1

! Number of eigenvalues (NEV) and eigenvectors (NCV) to compute for the
! Lanczos/Arnoldi problem in the Generalized Stability Theory (GST)
! analysis. NCV must be greater than NEV (see documentation below).

        NEV = 2           ! Number of eigenvalues
        NCV = 10          ! Number of eigenvectors

! Input/Output parameters.

        NRREC == 0
        LcycleRST == T
        NRST == 1600
        NSTA == 1
        NFLT == 1
        NINFO == 1

! Output history, average, diagnostic files parameters.

        LDEFOUT == T
        NHIS == 160
        NDEFHIS == 0
        NTSAVG == 1
        NAVG == 160
        NDEFAVG == 0
        NTSDIA == 1
        NDIA == 160
        NDEFDIA == 0

! Output tangent linear and adjoint models parameters.

        LcycleTLM == F
        NTLM == 80
        NDEFTLM == 0

```

```

LcycleADJ == F
  NADJ == 80
  NDEFADJ == 0

! Output check pointing GST restart parameters.

  LrstGST = F                ! GST restart switch
  MaxIterGST = 500          ! maximum number of iterations
  NGST = 10                 ! check pointing interval

! Relative accuracy of the Ritz values computed in the GST analysis.

  Ritz_tol = 1.0d-15

! Harmonic/biharmonic horizontal diffusion of tracer: [1:NAT+NPT,Ngrids].

  TNU2 == 0.0d0 0.0d0      ! m2/s
  TNU4 == 2*0.0d0          ! m4/s

! Harmonic/biharmonic, horizontal viscosity coefficient: [Ngrids].

  VISC2 == 50.0d0          ! m2/s
  VISC4 == 4.0d+8          ! m4/s

! Vertical mixing coefficients for active tracers: [1:NAT+NPT,Ngrids]

  AKT_BAK == 1.0d-6 1.0d-6 ! m2/s

! Vertical mixing coefficient for momentum: [Ngrids].

  AKV_BAK == 1.0d-5        ! m2/s

! Turbulent closure parameters.

  AKK_BAK == 5.0d-6        ! m2/s
  AKP_BAK == 5.0d-6        ! m2/s
  TKENU2 == 0.0d0         ! m2/s
  TKENU4 == 0.0d0         ! m4/s

! Generic length-scale turbulence closure parameters.

  GLS_P == 3.0d0           ! K-epsilon
  GLS_M == 1.5d0
  GLS_N == -1.0d0
  GLS_Kmin == 7.6d-6
  GLS_Pmin == 1.0d-12

  GLS_CMU0 == 0.5477d0
  GLS_C1 == 1.44d0
  GLS_C2 == 1.92d0
  GLS_C3M == -0.4d0
  GLS_C3P == 1.0d0
  GLS_SIGK == 1.0d0
  GLS_SIGP == 1.30d0

! Constants used in surface turbulent kinetic energy flux computation.

  CHARNOK_ALPHA == 1400.0d0 ! Charnok surface roughness
  ZOS_HSIG_ALPHA == 0.5d0   ! roughness from wave amplitude
  SZ_ALPHA == 0.25d0        ! roughness from wave dissipation

```

```

        CRGBAN_CW == 100.0d0          ! Craig and Banner wave breaking

! Constants used in momentum stress computation.

        RDRG == 3.0d-04              ! m/s
        RDRG2 == 3.0d-03             ! nondimensional
        Zob == 0.003d0               ! m - changed per K. Xu model
        Zos == 0.02d0                ! m

! Height (m) of atmospheric measurements for Bulk fluxes parameterization.

        BLK_ZQ == 10.0d0             ! air humidity
        BLK_ZT == 10.0d0             ! air temperature
        BLK_ZW == 10.0d0             ! winds

! Minimum depth for wetting and drying.

        DCRIT == 0.10d0              ! m

! Various parameters.

        WTYPE == 1
        LEVSFRC == 15
        LEVBFRC == 1

! Vertical S-coordinates parameters, [1:Ngrids].

        THETA_S == 5.0d0              ! 0 < THETA_S < 20
        THETA_B == 0.4d0              ! 0 < THETA_B < 1
        TCLINE == 50.0d0              ! m

! Mean Density and Brunt-Vaisala frequency.

        RHO0 = 1025.0d0               ! kg/m3
        BVF_BAK = 1.0d-5              ! 1/s2

! Time-stamp assigned for model initialization, reference time
! origin for tidal forcing, and model reference time for output
! NetCDF units attribute.

        DSTART = 972.0d0 !882.0d0          ! days
        TIDE_START = 0.0d0              ! days
        TIME_REF = 20000101.0d0         ! yyyyymmdd.dd

! Nudging/relaxation time scales, inverse scales will be computed
! internally, [1:Ngrids].

        TNUDG == 2*1.0d0               ! days
        ZNUDG == 0.0d0                 ! days
        M2NUDG == 0.0d0                ! days
        M3NUDG == 0.0d0                ! days

! Factor between passive (outflow) and active (inflow) open boundary
! conditions, [1:Ngrids]. If OBCFAC > 1, nudging on inflow is stronger
! than on outflow (recommended).

        OBCFAC == 0.0d0                ! nondimensional

! Linear equation of State parameters:

```

```

        R0 == 1027.0d0           ! kg/m3
        T0 == 10.0d0            ! Celsius
        S0 == 35.0d0            ! PSU
        TCOEF == 1.7d-4         ! 1/Celsius
        SCOEF == 7.6d-4         ! 1/PSU

! Slipperiness parameter: 1.0 (free slip) or -1.0 (no slip)

        GAMMA2 == 1.0d0

! Logical switches (TRUE/FALSE) to specify which variables to consider on
! tracers point Sources/Sinks (like river runoff): [1:NAT+NPT,Ngrids].
! See glossary below for details.

! LtracerSrc == T T           ! temperature, salinity, inert

! Starting (DstrS) and ending (DendS) day for adjoint sensitivity forcing.
! DstrS must be less or equal to DendS. If both values are zero, their
! values are reset internally to the full range of the adjoint integration.

        DstrS == 0.0d0           ! starting day
        DendS == 0.0d0           ! ending day

! Starting and ending vertical levels of the 3D adjoint state variables
! whose sensitivity is required.

        KstrS == 1               ! starting level
        KendS == 1               ! ending level

! Logical switches (TRUE/FALSE) to specify the adjoint state variables
! whose sensitivity is required.

Lstate(isFsur) == F           ! free-surface
Lstate(isUbar) == F           ! 2D U-momentum
Lstate(isVbar) == F           ! 2D V-momentum
Lstate(isUvel) == F           ! 3D U-momentum
Lstate(isVvel) == F           ! 3D V-momentum

! Logical switches (TRUE/FALSE) to specify the adjoint state tracer
! variables whose sensitivity is required (NT values are expected).

Lstate(isTvar) == F F         ! tracers

! Stochastic optimals time decorrelation scale (days) assumed for
! red noise processes.

        SO_decay == 2.0d0        ! days

! Logical switches (TRUE/FALSE) to specify the state surface forcing
! variable whose stochastic optimals is required.

S0state(isUstr) == T           ! surface u-stress
S0state(isVstr) == T           ! surface v-stress

! Logical switches (TRUE/FALSE) to specify the surface tracer forcing
! variable whose stochastic optimals is required (NT values are expected).

S0state(isTsur) == F F         ! surface tracer flux

! Stochastic optimals surface forcing standard deviation for

```



```

! dimensionalization.

SO_sdev(isUstr) == 1.0d0           ! surface u-stress
SO_sdev(isVstr) == 1.0d0           ! surface v-stress
SO_sdev(isTsur) == 1.0d0 1.0d0     ! NT surface tracer flux

! Logical switches (TRUE/FALSE) to activate writing of fields into
! HISTORY output file.

Hout(idUvel) == T                   ! 3D U-velocity
Hout(idVvel) == T                   ! 3D V-velocity
Hout(idWvel) == T                   ! 3D W-velocity
Hout(idOvel) == T                   ! omega vertical velocity
Hout(idUbar) == T                   ! 2D U-velocity
Hout(idVbar) == T                   ! 2D V-velocity
Hout(idFsur) == T                   ! free-surface
Hout(idBath) == T                   ! time-dependent bathymetry

Hout(idTvar) == T T                 ! temperature and salinity

Hout(idUsms) == T                   ! surface U-stress
Hout(idVsms) == T                   ! surface V-stress
Hout(idUbms) == T                   ! bottom U-stress
Hout(idVbms) == T                   ! bottom V-stress

Hout(idUbrs) == T                   ! bottom U-current stress
Hout(idVbrs) == T                   ! bottom V-current stress
Hout(idUbws) == T                   ! bottom U-wave stress
Hout(idVbws) == T                   ! bottom V-wave stress
Hout(idUbcs) == T                   ! bottom max wave-current U-stress
Hout(idVbcs) == T                   ! bottom max wave-current V-stress

Hout(idUbot) == T                   ! bed wave orbital U-velocity
Hout(idVbot) == T                   ! bed wave orbital V-velocity
Hout(idUbur) == F                   ! bottom U-velocity above bed
Hout(idVbvr) == F                   ! bottom V-velocity above bed

Hout(idW2xx) == F                   ! 2D radiation stress, Sxx component
Hout(idW2xy) == F                   ! 2D radiation stress, Sxy component
Hout(idW2yy) == F                   ! 2D radiation stress, Syy component
Hout(idU2rs) == F                   ! 2D radiation U-stress
Hout(idV2rs) == F                   ! 2D radiation V-stress
Hout(idU2Sd) == F                   ! 2D U-Stokes velocity
Hout(idV2Sd) == F                   ! 2D V-Stokes velocity

Hout(idW3xx) == F                   ! 3D radiation stress, Sxx component
Hout(idW3xy) == F                   ! 3D radiation stress, Sxy component
Hout(idW3yy) == F                   ! 3D radiation stress, Syy component
Hout(idW3zx) == F                   ! 3D radiation stress, Szx component
Hout(idW3zy) == F                   ! 3D radiation stress, Szy component
Hout(idU3rs) == F                   ! 3D U-radiation stress
Hout(idV3rs) == F                   ! 3D V-radiation stress
Hout(idU3Sd) == F                   ! 3D U-Stokes velocity
Hout(idV3Sd) == F                   ! 3D V-Stokes velocity

Hout(idWamp) == T                   ! wave height
Hout(idWlen) == T                   ! wave length
Hout(idWdir) == T                   ! wave direction
Hout(idWpbt) == T                   ! bottom wave period

```

```

Hout(idTsur) == T F      ! surface net heat and salt flux
Hout(idLhea) == T      ! latent heat flux
Hout(idShea) == T      ! sensible heat flux
Hout(idLrad) == T      ! longwave radiation flux
Hout(idSrad) == T      ! shortwave radiation flux
Hout(idevap) == F      ! evaporation rate
Hout(idrain) == F      ! precipitation rate

Hout(idDano) == T      ! density anomaly
Hout(idVvis) == T      ! vertical viscosity
Hout(idTdif) == T      ! vertical T-diffusion
Hout(idSdif) == T      ! vertical Salinity diffusion
Hout(idHsbl) == T      ! depth of surface boundary layer
Hout(idHbbl) == T      ! depth of bottom boundary layer
Hout(idMtke) == F      ! turbulent kinetic energy
Hout(idMtls) == F      ! turbulent length scale

! Logical switches (TRUE/FALSE) to activate writing of extra inert passive
! tracers other than biological and sediment tracers. An inert passive tracer
! is one that it is only advected and diffused. Other processes are ignored.
! These tracers include, for example, dyes, pollutants, oil spills, etc.
! NPT values are expected. However, these switches can be activated using
! compact parameter specification.

Hout(inert) == T      ! inert passive tracers

! Logical switches (TRUE/FALSE) to activate writing of exposed sediment
! layer properties into HISTORY output file. Currently, MBOTP properties
! are expected for the bottom boundary layer and/or sediment models:
!
!   Hout(idBott(isd50)),   isd50 = 1      ! mean grain diameter
!   Hout(idBott(idens)),   idens = 2      ! mean grain density
!   Hout(idBott(iwsed)),   iwsed = 3      ! mean settling velocity
!   Hout(idBott(itauc)),   itauc = 4      ! critical erosion stress
!   Hout(idBott(irlen)),   irlen = 5      ! ripple length
!   Hout(idBott(irhgt)),   irhgt = 6      ! ripple height
!   Hout(idBott(ibwav)),   ibwav = 7      ! wave excursion amplitude
!   Hout(idBott(izdef)),   izdef = 8      ! default bottom roughness
!   Hout(idBott(izapp)),   izapp = 9      ! apparent bottom roughness
!   Hout(idBott(izNik)),   izNik = 10     ! Nikuradse bottom roughness
!   Hout(idBott(izbio)),   izbio = 11     ! biological bottom roughness
!   Hout(idBott(izbfm)),   izbfm = 12     ! bed form bottom roughness
!   Hout(idBott(izbld)),   izbld = 13     ! bed load bottom roughness
!   Hout(idBott(izwbl)),   izwbl = 14     ! wave bottom roughness
!   Hout(idBott(iactv)),   iactv = 15     ! active layer thickness
!   Hout(idBott(ishgt)),   ishgt = 16     ! saltation height
!   Hout(idBott(idefx)),   idefx = 17     ! erosion flux
!   Hout(idBott(idnet)),   idnet = 18     ! erosion or deposition
!
!
!           1 1 1 1 1 1 1 1 1
!           1 2 3 4 5 6 7 8 9 0 1 2 3 4 5 6 7 8
Hout(idBott) == T T T T T T T T F F T F F T F F F

! Generic User parameters, [1:NUSER].

      NUSER = 0
      USER = 0.d0

! Input NetCDF file names, [1:Ngrids].

```

```

GRDNAME == ./External/roms_sedbiotoy_grd.nc
ININAME == ./External/roms_sedbiotoy_ini_sed_apr1.nc
ITLNAME == /dev/null
IRPNAME == /dev/null
IADNAME == /dev/null
CLMNAME == /dev/null
BRYNAME == /dev/null
FWDNAME == /dev/null
ADSNAME == /dev/null

! Input forcing NetCDF file name(s). The USER has the option to enter
! several files names per each nested grid. For example, the USER may
! have a different files for wind products, heat fluxes, rivers, tides,
! etc. The model will scan the file list and will read the needed data
! from the first file in the list containing the forcing field. Therefore,
! the order of the file names is very important. If multiple forcing
! files per grid, enter first all the file names for grid 1, then grid 2,
! and so on. Use a single line per entry with a continuation (\) symbol
! at the each entry, except the last one.

      NFFILES == 1                      ! number of forcing files

      FRCNAME == ./External/frc_sedbiotoy_waves2.nc

! Output NetCDF file names, [1:Ngrids].

      GSTNAME == ocean_gst.nc
      RSTNAME == ./OUTPUT/rst/rst_sedbiotoy_012.nc
      HISNAME == ./OUTPUT/his_sedbiotoy_012.nc
      TLMNAME == ocean_tlm.nc
      TLFNAME == ocean_tlf.nc
      ADJNAME == ocean_adj.nc
      AVGNAM == ./OUTPUT/avg/avg_sedbiotoy_012.nc
      DIANAME == ./OUTPUT/dia_sedbiotoy_012.nc
      STANAME == ./OUTPUT/sta_sedbiotoy_012.nc
      FLTNAME == ./OUTPUT/flt_sedbiotoy_012.nc

! Input ASCII parameter filenames.

      APARNAM = ROMS/External/s4dvar.in
      SPOSNAM = ROMS/External/stations.in
      FPOSNAM = ROMS/External/floats.in
      BPARNAM = ./External/bioFasham.in
      SPARNAM = ./External/sediment_sedbio_lowDb.in
      USRNAME = ROMS/External/MyFile.dat

!
! GLOSSARY:
! =====
!
!-----
! Application title (string with a maximum of eighty characters) and
! C-preprocessing flag.
!-----
!
! TITLE          Application title.
!
! MyAppCPP       Application C-preprocessing option.
!

```



```

! NPT      Number of inert (dyes, age, etc) passive tracer type variables
!           to advect and diffuse only. This parameter is only relevant
!           if CPP option T_PASSIVE is activated.
!
! NCS      Number of cohesive (mud) sediment tracer type variables. This
!           parameter is only relevant if CPP option SEDIMENT is
!           activated.
!
! NNS      Number of non-cohesive (sand) sediment tracer type variables.
!           This parameter is only relevant if CPP option SEDIMENT is
!           activated.
!
!           The total of sediment tracers is NST=NCS+NNS. Notice that
!           NST must be greater than zero (NST>0).
!
!-----
! Domain tile partition parameters.
!-----
!
! Model tile decomposition parameters for serial and parallel configurations
! which are used to determine tile horizontal range indices (Istr,Iend) and
! (Jstr,Jend). In some computers, it is advantageous to have tile partitions
! in serial applications.
!
! NtileI   Number of domain partitions in the I-direction (XI-coordinate).
!           It must be equal or greater than one.
!
! NtileJ   Number of domain partitions in the J-direction (ETA-coordinate).
!           It must be equal or greater than one.
!
! WARNING: In shared-memory (OpenMP), the product of NtileI and NtileJ must
!           be a MULTIPLE of the number of parallel threads specified with
!           the OpenMP environmental variable OMP_NUM_THREADS.
!
!           In distributed-memory (MPI), the product of NtileI and NtileJ
!           must be EQUAL to the number of parallel nodes specified during
!           execution with the "mprun" or "mpirun" command.
!
!-----
! Time-Stepping parameters.
!-----
!
! NTIMES   Total number time-steps in current run. If 3D configuration,
!           NTIMES is the total of baroclinic time-steps. If only 2D
!           configuration, NTIMES is the total of barotropic time-steps.
!
! DT       Time-Step size in seconds. If 3D configuration, DT is the
!           size of baroclinic time-step. If only 2D configuration, DT
!           is the size of the barotropic time-step.
!
! NDTFAST  Number of barotropic time-steps between each baroclinic time
!           step. If only 2D configuration, NDTFAST should be unity since
!           there is not need to splitting time-stepping.
!
!-----
! Model iteration loops parameters.
!-----
!
! ERstr    Starting ensemble run (perturbation or iteration) number.
!

```

```

! ERend      Ending  ensemble run (perturbation or iteration) number.
!
! Nouter     Maximum number of 4DVAR outer loop iterations.
!
! Ninner     Maximum number of 4DVAR inner loop iterations.
!
! Nintervals Number of time interval divisions for stochastic optimals
!           computations. It must be a multiple of NTIMES. The tangent
!           linear model (TLM) and the adjoint model (ADM) are integrated
!           forward and backward in different intervals. For example,
!           if Nintervals=3,
!
!           1           NTIMES/3           2*NTIMES/3           NTIMES
!           +.....+.....+.....+.....+
!           <=====> (1)
!                   <=====> (2)
!                               <=====> (3)
!
!           In the first iteration (1), the TLM is integrated forward from
!           1 to NTIMES and the ADM is integrated backward from NTIMES to 1.
!           In the second iteration (2), the TLM is integrated forward from
!           NTIMES/3 to NTIMES and the ADM is integrated backward from
!           NTIMES to NTIMES/3. And so on.
!
-----
! Eigenproblem parameters.
-----
!
! NEV        Number of eigenvalues to compute for the Lanczos/Arnoldi
!           problem. Notice that the model memory requirement increases
!           substantially as NEV increases. The GST requires NEV+1
!           copies of the model state vector. The memory requirements
!           are decreased in distributed-memory applications.
!
! NCV        Number of eigenvectors to compute for the Lanczos/Arnoldi
!           problem. NCV must be greater than NEV.
!
! At present, there is no a-priori analysis to guide the selection of NCV
! relative to NEV. The only formal requirement is that NCV > NEV. However
! in optimal perturbations, it is recommended to have NCV greater than or
! equal to 2*NEV. In Finite Time Eigenmodes (FTE) and Adjoint Finite Time
! Eigenmodes (AFTE) the requirement is to have NCV greater than or equal to
! 2*NEV+1.
!
! The efficiency of calculations depends critically on the combination of
! NEV and NCV. If NEV is large (greater than 10 say), you can use NCV=2*NEV+1
! but for NEV small (less than 6) it will be inefficient to use NCV=2*NEV+1.
! In complicated applications, you can start with NEV=2 and NCV=10. Otherwise,
! it will iterate for very long time.
!
-----
! Input/Output parameters.
-----
!
! NRREC      Switch to indicate re-start from a previous solution. Use
!           NRREC=0 for new solutions. In a re-start solution, NRREC
!           is the time index of the re-start NetCDF file assigned for
!           initialization. If NRREC is negative (said NRREC=-1), the
!           model will re-start from the most recent time record. That
!           is, the initialization record is assigned internally.

```

```

!           Notice that it is also possible to re-start from a history
!           or time-averaged NetCDF files.  If a history file is used
!           for re-start, it must contains all the necessary primitive
!           variables at all levels.
!
! LcycleRST Logical switch (T/F) used to recycle time records in output
!           re-start file.  If TRUE, only the latest two re-start time
!           records are maintained.  If FALSE, all re-start fields are
!           saved every NRST time-steps without recycling.  The re-start
!           fields are written at all levels in double precision.
!
! NRST      Number of time-steps between writing of re-start fields.
!
! NSTA      Number of time-steps between writing data into stations file.
!           Station data is written at all levels.
!
! NFLT      Number of time-steps between writing data into floats file.
!
! NINFO     Number of time-steps between print of single line information
!           to standard output.  If also determines the interval between
!           computation of global energy diagnostics.
!
!-----
!           Output history and average files parameters.
!-----
!
! LDEFOUT   Logical switch (T/F) used to create new output files when
!           initializing from a re-start file, abs(NRREC) > 0.  If TRUE
!           and applicable, a new history, average, diagnostic and
!           station files are created during the initialization stage.
!           If FALSE and applicable, data is appended to an existing
!           history, average, diagnostic and station files.  See also
!           parameters NDEFHIS, NDEFavg and NDEFDIA below.
!
! NHIS      Number of time-steps between writing fields into history file.
!
! NDEFHIS   Number of time-steps between the creation of new history file.
!           If NDEFHIS=0, the model will only process one history file.
!           This feature is useful for long simulations when history files
!           get too large; it creates a new file every NDEFHIS time-steps.
!
! NTSavg    Starting time-step for the accumulation of output time-averaged
!           data.
!
! NAVG      Number of time-steps between writing time-averaged data
!           into averages file.  Averaged date is written for all fields.
!
! NDEFavg   Number of time-steps between the creation of new average
!           file.  If NDEFavg=0, the model will only process one average
!           file.  This feature is useful for long simulations when
!           average files get too large; it creates a new file every
!           NDEFavg time-steps.
!
! NTSdia    Starting time-step for the accumulation of output time-averaged
!           diagnostics data.
!
! NDIA      Number of time-steps between writing time-averaged diagnostics
!           data into diagnostics file.  Averaged date is written for all
!           fields.
!

```

```

! NDEFDIA      Number of time-steps between the creation of new time-averaged
!              diagnostics file.  If NDEFDIA=0, the model will only process one
!              diagnostics file.  This feature is useful for long simulations
!              when diagnostics files get too large; it creates a new file
!              every NDEFDIA time-steps.
!
!-----
! Output tangent linear and adjoint model parameters.
!-----
!
! LcycleTLM    Logical switch (T/F) used to recycle time records in output
!              tangent linear file.  If TRUE, only the latest two time
!              records are maintained.  If FALSE, all tangent linear fields
!              are saved every NTLM time-steps without recycling.
!
! NTLM         Number of time-steps between writing fields into tangent linear
!              model file.
!
! NDEFTLM     Number of time-steps between the creation of new tangent linear
!              file.  If NDEFTLM=0, the model will only process one tangent
!              linear file.  This feature is useful for long simulations when
!              output NetCDF files get too large; it creates a new file every
!              NDEFTLM time-steps.
!
! LcycleADJ    Logical switch (T/F) used to recycle time records in output
!              adjoint file.  If TRUE, only the latest two time records are
!              maintained.  If FALSE, all tangent linear fields re saved
!              every NADJ time-steps without recycling.
!
! NADJ        Number of time-steps between writing fields into adjoint model
!              file.
!
! NDEFADJ     Number of time-steps between the creation of new adjoint file.
!              If NDEFADJ=0, the model will only process one adjoint file.
!              This feature is useful for long simulations when output NetCDF
!              files get too large; it creates a new file every NDEFADJ
!              time-steps.
!
!-----
! Generalized Stability Theory (GST) analysis parameters.
!-----
!
! LrstGST      Logical switch (TRUE/FALSE) to restart GST analysis.  If TRUE,
!              the check pointing data is read in from the GST restart NetCDF
!              file.  If FALSE and applicable, the check pointing GST data is
!              saved and overwritten every NGST iterations of the algorithm.
!
! MaxIterGST   Maximum number of GST algorithm iterations.
!
! NGST        Number of GST iterations between storing of check pointing
!              data into NetCDF file.  The restart data is always saved if
!              MaxIterGST is reached without convergence.  It is also saved
!              when convergence is achieved.  It is always a good idea to
!              save the check pointing data at regular intervals so there
!              is a mechanism to recover from an unexpected interruption
!              in this very expensive computation.  The check pointing data
!              can be used also to recompute the Ritz vectors by changing
!              some of the parameters, like convergence criteria (Ritz_tol)
!              and number of Arnoldi iterations (iparam(3)).
!

```



```

! Ritz_tol      Relative accuracy of the Ritz values computed in the GST
!               analysis.
!
!-----
! Harmonic/Biharmonic horizontal diffusion for active tracers.
!-----
!
! TNU2          Lateral, harmonic, constant, mixing coefficient (m2/s) for
!               active (NAT) and inert (NPT) tracer variables.  If variable
!               horizontal diffusion is activated, TNU2 is the mixing
!               coefficient for the largest grid-cell in the domain.
!
! TNU4          Lateral, biharmonic, constant, mixing coefficient (m4/s) for
!               active (NAT) and inert (NPT) tracer variables.  If variable
!               horizontal diffusion is activated, TNU4 is the mixing
!               coefficient for the largest grid-cell in the domain.
!
!-----
! Harmonic/biharmonic horizontal viscosity coefficients.
!-----
!
! VISC2         Lateral, harmonic, constant, mixing coefficient (m2/s) for
!               momentum.  If variable horizontal viscosity is activated, UVNU2
!               is the mixing coefficient for the largest grid-cell in the
!               domain.
!
! VISC4         Lateral, biharmonic, constant mixing coefficient (m4/s) for
!               momentum.  If variable horizontal viscosity is activated, UVNU4
!               is the mixing coefficient for the largest grid-cell in the
!               domain.
!
!-----
! Vertical mixing coefficients for active tracers.
!-----
!
! AKT_BAK       Background vertical mixing coefficient (m2/s) for active
!               (NAT) and inert (NPT) tracer variables.
!
!-----
! Vertical mixing coefficient for momentum.
!-----
!
! AKV_BAK       Background vertical mixing coefficient (m2/s) for momentum.
!
!-----
! Turbulent closure parameters.
!-----
!
! AKK_BAK       Background vertical mixing coefficient (m2/s) for turbulent
!               kinetic energy.
!
! AKP_BAK       Background vertical mixing coefficient (m2/s) for turbulent
!               generic statistical field, "psi".
!
! TKENU2        Lateral, harmonic, constant, mixing coefficient (m2/s) for
!               turbulent closure variables.
!
! TKENU4        Lateral, biharmonic, constant mixing coefficient (m4/s) for
!               turbulent closure variables.
!

```

```

-----
! Generic length-scale turbulence closure parameters.
-----
!
! GLS_P      Stability exponent (non-dimensional).
!
! GLS_M      Turbulent kinetic energy exponent (non-dimensional).
!
! GLS_N      Turbulent length scale exponent (non-dimensional).
!
! GLS_Kmin   Minimum value of specific turbulent kinetic energy
!
! GLS_Pmin   Minimum Value of dissipation.
!
! Closure independent constraint parameters (non-dimensional):
!
! GLS_CMU0   Stability coefficient.
!
! GLS_C1     Shear production coefficient.
!
! GLS_C2     Dissipation coefficient.
!
! GLS_C3M    Buoyancy production coefficient (minus).
!
! GLS_C3P    Buoyancy production coefficient (plus).
!
! GLS_SIGK   Constant Schmidt number (non-dimensional) for turbulent
!            kinetic energy diffusivity.
!
! GLS_SIGP   Constant Schmidt number (non-dimensional) for turbulent
!            generic statistical field, "psi".
!
! Suggested values for various parameterizations:
!
!            k-k1          k-epsilon      k-omega          gen
!
!            GLS_P = 0.d0          3.0d0          -1.0d0          2.0d0
!            GLS_M = 1.d0          1.5d0          0.5d0          1.0d0
!            GLS_N = 1.d0          -1.0d0         -1.0d0         -0.67d0
!            GLS_Kmin = 5.0d-6      7.6d-6         7.6d-6         1.0d-8
!            GLS_Pmin = 5.0d-6      1.0d-12        1.0d-12        1.0d-8
!
!            GLS_CMU0 = 0.5544d0    0.5477d0       0.5477d0       0.5544d0
!            GLS_C1 = 0.9d0          1.44d0         0.555d0        1.00d0
!            GLS_C2 = 0.52d0         1.92d0         0.833d0        1.22d0
!            GLS_C3M = 2.5d0         -0.4d0         -0.6d0         0.1d0
!            GLS_C3P = 1.0d0         1.0d0          1.0d0          1.0d0
!            GLS_SIGK = 1.96d0       1.0d0          2.0d0          0.8d0
!            GLS_SIGP = 1.96d0       1.30d0         2.0d0          1.07d0
!
-----
! Constants used in the various formulation of surface turbulent kinetic
! energy flux in the GLS.
-----
!
! CHARNOK_ALPHA   Charnok surface roughness,
!                 Zos:   (charnok_alpha * u_star**2) / g
!
! ZOS_HSIG_ALPHA  Roughness from wave amplitude,
!                 Zos:   zos_hsig_alpha * Hsig

```

```

!
! SZ_ALPHA      Surface flux from wave dissipation,
!               flux: dt * sz_alpha * Wave_dissip
!
! CRGBAN_CW     Surface flux due to Craig and Banner wave breaking,
!               flux: dt * crgban_cw * u_star**3
!
!-----
! Constants used in the computation of momentum stress.
!-----
!
! RDRG          Linear bottom drag coefficient (m/s).
!
! RDRG2         Quadratic bottom drag coefficient.
!
! Zob           Bottom roughness (m).
!
! Zos           Surface roughness (m).
!
!-----
! Height of atmospheric measurements for bulk fluxes parameterization.
!-----
!
! BLK_ZQ        Height (m) of surface air humidity measurement. Usually,
!               recorded at 10 m.
!
! BLK_ZT        Height (m) of surface air temperature measurement. Usually,
!               recorded at 2 or 10 m.
!
! BLK_ZW        Height (m) of surface winds measurement. Usually, recorded
!               at 10 m.
!
!-----
! Wetting and drying parameters.
!-----
!
! DCRIT         Minimum depth (m) for wetting and drying.
!
!-----
! Jerlow Water type.
!-----
!
! WTYPE         Jerlov water type: an integer value from 1 to 5.
!
!-----
! Body-force parameters. Used when CPP option BODYFORCE is activated.
!-----
!
! LEVSFRC       Deepest level to apply surface momentum stress as a body-force.
!
! LEVBFRFC      Shallowest level to apply bottom momentum stress as a body-
force.
!
!-----
! Vertical S-coordinates parameters.
!-----
!
! THETA_S       S-coordinate surface control parameter, [0 < theta_s < 20].
!
! THETA_B       S-coordinate bottom control parameter, [0 < theta_b < 1].

```

```

!
! TCLINE      Width (m) of surface or bottom boundary layer in which
!             higher vertical resolution is required during stretching.
!
!             WARNING:  Users need to experiment with these parameters.  We
!             have found out that the model goes unstable with
!             high values of THETA_S.  In steep and very tall
!             topography, it is recommended to use THETA_S < 3.0.
!
!-----
! Mean Density and background Brunt-Vaisala frequency.
!-----
!
! RHOO        Mean density (Kg/m3) used when the Boussinesq approximation
!             is inferred.
!
! BVF_BAK     Background Brunt-Vaisala frequency squared (1/s2).  Typical
!             values for the ocean range (as a function of depth) from
!             1.0E-4 to 1.0E-6.
!
!-----
! Time Stamps.
!-----
!
! DSTART      Time stamp assigned to model initialization (days).  Usually
!             a Calendar linear coordinate, like modified Julian Day.  For
!             Example:
!
!             Julian Day = 1   for   Nov 25, 0:0:0 4713 BCE
!             modified Julian Day = 1   for   May 24, 0:0:0 1968 CE GMT
!
!             It is called truncated or modified Julian day because an offset
!             of 2440000 needs to be added.
!
! TIDE_START  Reference time origin for tidal forcing (days).  This is the
!             time used when processing input tidal model data.  It is needed
!             in routine "set_tides" to compute the correct phase lag with
!             respect ROMS/TOMS initialization time.
!
! TIME_REF    Reference time (yyyymmdd.f) used to compute relative time:
!             elapsed time interval since reference-time.  The "units"
!             attribute takes the form "time-unit since reference-time".
!             This parameter also provides information about the calendar
!             used:
!
!             If TIME_REF = -2, model time and DSTART are in modified Julian
!             days units.  The "units" attribute is:
!
!             'time-units since 1968-05-23 00:00:00 GMT'
!
!             If TIME_REF = -1, model time and DSTART are in a calendar
!             with 360 days in every year (30 days each month).  The "units"
!             attribute is:
!
!             'time-units since 0000-01-01 00:00:00'
!
!             If TIME_REF = 0, model time and DSTART are in a common year
!             calendar with 365.25 days.  The "units" attribute is:
!
!             'time-units since 0000-01-01 00:00:00'
!

```

```

!
!       If TIME_REF > 0, model time and DSTART are the elapsed time
!       units since specified reference time.  For example,
!       TIME_REF=20020115.5 will yield the following attribute:
!
!               'time-units since 2002-01-15 12:00:00'
!
!-----
! Nudging/relaxation time scales, inverse scales will be computed internally.
!-----
!
! When passive/active open boundary conditions are activated, these nudging
! values correspond to the passive (outflow) nudging time scales.
!
! TNUDG      Nudging time scale (days) for active tracer variables.
!             (1:NAT+NPT,1:Ngrids) values are expected.
!
! ZNUDG      Nudging time scale (days) for free-surface.
!
! M2NUDG     Nudging time scale (days) for 2D momentum.
!
! M3NUDG     Nudging time scale (days) for 3D momentum.
!
! OBCFAC     Factor between passive (outflow) and active (inflow) open
!             boundary conditions.  The nudging time scales for the
!             active (inflow) conditions are obtained by multiplying
!             the passive values by OBCFAC.  If OBCFAC > 1, nudging on
!             inflow is stronger than on outflow (recommended).
!
!-----
! Linear equation of State parameters.
!-----
!
! Ignoring pressure, the linear equation of state is:
!
!             rho(:,:,) = R0 - R0 * TCOEF * (t(:,:,:,itemp) - T0)
!                   + R0 * SCOEF * (t(:,:,:,isalt) - S0)
!
! Typical values:      R0 = 1027.0   kg/m3
!                   T0 = 10.0      Celsius
!                   S0 = 35.0      PSU
!                   TCOEF = 1.7d-4  1/Celsius
!                   SCOEF = 7.6d-4  1/PSU
!
! R0           Background density value (Kg/m3) used in Linear Equation of
!             State.
!
! T0           Background potential temperature (Celsius) constant.
!
! S0           Background salinity (PSU) constant.
!
! TCOEF        Thermal expansion coefficient in Linear Equation of State.
!
! SCOEF        Saline contraction coefficient in Linear Equation of State.
!
!-----
! Slipperiness parameter.
!-----
!
! GAMMA2      Slipperiness variable, either 1.0 (free slip) or -1.0 (no slip).

```

```

!-----
! Adjoint sensitivity parameters.
!-----
!
! DstrS      Starting day for adjoint sensitivity forcing.
!
! DendS      Ending   day for adjoint sensitivity forcing.
!
!            The adjoint forcing is applied at every time step according to
!            desired state functional stored in the adjoint sensitivity
!            NetCDF file. DstrS must be less or equal to DendS. If both
!            values are zero, their values are reset internally to the full
!            range of the adjoint integration.
!
! KstrS      Starting vertical level of the 3D adjoint state variables whose
!            sensitivity is required.
!
! KendS      Ending   vertical level of the 3D adjoint state variables whose
!            sensitivity is required.
!
! Lstate     Logical switches (TRUE/FALSE) to specify the adjoint state
!            variables whose sensitivity is required.
!
!            Lstate(isFsur):  Free-surface
!            Lstate(isUbar):  2D U-momentum
!            Lstate(isVbar):  2D V-momentum
!            Lstate(isUvel):  3D U-momentum
!            Lstate(isVvel):  3D V-momentum
!            Lstate(isTvar):  Traces (NT values expected)
!
!-----
! Stochastic optimals parameters.
!-----
!
! SO_decay   Stochastic optimals time decorrelation scale (days) assumed
!            for red noise processes.
!
! SOstate    Logical switches (TRUE/FALSE) to specify the state surface
!            forcing variable whose stochastic optimals is required.
!
!            SOstate(isUstr): surface u-stress
!            SOstate(isVstr): surface v-stress
!            SOstate(isTsur): surface tracer flux (NT values expected)
!
! SO_sdev    Stochastic optimals surface forcing standard deviation for
!            dimensionalization.
!
!            SO_sdev(isUstr): surface u-stress
!            SO_sdev(isVstr): surface v-stress
!            SO_sdev(isTsur): surface tracer flux (NT values expected)
!
!-----
! Logical switches (T/F) to activate writing of fields into HISTORY file.
!-----
!
! Hout(idUvel) Write out 3D U-velocity component.
! Hout(idVvel) Write out 3D V-velocity component.
! Hout(idWvel) Write out 3D W-velocity component.
! Hout(idOvel) Write out 3D omega vertical velocity.
! Hout(idUbar) Write out 2D U-velocity component.

```

```

! Hout(idVbar) Write out 2D V-velocity component.
! Hout(idFsur) Write out free-surface.
! Hout(idBath) Write out time-dependent bathymetry.
!
! Hout(idTvar) Write out active (NAT) tracers: temperature and salinity.
!
! Hout(idUsms) Write out surface U-momentum stress.
! Hout(idVsms) Write out surface V-momentum stress.
! Hout(idUbms) Write out bottom U-momentum stress.
! Hout(idVbms) Write out bottom V-momentum stress.
!
! Hout(idUbrs) Write out current-induced, U-momentum stress.
! Hout(idVbrs) Write out current-induced, V-momentum stress.
! Hout(idUbws) Write out wind-induced, bottom U-wave stress.
! Hout(idVbws) Write out wind-induced, bottom V-wave stress.
! Hout(idUbcs) Write out bottom maximum wave and current U-stress.
! Hout(idVbcs) Write out bottom maximum wave and current V-stress.
!
! Hout(idUbot) Write out wind-induced, bed wave orbital U-velocity.
! Hout(idVbot) Write out wind-induced, bed wave orbital V-velocity.
! Hout(idUbur) Write out bottom U-velocity above bed.
! Hout(idVbvr) Write out bottom V-velocity above bed.
!
! Hout(idW2xx) Write out 2D radiation stress, Sxx component.
! Hout(idW2xy) Write out 2D radiation stress, Sxy component.
! Hout(idW2yy) Write out 2D radiation stress, Syy component.
! Hout(idU2rs) Write out 2D U-radiation stress.
! Hout(idV2rs) Write out 2D V-radiation stress.
! Hout(idU2Sd) Write out 2D U-Stokes velocity.
! Hout(idV2Sd) Write out 2D V-Stokes velocity.
!
! Hout(idW3xx) Write out 3D radiation stress, Sxx component.
! Hout(idW3xy) Write out 3D radiation stress, Sxy component.
! Hout(idW3yy) Write out 3D radiation stress, Syy component.
! Hout(idW3zx) Write out 3D radiation stress, Szx component.
! Hout(idW3zy) Write out 3D radiation stress, Szy component.
! Hout(idU3rs) Write out 3D U-radiation stress.
! Hout(idV3rs) Write out 3D V-radiation stress.
! Hout(idU3Sd) Write out 3D U-Stokes velocity.
! Hout(idV3Sd) Write out 3D V-Stokes velocity.
!
! Hout(idWamp) Write out wave height.
! Hout(idWlen) Write out wave length.
! Hout(idWdir) Write out wave direction.
!
! Hout(idTsur) Write out surface net heat and salt flux
! Hout(idLhea) Write out latent heat flux.
! Hout(idShea) Write out sensible heat flux.
! Hout(idLrad) Write out long-wave radiation flux.
! Hout(idSrad) Write out short-wave radiation flux.
! Hout(iddevap) Write out evaporation rate.
! Hout(idrain) Write out precipitation rate.
!
! Hout(idDano) Write out density anomaly.
! Hout(idVvis) Write out vertical viscosity coefficient.
! Hout(idTdif) Write out vertical diffusion coefficient of temperature.
! Hout(idSdif) Write out vertical diffusion coefficient of salinity.
! Hout(idHsbl) Write out depth of oceanic surface boundary layer.
! Hout(idHbbl) Write out depth of oceanic bottom boundary layer.
! Hout(idMtke) Write out turbulent kinetic energy.

```

```

! Hout(idMtls) Write out turbulent kinetic energy times length scale.
!
! Hout(inert) Write out extra inert passive tracers.
!
! Hout(idBott) Write out exposed sediment layer properties, 1:MBOTP.
!
-----
! Generic User parameters.
-----
!
! NUSER      Number of User parameters to consider (integer).
! USER      Vector containing user parameters (real array). This array
!            is used with the SANITY_CHECK to test the correctness of
!            the tangent linear adjoint models. It contains information
!            of the model variable and grid point to perturb:
!
!            INT(user(1)): tangent state variable to perturb
!            INT(user(2)): adjoint state variable to perturb
!                           [isFsur=1] free-surface
!                           [isUbar=2] 2D U-momentum
!                           [isVbar=3] 2D V-momentum
!                           [isUvel=4] 3D U-momentum
!                           [isVvel=5] 3D V-momentum
!                           [isTvar=6] First tracer (temperature)
!                           [ ... ]
!                           [isTvar=?] Last tracer
!
!            INT(user(3)): I-index of tangent variable to perturb
!            INT(user(4)): I-index of adjoint variable to perturb
!            INT(user(5)): J-index of tangent variable to perturb
!            INT(user(6)): J-index of adjoint variable to perturb
!            INT(user(7)): K-index of tangent variable to perturb, if 3D
!            INT(user(8)): K-index of adjoint variable to perturb, if 3D
!
!            Set tangent and adjoint parameters to the same values
!            if perturbing and reporting the same variable.
!
-----
! Input/output NetCDF file names (string with a maximum of eighty characters).
-----
!
! GRDNAME    Input grid file name.
! ININAME    Input nonlinear initial conditions file name. It can be a
!            re-start file.
! IRPNAME    Input representer model initial conditions file name.
! ITLNAME    Input tangent linear model initial conditions file name.
! IADNAME    Input adjoint model initial conditions file name.
! FRCNAME    Input forcing fields file name.
! CLMNAME    Input climatology fields file name.
! BRYNAME    Input open boundary data file name.
! FWDNAME    Input forward solution fields file name.
! ADSNAME    Input adjoint sensitivity functional file name.
!
! GSTNAME    Output GST analysis re-start file name.
! RSTNAME    Output re-start file name.
! HISNAME    Output history file name.
! TLFNAME    Output impulse forcing for tangent linear (TLM and RPM) models.
! TLMNAME    Output tangent linear file name.
! ADJNAME    Output adjoint file name.
! AVGNAMES   Output averages file name.

```



```
! DIANAME      Output diagnostics file name.
! STANAME      Output stations file name.
! FLTNAME      Output floats file name.
!
!-----
! Input ASCII parameters file names.
!-----
!
! APARNAM      Input assimilation parameters file name.
! SPOSNAM      Input stations positions file name.
! FPOSNAM      Input initial drifters positions file name.
! BPARNAM      Input biological parameters file name.
! SPARNAM      Input sediment transport parameters file name.
! USRNAME      USER's input generic file name.
!
```

sediment_sedbio.in

```
!
!   ROMS/TOMS Cohesive and Non-cohesive Sediment Model Parameters.
!
!svn $Id: sediment_estuary_test.in 34 2007-04-27 04:40:21Z arango $
!===== Hernan G. Arango =====
!   Copyright (c) 2002-2007 The ROMS/TOMS Group
!   Licensed under a MIT/X style license
!   See License_ROMS.txt
!=====
!
! Input parameters can be entered in ANY order, provided that the parameter
! KEYWORD (usually, upper case) is typed correctly followed by "=" or "=="
! symbols. Any comment lines are allowed and must begin with an exclamation
! mark (!) in column one. Comments may appear to the right of a parameter
! specification to improve documentation. All comments will ignored during
! reading. Blank lines are also allowed and ignored. Continuation lines in
! a parameter specification are allowed and must be preceded by a backslash
! (\). In some instances, more than one value is required for a parameter.
! If fewer values are provided, the last value is assigned for the entire
! parameter array. The multiplication symbol (*), without blank spaces in
! between, is allowed for a parameter specification. For example, in a two
! grids nested application:
!
!   AKT_BAK == 2*1.0d-6  2*5.0d-6           ! m2/s
!
! indicates that the first two entries of array AKT_BAK, in fortran column-
! major order, will have the same value of "1.0d-6" for grid 1, whereas the
! next two entries will have the same value of "5.0d-6" for grid 2.
!
! In multiple levels of nesting and/or multiple connected domains step-ups,
! "Ngrids" entries are expected for some of these parameters. In such case,
! the order of the entries for a parameter is extremely important. It must
! follow the same order (1:Ngrids) as in the state variable declaration. The
! USER may follow the above guidelines for specifying his/her values. These
! parameters are marked by "==" plural symbol after the KEYWORD.
!=====
!
!-----
!   Sediment model control switch.
!-----
!
! Switch is used to control sediment model computation within nested and/or
! multiple connected grids, [1:Ngrids].
!
!   Lsediment == T
!-----
!   General sediment bed model controls.
!-----
!
! Depositional bed layer thickness criteria to create a new layer (m). If
! deposition exceeds this value, then a new layer is created, [1:Ngrids].
!
!   NEWLAYER_THICK == 0.005d0
!
! Bed load transport rate coefficient. [1:Ngrids].
!
!   BEDLOAD_COEFF == 0.05d0
```

```

!-----
! Suspended Cohesive Sediment Parameters, [1:NCS,1:Ngrids] values expected.
!-----
! Median sediment grain diameter (mm).
! added by kxu, mud_01, 02, 03
!           seabed1, seabed2, seabed3
!           micro-floc, macro-floc, sand

MUD_SD50 == 0.015d0 0.063d0 0.125d0

! Sediment concentration (kg/m3).

MUD_CSED == 0.0d0 0.0d0 0.0d0

! Sediment grain density (kg/m3).

MUD_SRHO == 2650.0d0 2650.0d0 2650.0d0

! Particle settling velocity (mm/s).

MUD_WSED == 0.1d0 1.0d0 10.0d0

! Surface erosion rate (kg/m2/s).

MUD_ERATE == 5.0d-5 5.0d-5 5.0d-5

! Critical shear for erosion and deposition (N/m2).

MUD_TAU_CE == 0.03d0 0.08d0 0.10d0
! MUD_TAU_CE == 0.03d0 10.08d0 0.10d0
MUD_TAU_CD == 0.01d0 0.01d0 0.01d0

! Porosity (nondimensional: 0.0-1.0): Vwater/(Vwater+Vsed).

MUD_POROS == 0.8d0 0.8d0 0.8d0

! Lateral, harmonic and biharmonic, constant, diffusion coefficient.

MUD_TNU2 == 0.0d0 0.0d0 0.0d0 ! m2/s
MUD_TNU4 == 0.0d0 0.0d0 0.0d0 ! m4/s

! Vertical diffusion coefficients.

MUD_AKT_BAK == 5.0d-6 5.0d-6 5.0d-6 ! m2/s

! Sediment Bed Biodiffusion coefficients - jjb Birchler@vims.edu - July '11

MUD_DBMX == 3.0d-12 3.0d-12 3.0d-12 !m2/s ! Db=1cm2/yr
MUD_DBMM == 5.0d-14 5.0d-14 5.0d-14 !m2/s

! Nudging/relaxation time scales, inverse scales will be computed
! internally.

MUD_TNUGD == 0.0d0 0.0d0 0.0d0 ! days

! Morphological time scale factor (greater than or equal to 1.0). A
! value of 1.0 has no scale effect.

MUD_MORPH_FAC == 1.0d0 1.0d0 1.0d0 ! nondimensional

```

! Logical switches (TRUE/FALSE) to specify which variables to consider on
! tracers point Sources/Sinks (like river runoff). See glossary below for
! details.

! MUD_Ltracer == T T F
! MUD_Ltsrc == T T F !jjb 8/13

! Logical switch (TRUE/FALSE) to activate writing of cohesive sediment
! into HISTORY output file.

Hout(idmud) == T ! suspended concentration
Hout(iMfrac) == T ! bed layer fraction
Hout(iMmass) == T ! bed layer mass
Hout(iMUbld) == T ! bed load at U-points
Hout(iMVbld) == T ! bed load at V-points
Hout(idbdom) == T ! bed OM concentration
Hout(idtgeoch) == T T T T ! wc geochron tracers

!-----
! Non-cohesive Sediment Parameters, [1:NNS,1:Ngrids] values expected.
!-----

! Median sediment grain diameter (mm).

SAND_SD50 == 1.0d0

! Sediment concentration (kg/m3).

SAND_CSED == 0.0d0

! Sediment grain density (kg/m3).

SAND_SRHO == 2650.0d0

! Particle settling velocity (mm/s).

SAND_WSED == 1.0d0

! Surface erosion rate (kg/m2/s).

SAND_ERATE == 5.0d-4

! Critical shear for erosion and deposition (N/m2).

SAND_TAU_CE == 0.1d0

SAND_TAU_CD == 0.1d0

! Porosity (nondimensional: 0.0-1.0): $V_{water}/(V_{water}+V_{sed})$.

SAND_POROS == 0.5d0

! Lateral, harmonic and biharmonic, constant, diffusion coefficient.

SAND_TNU2 == 0.0d0 ! m2/s

SAND_TNU4 == 0.0d0 ! m4/s

! Vertical diffusion coefficients.

SAND_AKT_BAK == 5.0d-6 ! m2/s

```

! Nudging/relaxation time scales, inverse scales will be computed
! internally.

SAND_TNUDG == 0.0d0                ! days

! Morphological time scale factor (greater than or equal to 1.0). A
! value of 1.0 has no scale effect.

SAND_MORPH_FAC == 1.0d0 1.0d0 1.0d0    ! nondimensional

!=====

! Tracer Bed Biodiffusion coefficients - jjbirchler@vims.edu - July '11

!   TRC_DBMX == 3.0d-13 3.0d-13 3.0d-13
!   TRC_DBMN == 5.0d-14 5.0d-14 5.0d-14

!=====

! Logical switches (TRUE/FALSE) to activate writing of non-cohesive
! sediment into HISTORY output file.

Hout(idsand) == T                    ! suspended concentration
Hout(iSfrac) == T                    ! bed layer fraction
Hout(iSmass) == T                    ! bed layer mass
Hout(iSubld) == T                    ! bed load at U-points
Hout(iSVbld) == T                    ! bed load at V-points

!-----
! Bed layer and bottom sediment parameters, [1:Ngrids] values expected.
!-----

Hout(ithck) == T                    ! sediment layer thickness
Hout(iaged) == T                    ! sediment layer age
Hout(iporo) == T                    ! sediment layer porosity
Hout(idiff) == F                    ! biodiffusivity
!
!   GLOSSARY:
!   =====
!-----
! Sediment model control switch, [1:Ngrids].
!-----
!
!   Lsediment      Switch to control sediment model computation within nested
!                  and/or multiple connected grids. By default this switch
!                  is set to TRUE in "mod_scalars" for all grids. The USER
!                  has the option, for example, to compute sediment in just
!                  one of the nested grids. If so, this switch needs to be
!                  consistent with the dimension parameter NST in input
!                  script (ocean.in). In order to make the model more
!                  efficient in memory usage, NST(:) should be zero in
!                  such grids.
!
!-----
! General sediment bed model controls, [1:Ngrids] values are expected.
!-----
!
!   NEWLAYER_THICK Depositional bed layer thickness criteria to create a new
!                  layer (m). If deposition exceeds this value, then a new

```

```

!           layer is created.
!
!   BEDLOAD_COEFF   Bed load transport rate coefficient.
!
!-----
! Suspended Cohesive Sediment KEYWORDS, [1:NCS,1:Ngrids] values expected.
!-----
!
!   MUD_SD50        Median sediment grain diameter (mm).
!
!   MUD_CSED        Sediment concentration (kg/m3). It may be used to initialize
!                   sediment fields using analytical expressions.
!
!   MUD_SRHO        Sediment grain density (kg/m3).
!
!   MUD_WSED        Particle settling velocity (mm/s).
!
!   MUD_ERATE       Surface erosion rate (kg/m2/s).
!
!   MUD_TAU_CE      Critical shear for erosion (N/m2).
!
!   MUD_TAU_CD      Critical shear for deposition (N/m2).
!
!   MUD_POROS       Porosity (nondimensional: 0.0-1.0): Vwater/(Vwater+Vsed).
!
!   MUD_TNU2        Lateral, harmonic, constant, mixing coefficient (m2/s),
!                   TNU2(idsed(i)) with i=1:NCS.  If variable horizontal
!                   diffusion is activated, TNU2 is the mixing coefficient
!                   for the largest grid-cell in the domain.
!
!   MUD_TNU4        Lateral, biharmonic, constant, mixing coefficient (m4/s),
!                   TNU4(idsed(i)) with i=1:NCS.  If variable horizontal
!                   diffusion is activated, TNU4 is the mixing coefficient
!                   for the largest grid-cell in the domain.
!
!   MUD_AKT_BAK     Background vertical mixing coefficient (m2/s),
!                   AKT_BAK(idsed(i)) with i=1:NCS.
!
!   MUD_TNUDG       Nudging time scale (days), TNUDG(idsed(i)) with i=1:NCS.
!                   Inverse scale will be computed internally.
!
!   MUD_MORPH_FAC  Morphological time scale factor (nondimensional; greater
!                   than or equal to 1.0). A value of 1.0 has no scale
!                   effect.
!
!   Hout(idmud)     Logical switches to activate writing of cohesive sediment
!                   concentration into HISTORY NetCDF file,
!                   HOUT(idTvar(idsed(i))) with i=1:NCS.
!
!   Hout(imfrac)    Logical switches to activate writing of cohesive sediment
!                   class fraction composition of each bed layer into HISTORY
!                   NetCDF file, HOUT(idfrac(i)) with i=1,NCS.
!
!   Hout(iMmass)    Logical switches to activate writing of cohesive sediment
!                   mass of each bed layer into HISTORY NetCDF file,
!                   HOUT(idsed(i)) with i=1,NCS.
!
!   Hout(iMubld)    Logical switches to activate writing of cohesive sediment
!                   bed load at U-points into HISTORY NetCDF file,
!                   HOUT(idsed(i)) with i=1,NCS.
!

```

```

!
! Hout(iMVbld)      Logical switches to activate writing of cohesive sediment
!                   bed load at V-points into HISTORY NetCDF file,
!                   HOUT(idsed(i)) with i=1,NCS.
!
-----
! Suspended Non-cohesive Sediment KEYWORDS, [1:NNS,1:Ngrids] values expected.
-----
!
! SAND_SD50         Median sediment grain diameter (mm).
!
! SAND_CSED         Sediment concentration (kg/m3). It may be used to initialize
!                   sediment fields using analytical expressions.
!
! SAND_SRHO         Sediment grain density (kg/m3).
!
! SAND_WSED         Particle settling velocity (mm/s).
!
! SAND_Erate        Surface erosion rate (kg/m2/s).
!
! SAND_TAU_CE       Critical shear for erosion (N/m2).
!
! SAND_TAU_CD       Critical shear for deposition (N/m2).
!
! SAND_POROS        Porosity (nondimensional: 0.0-1.0): Vwater/(Vwater+Vsed).
!
! SAND_TNU2         Lateral, harmonic, constant, mixing coefficient (m2/s),
!                   TNU2(idsed(i)) with i=NCS+1:NST. If variable horizontal
!                   diffusion is activated, TNU2 is the mixing coefficient
!                   for the largest grid-cell in the domain.
!
! SAND_TNU4         Lateral, biharmonic, constant, mixing coefficient (m4/s),
!                   TNU4(idsed(i)) with i=NCS+1:NST. If variable horizontal
!                   diffusion is activated, TNU4 is the mixing coefficient
!                   for the largest grid-cell in the domain.
!
! SAND_AKT_BAK      Background vertical mixing coefficient (m2/s),
!                   AKT_BAK(idsed(i)) with i=NCS+1:NST.
!
! SAND_TNUDG        Nudging time scale (days), TNUDG(idsed(i)) with i=NCS+1:NST.
!                   Inverse scale will be computed internally,
!
! SAND_MORPH_FAC    Morphological time scale factor (nondimensional; greater
!                   than or equal to 1.0). A value of 1.0 has no scale effect.
!
! Hout(idsand)      Logical switches to activate writing of non-cohesive
!                   sediment concentration into HISTORY NetCDF file,
!                   HOUT(idTvar(idsed(i))) with i=1:NCS+1,NST.
!
! Hout(iSfrac)      Logical switches to activate writing of non-cohesive
!                   sediment class fraction composition of each bed layer
!                   into HISTORY NetCDF file, HOUT(idfrac(i)) with
!                   i=NCS+1,NST.
!
! Hout(iSmass)      Logical switches to activate writing of non-cohesive
!                   sediment mass of each bed layer into HISTORY NetCDF file,
!                   HOUT(idsed(i)) with i=NCS+1,NST.
!
! Hout(iSubld)      Logical switches to activate writing of non-cohesive
!                   sediment bed load at U-points into HISTORY NetCDF file,

```

```

!           HOUT(idsed(i)) with i=NCS+1,NST.
!
!  Hout(iSVbld)   Logical switches to activate writing of non-cohesive
!                 sediment bed load at V-points into HISTORY NetCDF file,
!                 HOUT(idsed(i)) with i=NCS+1,NST.
!
!-----
! Bed layer and bottom sediment KEYWORDS, [1:Ngrids] values expected.
!-----
!
!  Hout(ithck)    Sediment layer thickness.
!
!  Hout(iaged)    Sediment layer age.
!
!  Hout(iporo)    Sediment layer porosity.
!
!  Hout(idiff)    Biodiffusivity at the bottom of each layer.

```


VITA

Justin J. Birchler

Born in Ann Arbor, MI on 4 September 1988. Graduated from Pioneer High School, Ann Arbor, MI in June 2006. Earned B.S. in Marine Science from Coastal Carolina University, Conway, SC in May 2010. Entered M.S. program in the College of William & Mary, School of Marine Science, Gloucester Point, VA in August 2010.